

POLITECNICO DI TORINO

**MASTER'S DEGREE PROGRAM IN
ENERGY AND NUCLEAR ENGINEERING**



MASTER'S DEGREE THESIS

**Energy, exergy and exergo-economic analysis of an ORC biomass
cogeneration system integrated with an hybrid solar thermal solution**

SUPERVISORS

**Leone Pierluigi
Lanzini Andrea
Baranda Ribeiro Jose Manuel**

CANDIDATE

Danilo Cantone

ACADEMIC YEAR 2018 / 2019

Index

Abstract	i
List of figures.....	iii
Abbreviations and acronyms	v
List of symbols	vii
Acknowledgements.....	xi
1. Introduction	1
2. Case studies	9
2.1 Biomass system layout.....	10
2.2 Hybrid biomass-solar plant layout and control systems	14
3. Methodology.....	19
3.1 Biomass plant model.....	19
3.1.1 ORC cycle model.....	19
3.1.2 Vertical biomass firetube boiler model.....	31
3.2 Exergy and exergoeconomic analysis.....	35
3.2.1 Exergy analysis.....	35
3.2.2 Exergoeconomic analysis.....	38
3.2.3 Design improvement and optimization.....	44
3.3 Hybrid biomass-solar plant model.....	46
4. Results.....	51
4.1 Biomass plant results	51
4.2 Exergy and exergoeconomic results	61
4.3 Hybrid biomass-solar plant results	74
5. Conclusion.....	85
Bibliography.....	88
Appendix	95
Appendix A.....	95
Appendix B.....	96
Appendix C.....	97
Appendix D.....	107
Appendix E	110
Appendix F.....	114
Appendix G.....	118

Abstract

The purpose of this thesis is to investigate a low-temperature and biomass-powered cogeneration prototype, innovative in the Portuguese market, proposed by the SCIVEN company, spin-off of the University of Coimbra.

The case study of a swimming pool water heater is presented, in which the water has a thermal load between 80 and 150 kW_{th}, with an inlet temperature between 25 and 27 °C and an outlet temperature between 30 and 32 °C.

The peculiarity of the plant is that it uses a hot water (up to 95 °C) boiler to have fewer legislative constraints during construction and maintenance. This thermal source is so used to evaporate and superheat the R245fa working fluid of an Organic Rankine Cycle (ORC) up to 90 °C. Moreover, particular attention was dedicated to the heat exchangers, to which was applied the moving boundary method.

Through the MATLAB software, the energetic, exergetic and exergoeconomic conditions of the combustion chamber and the cogeneration cycle were analysed in design and off design conditions.

Thermodynamic analysis showed a maximum electrical efficiency of 6.62% for a condenser capacity of 140 kW_{th}. For different condenser thermal powers, there was also discovered a pool temperature control strategy, able to increase, compared to the worst operating condition, the electrical efficiency of 0.45% and the net electric power produced of 16%. Finally, for each benchmark, the ranges of the thermodynamic conditions have been reported to carry out future thermo-mechanical analyses.

The exergetic and exergoeconomic analysis were conducted on the full range of operating conditions on the condenser to minimize the cost of exergy. It emerged that the component with the greatest irreversibility is the combustion chamber, between 89.6 and 93%, followed by the evaporator, between 5.9 and 3.3%. Finally, since the combustion chamber has the highest sum of the cost rate and the exergy destruction, it was decided to reduce its contribution to the plant by preheating the organic fluid with an hybrid solar thermal system.

The solar system has been sized, thought Polysun software, both to preheat the organic fluid and to generate hot water for the showers of a system of 250 daily users. The plant was analysed with two different technologies, the vacuum tube and the flat plate. The optimization on panel surface allows a pellet savings of 21.9 $\left[\frac{\text{ton}}{\text{year}}\right]$ and 19.4 $\left[\frac{\text{ton}}{\text{year}}\right]$ respectively. Finally, was evaluated the NPV of the solutions proposed without incentives and considering those of the Italian and Portuguese states.

Keywords

Cogeneration, Swimming pool water heating system, ORC, Exergy and exergoeconomic analysis, Biomass-solar thermal hybrid system.

List of figures

Figure 2.1 Scheme of the hybrid, biomass-solar, low temperature ORC cogeneration plant.....	9
Figure 2.2 Scheme of the ORC cogeneration plant fuelled by biomass	10
Figure 2.3 Evolution of the isentropic efficiency of the turbine as function of the pressure ratio	12
Figure 2.4 Hybrid biomass-solar plant scheme	15
Figure 2.5 Hybrid solution, only water preheating condition	16
Figure 2.6 Hybrid solution, only ORC preheating condition.....	16
Figure 2.7 Hybrid solution, ORC and water preheating condition.....	17
Figure 2.8 Hybrid solution, ORC and water preheating condition, with the use of the three-valve in order to reach at most the boiling point	17
Figure 3.1 Block diagram of the ORC cycle model	21
Figure 3.2 Moving boundaries principle in heat exchangers: evaporator (left), condenser (right)	23
Figure 3.3 Time elapsed during simulation with variable condenser power	29
Figure 3.4 Time elapsed during simulation with variable condenser temperature inlet (Left); Time elapsed during simulation with variable condenser temperature outlet (Right)	29
Figure 3.5 Definition of the optimal area through the solar factor and the system efficiency [82].....	49
Figure 4.1 Evolution of electrical efficiency with different temperatures of pool water inlet	51
Figure 4.2 Evolution of the isentropic efficiency of the turbine and of the ratio between the mass flow rates with different pool water inlet temperatures.....	52
Figure 4.3 Evolution of the pressure ratio with different pool water inlet temperatures	53
Figure 4.4 Evolution of the electrical efficiency with different variations of pool water temperature.....	54
Figure 4.5 Extreme cases of electrical efficiency recorded in the range analyzed in the condenser.....	55
Figure 4.6 Evolution of thermal efficiency with different temperatures of pool water inlet	55
Figure 4.7 Evolution of the thermal efficiency with different variations of pool water temperature.....	56
Figure 4.8 Evolution of Primary Energy Savings with different temperatures of pool water inlet.....	57
Figure 4.9 Evolution of Primary Energy Savings with different variations of pool water temperature.....	57
Figure 4.10 Exergies of the streams in the operating condition that provides the greatest electrical efficiency of the system	62
Figure 4.11 Irrevesibilities of the components in the operating condition that provides the greatest electrical efficiency of the system.....	63

Figure 4.12 Exergy efficiency of the components in the operating condition that provides the greatest electrical efficiency of the system.....	63
Figure 4.13 Exergy cost of the streams in the operating condition that provides the greatest electrical efficiency of the system.....	64
Figure 4.14 Unit exergy cost of the streams in the operating condition that provides the greatest electrical efficiency of the system.....	64
Figure 4.15 Exergo economic cost of the streams in the operating condition that provides the greatest electrical efficiency of the system.....	65
Figure 4.16 Unit of exergo economic cost of the streams in the operating condition that provides the greatest electrical efficiency of the system.....	66
Figure 4.17 Evolution of the unit of exergo economic cost of the mechanical product with different inlet pool water temperatures	67
Figure 4.18 Evolution of the unit of exergo economic cost of the mechanical product with the same inlet and different outlet of pool water temperature.....	68
Figure 4.19 Extreme cases of the unit of exergo economic cost of the mechanical product recorded in the range analyzed in the condenser	68
Figure 4.20 Evolution of the unit of exergo economic cost of the thermal product with different temperatures of pool water inlet.....	69
Figure 4.21 Evolution of the unit of exergo economic cost of the thermal product with the same outlet and different inlet of pool water temperature.....	70
Figure 4.22 Evolution of the exergo economic cost of the thermal product and the outlet water condenser exergy with different pool water inlet temperatures.....	70
Figure 4.23 Extreme cases of the unit of exergo economic cost of the thermal product recorded in the range analyzed in the condenser	71
Figure 4.24 Relationship between SF and SE in the analysed cases	75
Figure 4.25 Vacuum tube, temperature evolution first week	77
Figure 4.26 Vacuum tube, temperature evolution twenty-sixth week	77
Figure 4.27 Flat plate, temperature evolution first week	77
Figure 4.28 Flat plate, temperature evolution twenty-sixth week	78
Figure 4.29 Annual thermal energy flow of a biomass system, for heating 10000 litres/day	79
Figure 4.30 Annual thermal energy flow of a hybrid solar plant, with vacuum panels (absorber area of 90.3 m ²), for heating 10000 litres/day.....	79
Figure 4.31 Annual thermal energy flow of a hybrid solar plant, with flat plate panels (absorber area of 88,54 m ²), for heating 10000 litres/day.....	79
Figure 4.32 Net Present Value of the vacuum tube and flat plate technologies without state incentives.....	82

Abbreviations and acronyms

BCR	Benefit-Cost Ratio
BEC	Bare Erected Cost
CEO	Chief Executive Officer
CAPEX	CAPital EXpenditure
CBE	Centro da Biomassa para a Energia
CHP	Combined Heat and Power
COND	Condensator
DHW	Domestic Hot Water
DRF	Discount Rate Factor
EES	Engineering Equation Solver
EMRP	Equity Market Risk Premium
EPC	European Pellet Council
EPCC	Engineering, Procurement and Construction
EVA	Evaporator
EVP	EVacuated Plate
EVT	EVacuated Tube
GHE	Geothermal/Ground Heat Exchanger
GHG	Greenhouse Gases
GHP	Geothermal Heat Pump
HFE	Hydrofluoroether
IEA	International Energy Agency
IRS	Interest Rate Swap
LEBS	Laboratório Especializado em Biocombustíveis Sólidos
LHV	Lower Heating Value
NETL	National Energy Technology Laboratory
NPV	Net Present Value
NSL	Not Selective absorber Layer
OPEX	OPerating EXpense
ORC	Organic Rankine Cycle
PCM	Phase Change Material
PB	Pay Back
PES	Primary Energy Savings
RES	Renewable Energy Sources
R&D	Research and Development
SEL	Selective External absorber Layer
SPB	Simple Pay Back
TASC	Total As Spent Cost
TOC	Total Overnight Cost

Abbreviations and acronyms

TPC	Total Plant Cost
TRNSYS	TRaNsient SYstem Simulation program
TURB	Turbine
UGL	Unglazed solar panel
UNFCCC	United Nations Framework Convention on Climate Change
UNI	Italian National Unification

List of symbols

Symbol	Units	Name
A	m^2	Area
AF	-	Availability Factor
c	$\frac{\text{€}}{MWh}$	Unit exergoeconomic cost
C	$\frac{\text{€}}{s}$	Exergoeconomic cost of a flow
c_p	$\frac{J}{kg \cdot K}$	Specific heat capacity
CD	$\frac{\text{€}}{s}$	Cost rate of irreversibility
D_e	m	Entrance diameter of plate heat exchanger
e	$\frac{W}{mol}$	Specific exergy
\dot{E}	W	Exergy
E_G	$\frac{kWh}{year}$	Total yearly solar irradiance
f	%	Exergoeconomic factor
G	$\frac{kg}{s \cdot m^2}$	Mass flow rate per unit cross-section area
h	$\frac{J}{kg} \cdot \frac{W}{m^2 \cdot K}$	Specific enthalpy, heat transfer coefficient
i	W	Irreversibility, exergy destruction rate
I	€	Investment
k^*	-	Unit exergetic cost
L	m	Plate heat exchanger length
\dot{m}	$\frac{kg}{s}$	Mass flow rate
N_p	-	Number of plates of the heat exchanger

List of symbols

Nu	-	Nusselt number
ϕ	-	Enlargement factor of plate heat exchanger
P	Pa	Pressure
p_{co}	m	Longitudinal step of plate heat exchanger
PES	%	Primary Energy Savings
Pr	-	Prandtl number
\dot{Q}	W	Thermal power
\dot{Q}_s	$\frac{kWh}{year}$	Solar heat yield in one year
R	$\frac{J}{mol \cdot K}$	Universal gas constant
R_f	$\frac{m^2 \cdot K}{W}$	Fouling factor
r_p	-	Turbine pressure ratio
Re	-	Reynolds number
s	$\frac{J}{kg \cdot K}$	Specific entropy
SE	%	System efficiency
SF	%	Solar fraction
T	K	Temperature
t_c	m	Thickness of channels of plate heat exchanger
U	$\frac{W}{m^2 K}$	Global heat transfer coefficient
V	m^3	Volume
w	m	Plate heat exchanger width
W	W	Mechanical power
x	-	Molar fraction

Z	$\frac{\text{€}}{\text{s}}$	Cost rate of component
-----	-----------------------------	------------------------

Greek letters

β	$^{\circ}$	Channel angle of the plate heat exchanger
ε	%	Exergetic efficiency
η	%	Energetic efficiency

Subscripts

as	As received
B	Swimming pool water
BIO	Biomass
c	Cold
CC	Combustion chamber
ch	Chemical
CHP	Combined Heat and Power
COND	Condenser
CV	Control Volume
d	Dry basis
DHW	Domestic Hot Water
EG	Exhausted gases
el	Electrical
EVA	Evaporator
f	Formation
g	Gaseous
h	Hot
iso	Isentropic

List of symbols

kin	Kinetic
l	Liquid
me	Mechanical
p	Product
ph	Physical
pot	Potential
r	Resource
SP	Swimming pool
STO	Storage
th	Thermal

Acknowledgements

First of all, I would like to express my sincere gratitude to my parents, Giovanni Cantone and Maria Marchese, and to my sister, Sharon Cantone, source of inspiration and always by my side ready to support me.

I am grateful to Professor Baranda for the continuous support of my master thesis, for his knowledge, motivation and availability. With his experience, he gave me a remarkable contribution every moment of research and writing of this thesis. I also thank the Professors Leone and Lanzini, for their help and suggestions, which allowed me to improve the elaborate.

My sincere thanks also go to Eduardo Costa, who offered me the opportunity to join the company SCIVEN as an intern and which allowed me to collaborate with very competent people, such as Marcio Santos and João Pereira.

Last but not least, I would like to mention and thank my girlfriend, Giulia Grazioli, and my friends, especially Salvatore Vaianella, Fabrizio Pappalardo, Alberto Giammarini, Paolo Elia Bortignon, Giuseppe Calderoni, Chiara Bosso and Jônatas Manzolli with whom I shared joys, sacrifices and successes. The affection and support they gave me make this goal even more precious.

1. Introduction

From 1960 to 2012, the world population increased from almost three billion to seven billion [1]. This hyperbolic evolution of the population growth rate, which was demonstrated by several mathematical macro models [2], has already begun to decline. Nowadays the population is still increasing and, according to projections [1], the world population will reach about nine billion by 2050.

To satisfy the demand for goods and services, in a world that continues to grow both in terms of population and technology [2], over the last few decades it was necessary to increase the exploitation of energy resources [3]. This uncontrolled exploitation has generated serious concerns regarding both the limited fossil fuel reserves and the climate changes caused by the emission of greenhouse gases related to energy conversion processes. To reduce these environmental problems, different international agreements have been signed, such as the Kyoto protocol [4] and the Paris agreement [5]. If the set objectives are respected, according to the World Energy Outlook 2018 projections [6], it will be necessary to install more efficient energy systems and increase the share of renewables within the global primary energy, from 14% in 2017 to 20% in 2040. These renewable resources constitute a valid solution to the problems listed above as they have a higher energy production rate compared to the exploitation rate and at the same time are characterized by low or zero greenhouse gas emissions.

As renewable resources present many advantages, they could entail several benefits if applied to energy-intensive installations. These facilities also include sports centres because, despite they belong to the building sector, they have quite different energy requirements when compared with services and residential buildings [7]. Indoor swimming pools are included in the facilities that require the highest energy operating costs among sports buildings. Therefore, swimming pools can be defined as processing plants rather than just regular buildings as stated in the literature [8], [9]. For indoor swimming pools, the average primary energy consumption per usable area per year is $666.1 \frac{kWh}{m^2 \cdot year}$ and the correlated greenhouse gas emissions are $181.8 \frac{kg CO_2}{m^2 \cdot year}$ [10]. However, these reference values may have small variations related to different parameters such as the sporting activity, the opening hours, the period of year, the geographical location of the building, the usable area, the water surface, the age of the building, the number of visitors and the average water temperature [7]. These data show that swimming pools are included in a sector that requires a considerable amount of energy, which may have considerable emission reduction of GHG when the conversion system is replaced.

The high energy consumption levels of swimming pools are caused by the need to provide appropriate thermal comfort conditions to its occupants, such as a predetermined temperature and relative humidity range, and to counterbalance losses, mainly those due to evaporation and water exchange. Typically, indoor swimming pools use two types of energy sources: thermal for pool water, domestic hot water for showers and space heating,

and electricity to power water pumping systems, lighting systems, rotating equipment, air cooling and dehumidifying processes [7].

A cogeneration plant would therefore be able to satisfy these needs. There are already some cogeneration plants powered by biomass in R&D phase or on the market [11], however only few plants have a nominal power below 15 kW_{el} [12] [13] [14]. For the cogeneration case in question, in which a low temperature thermal source is used and an electric power lower than 15 kW_{el} is required, was noted that the electrical efficiency of the ORC plants (Organic Rankine Cycle) is greater than the one of traditional steam turbine systems [15]. Furthermore, these plants can minimize the losses associated with transporting energy since they produce energy locally and by using organic fluids instead of water, evaporation occurs at lower temperatures and pressures. Biomass is the renewable energy source, which follows the variation of thermal and electric energy requirements by the users of such cogeneration plants without being affected by weather variations. The installation of a biomass cogeneration plant with ORC cycle is also ideal for both thermal and electrical needs of swimming pools since, compared to other sectors, there is the greatest conversion efficiency and the highest return on investment [16].

The use of biomass as an energy resource can be fully considered renewable since the combustion process simply returns to the atmosphere the same amount of CO₂ that was absorbed during the plants' growth. The processes of CO₂ sequestration and re-emission into the atmosphere can take place at different times, depending on the CO₂ capture rate during growth. By controlling the rate of growth and harvest, a zero CO₂ emission rate could be obtained [17]. The control of the CO₂ emission also occurs through fire prevention. Proper forest management locally reduces the stock of carbonaceous energy contained in the forest, making fires less intense and more easily controlled [18]. Therefore, the development of new biomass technologies in the market can transform the waste of such process into a sustainable energy resource. Due to the innumerable advantages linked to the use of biomass as an energy source, several studies on biomass have recently been conducted. One interesting in-depth analysis suggested, in which are contemplated additional information on the topic, as biomass characterization, availability, processing, transport and its market, on the Portuguese scenario, is the annual report developed by Carlos Ferreira in Renature project [19].

Due to the high energy consumption required to power this cogeneration plant, is required the use of tools capable of performing a deep system analysis. Among the energy and economic analyses currently carried out on energy plants, exergo economic analysis reveals as interesting. This tool can allocate the costs of the different streams of the thermal plant and allows to understand if improvements are needed regarding thermodynamic efficiency or the cost of capital.

The significant energy demands of the pools, the related possibilities of reducing operating costs by replacing old plants with renewable sources and the advantages linked to cogeneration, use of biomass and ORC for small plants explain why different thermal,

economic and thermoeconomic analyses have been conducted in these areas of the scientific literature.

Despite the presence in the market of both outdoor and indoor pools, scientific research has focused mainly on indoor because they are the only ones that can ensure a constant service during the year. The considerable thermal losses of outdoor pools indeed are such as not to guarantee an annual service that is economically feasible. In fact, according to the results reported by Dimitris Al. Katsaprakakis, by applying passive systems to outdoor swimming pools, such as the inclusion of the enclosure and a floating insulation cover on the pools' surface whenever they are not used, operating costs can be reduced by approximately 92% [20]. Moreover, according to the literature, the main portion of energy required in indoor swimming pools is related to the thermal one. For example, a study conducted on 855 Italian swimming pool shows that thermal energy consumption is five times higher than the electricity one [21]. These trends are also recorded in the consumption of five Portuguese swimming pools, with a thermal demand in the range of 66% to 77% of the facility's total energy consumption [7], and in the consumption recorded in a Greek pool where the thermal energy, in the course of three different years, ranged from 72% to 77% of total consumption [22]. The huge amount of thermal energy required to heat up the swimming pool water has led Zuccari et al. to carry out an in-depth analysis of the distribution of these heat needs. The results show that about 38% of this heat is related to the heating of water replacements and the remaining 62% is represented by evaporation (60%) and convection (2%) losses, while conduction is negligible [21]. These sources of loss are determined by the operating conditions imposed by national regulations and by sports regulations. For example, the International Swimming Federation mandates that pool water temperature for swimming is between 25 and 28°C [23] and the UNI 10637:2015 imposes pool water temperature 28°C, air temperature 27°C and relative humidity 70% [21]. Replacement water flow is calculated based on consumption for evaporation, minimum daily water replacement provided by UNI10637 and full water replacement (once a year) [21].

Most of the indoor swimming pools currently operating have a gas or oil-based boilers water heating systems, that are a source of significant operational costs and pollutant emissions. For example, according to the survey conducted by Mousia et al., 43% of Greek swimming pools have a water heating system based on oil combustion and 35% on natural gas one [24]. Therefore, in recent years several searches have been conducted to find new, renewable and more efficient energy conversion plant. For these reasons, in the scientific literature, each new heating system plant solution is compared with the old one. Marinopoulos et al. [22] have analyzed the advantages related to the application of renewable technologies in a municipal swimming pool located in Thessaloniki, Greece, initially heated with two gas-boilers of 1100 kW. Three different technologies have been designed for this pool, i.e. solar collectors, photovoltaic and ground heat pumps. Regarding the solar collectors, a closed loop system with flat-plate collectors was chosen, which covers 60% of the area of the pool; about photovoltaics, it was proposed to install 120 units with a total area of 152 m² and a power of 29 kW, with a photovoltaic efficiency of 19% and finally for ground heat pumps, two 600 kW units are considered necessary

1. Introduction

for the case of open pool and two 300 kW units for indoor one. For these cases, the Benefit cost ratio (BCR) and the Payback period were calculated assuming the inflation rate equal to 2.5%, the discount rate equal to 6% and an analysis period of 20 years. In addition, a profit of 70 € per ton of CO₂ was also assumed, following the values reported by the Federal Environment Agency [25]. The comparison between the different technologies, for open and closed swimming pools, is reported in Table 1.1.

Table 1.1 Economic comparison between different renewable technologies used in swimming pools

Technology	Benefit-cost ratio (BCR)	Payback period
Solar panels (open)	3.53	3.8
Solar panels (closed)	7.57	1.8
Photovoltaic panels	1.45	7.6
Heat pump (open)	2.34	5.8
Heat pump (closed)	2.00	6.9

From the comparison of such technologies, the application of thermal solar panels is the most interesting at a financial level to be coupled with gas boilers. Specifically, the solar thermal system applied to indoor pools is the best in terms of reducing operating costs, since has a payback period of only 1.8 years.

The study conducted by Katsaprakakis [20], in addition of showing the advantages associated with the application of passive systems as listed above, highlights the reduction in annual operating costs linked to the replacement of the existing oil heating system with exclusively renewable plants. The analysis was based on the real data of two swimming pools, an Olympic one (50x20 m) and a small one (25x6 m), in the Municipal Sports Center in Arkalochori (Crete). Specifically, the author analyses, starting from the case of an indoor swimming pool, five different cases, namely biomass heater burning olive kernel, biomass heater burning biomass pellets, combi solar-heater system burning olive kernel, combi solar-heater system burning biomass pellets and geothermal heat pump (GHP) co-operating with vertical GHE (GHP and GHE system). The author considers the use of olive kernels as abundant and low cost (80 €/tn) on the island of Crete. The sizing results are as follows: a biomass heater of 230 kW for biomass heater burning technology only, an area of 98 m² for the plant with olive kernel fuel and 262 m² for biomass for the biomass technologies combined with solar technology, using selective coating collectors, and finally 43 boreholes with 42.2 m of depth for borehole and 5 heat pumps with a nominal heating/cooling power of 33.3/44.8 kW.

Table 1.2 Economic comparison between different energy sources used to produce heat in swimming pools

Technology	Total set-up cost (€)	System annual operating cost (€)	Annual operation cost reduction (%)
Oil heater (indoor pools)	-	28332	-
Biomass heater burning olive kernel	49890	4170	85.3
Biomass heater burning biomass pellets	49890	12771	54.9
Combi solar-heater system burning olive kernel	104590	2831	90.0
Combi solar-heater system burning biomass pellets	170190	6204	78.1
GHP e GHE system	243000	4977	82.4

This study shows that replacing the oil installation can result in annual cost reductions of between 55 and 90%. Specifically, it should be noted that the greatest advantages are registered using the most convenient on-site fuel. The geothermal plant has annual cost reductions approximately similar to those of the biomass heater burning olive kernel and the combi solar-heater system burning olive kernel, however it has initial investment costs between five and two times respectively higher. Furthermore, the study shows that the application of a hybrid system leads to additional annual savings of between 5 and 23%. The payback time study, which also includes the installation of passive technologies, shows a period of between 2.59 years and 2.96 years for biomass-based technologies and 3.16 years for geothermal technology.

Calise et al. [26] conducted a case study in a university indoor swimming pool centre, located in Naples, South of Italy, in which thermal demand was met by a hybrid solar thermal and natural gas boiler. This study analyses the possibility of replacing 64 m² of the existing obsolete flat-plate solar thermal collector. The results obtained using different solar technologies, such as unglazed (UGL), flat plate without selective absorber (NSL), flat plate with a selective absorber (SEL), evacuated tube (EVT) and evacuated flat plate (EVP), from the TRNSYS simulation, show that the best energy and economic performance is achieved by evacuated solar thermal collectors. The Simple Pay Back (SPB) period results in about 14 years without incentives and it decreases to 5 years considering the Italian incentive policy.

Therefore, from the scientific researches mentioned above, appears clear that renewable heating technologies are more efficient than fossil ones. Specifically, solar and biomass-based systems are, between renewables, the most advantageous in terms of energy and return on investment.

To guarantee the services offered by the swimming pools, as previously mentioned, both the thermal source and the electric source are necessary, however it is noted that such systems generally only have an autonomous water heating system and buy electricity from the grid. This is mainly related to the greater simplicity of construction of the conversion plant, lower investment costs and a technology, based on renewable sources, not fully diffused for the range required by these users.

Despite the not yet commercial status of the technology for $P_{el} < 50 \text{ kW}_{el}$ [27], however, it is noted that some small-scale cogeneration plants based on biomass and solar radiation have already been designed and installed.

A relevant analysis in the use of the solar thermal hybrid resource, with a parametric study based on the proportions of the resources provided, is that developed by Jradi et al. on a micro-CHP system, based on the circulation of the environmentally friendly HFE 7100 working fluid, capable of generating 500 W as a peak of electric current [28]. The results of this study, conducted on a total heat input of 24.23 kW, show that this plant can have a thermal efficiency between 61.23% and 75.96% and an electrical efficiency between 8.49% and 10.83%, if only the solar energy or biomass is used. From the comparison of the efficiency ranges, appears immediately evident that the parameters with greater value, those related to the use of biomass only, are linked to the certainty of the evaporator water inlet temperature (120 °C), while the lower ones are linked to the uncertainty of the solar resource, not able to supply the hot resource in the same conditions. Similar results were obtained from a hybrid solar-biomass ORC plant, with a nominal electric nominal power greater than 60 kW. Even though this survey it has been shown that, in the case of passing from a simple solar system to a hybrid solution with PCM storage, it is possible to increase the electrical efficiency from 3.4 to 9.6% [29].

Even though cogeneration plants with small-capacity organic fluid, around 10 kW_{el}, are not a widely distributed technology, it is noted from the aforementioned works that it is preferred to use mainly solar concentrators to increase the temperature of the motor fluid vapour and, consequently, the electrical efficiency.

Finally, to understand the potential of biomass savings for a hybrid cogeneration ORC plant, the study, carried out on a plant installed in southern Italy, is mentioned. It has demonstrated that the hybrid biomass-solar solution guarantees biomass savings higher than 21% compared to the simple biomass-fired CHP units [27].

Summarizing, in the literature review, was noted the lack of studies of small-scale organic hybrid cogeneration plants in which solar thermal technologies, different from the concentration one, such as vacuum panels, are considered. The main cause is that these installations, have a single thermal product, besides having as objective the maximization of the hours in which the plant is powered exclusively by solar energy, which generally required a high temperature source. It is therefore considered necessary to fill this gap by trying to propose an innovative solution coming from the combination of two technologies that are already fully widespread, namely solar thermal for preheating the domestic hot water and a cogeneration plant, fed by pellets, capable of produce a

thermal source suitable both for heating the water in the pools and the water in the showers.

The novelty of the plant, that will be presented in the following chapters, is the investigation of a cogeneration hybrid system, with vacuum solar panels, able to preheat, in relation of the climatic conditions, both the circuit with organic fluid and that of the domestic hot water. By implementing the control strategy that dissipates the solar thermal energy in both fluids, which have different temperatures, the exploitation of the energy absorbed by the panels is maximized and the thermal losses of the panel are reduced due to the complete removal of the heat. From the combination of the two circuits it will be noted that the hot solar fluid will not be exclusively linked to the temperature reached by the storage. Therefore, it will be possible to reduce the hours of stagnation by being able to transfer the heat accumulated to the ORC fluid, temperature of which remains low, i.e. the temperature reached at the pump outlet (T_1).

Having established the state of the art of the technologies considered, it finally considered necessary to focus attention also on exergetic and exergoeconomic studies carried out in the past on small biomass-based Organic Rankine Cycle, since they will be the subject of discussion in the studied plant.

For instance, Açıkkalp et al. [30] carried out detailed exergy and exergoeconomic evaluation of a micro CHP system based on a biomass boiler and a steam engine. It was found that the highest exergy destruction rate, corresponding to more than 90% of the whole system, was placed in the boiler while the lowest was in the heat exchanger. To obtain improvements in terms of exergy efficiency as well as the economics of the entire system, in accordance with the results obtained, the author suggests increasing the efficiency of the boiler. Creyx et al. [31], performing a detailed exergetic analysis of a biomass-fuelled micro-CHP system with an Ericsson engine, reported that the highest exergy destruction was linked to solid biomass combustion. The results also showed that the exergy destruction in the heat exchanger supplying was correlated to the thermal power exchanged. Nur and Sunoto [32] performed an exergy analysis on a small biomass-fed Organic Rankine Cycle (ORC) electrical power plant. The plant, since it has turbine outlet conditions of about 90 °C, was considered both in the case with and without regenerator. From the comparison it emerged that, for such thermal levels and for the only production of electricity, the plant with the regenerator showed the lowest value of the total exergy destruction. It was found that the largest exergy destruction occurs during processes, for both configurations, are at combustion part, followed by evaporator, condenser, expander, and pump. He concluded through a parametric analysis that as the ambient temperature increased, the exergy destruction in the combustion chamber and condenser decreased, reducing the total exergy destruction of the system during the process. Pereira et al. [33], in addition to providing a detailed list of the main ORC manufacturers, with their fields of application and power range, investigated, for Micro ORC cogeneration biomass system, the correlation between the thermal power supplied to ORC and the output thermal and net electrical power. From the results of the research, it emerged that for the domestic-scale CHP system 37 kW_{th} are required to obtain 30

kWth and 4 kW of net electrical power. Finally, in the range of thermal power input between 20 and 300 kW, from the published results of the plant an electric efficiency between 8 and 10% [34]. Algieri and Morrone [35] have conducted a techno-economic analysis of a cogeneration biomass-fired ORC system for single-family. The results of the parametric analysis of the evaporation temperature of the ORC fluid, in the range between 200 and 337 °C, show an increase in both electrical and cogeneration efficiency. For the thermodynamic conditions analyzed it was also found that by applying an internal heat exchanger to the traditional cycle it was possible to have an improvement in electrical efficiency of between 2 and 5% while an improvement in the efficiency of the entire system in the range between 5 and 10%. From the economic analysis, it emerged instead that the payback period is about 8 years when the specific ORC is fixed to $10,000 \frac{\text{€}}{\text{kW}_{el}}$ and is reduced to about 4 years if the specific cost is $5000 \frac{\text{€}}{\text{kW}_{el}}$. From the recent research conducted by Tocci et al. [36] has emerged that the scarce diffusion of ORC technology in the small-scale power range is caused by the lack of data diffused in the scientific literature.

As reported in the above cases, different analyses were carried out on small-scale biomass and ORC plants. A thorough thermal and economic analysis on an ORC pellet-fuelled cogeneration plant to meet the requirements of an indoor swimming pool is still pending in the literature. In the ORC implants treated in the scientific articles, it is also noted that the various analyses are carried out exclusively in the design conditions without focusing the off-design one. It is deemed necessary to carry out a more detailed off-design analysis in case of systems that are subject to significant variations in requests from users, as in the case study treated in the following thesis. For these reasons, the aim of this thesis is the study of an ORC cogeneration plant, both in design and off-design conditions, capable of satisfying energy carriers required by indoor swimming pools, i.e. the electric current and the hot water at medium and low temperature, an exergoeconomic analysis and finally the investigation of the biomass savings related to a novel hybrid biomass and solar thermal plant.

After this first chapter dedicated to the introduction, the motivation and the presentation of the current state of art, the following thesis is divided into four main parts. In the first part are presented the main characteristics of the systems that will be simulated, in the second one is described the mathematical models of the different case studies, created for the extrapolation of data necessary to the analysis, and finally there are two chapters devoted respectively to the presentation of the results obtained and to the conclusions.

2. Case studies

This chapter aims to illustrate in-depth the plant solutions necessary to fulfil the thermal demands of a swimming pool sports centre. As mentioned in the introduction, for this specific service, the main heat flow requirements are related to the pool and shower water warming process.

Initially, the amount of thermal energy related to the pool water heating will be fully provided by a cogeneration plant, powered by pellets, while subsequently this solution will be expanded with a solar plant, able to pre-heat the cogeneration working fluid and simultaneously warming up the domestic hot water for showers.

The hybrid solution, designed in this thesis for the case under analysis, is shown in Figure 2.1.

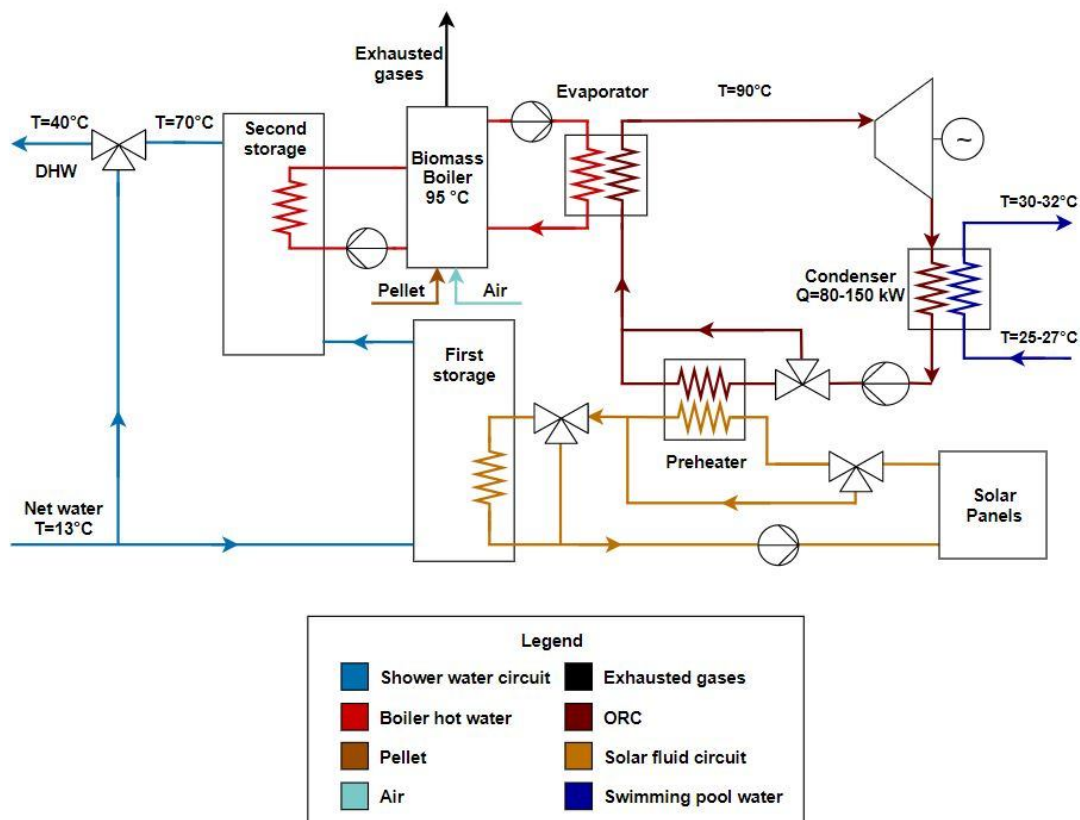


Figure 2.1 Scheme of the hybrid, biomass-solar, low temperature ORC cogeneration plant

In the following sections, the principal characteristics of both cases will be listed, such as the technical data of the components used, the thermochemical properties of the fuel adopted and the control systems.

2.1 Biomass system layout

The biomass plant examined consists of a CHP system, powered by the energy realized by the pellet combustion, that follows the thermal request of the users, as shown in Figure 2.2.

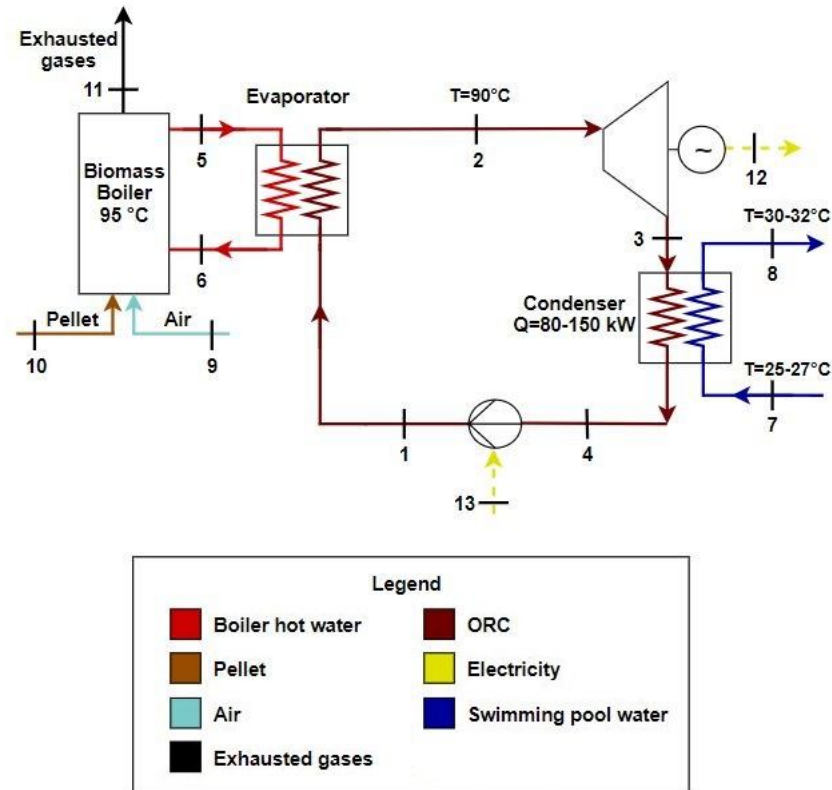


Figure 2.2 Scheme of the ORC cogeneration plant fuelled by biomass

To simplify the explanation of the physical and mathematical biomass cogeneration model, the following thesis will use thermodynamic benchmarks according to the numbering adopted in Figure 2.2. The simplified version of the system consists of the following main components: a vertical firetube biomass boiler, an evaporator, a turbine, a condenser and a recirculation pump.

The biomass cogeneration plant consists of 3 different loops that are respectively:

- the closed circuit of hot water at high temperature, from 5 to 6, in which flows the mass flow rate $\dot{m}_{H_2O_B}$;
- the closed circuit of ORC fluid, from 1 to 4, in which flows the mass flow rate \dot{m}_{ORC} ;
- the open circuit of hot water at low temperature, from 7 to 8, in which flows the mass flow rate $\dot{m}_{H_2O_{SP}}$.

The core of the cogeneration plant is the working fluid loop. The organic fluid flows in the liquid and vapour phases through the internal closed-circuit following the well-

known Rankine cycle. Firstly, from 1 to 2, the liquid fluid is heated and vaporizes in the evaporator, then from 2 to 3, the vapour fluid expands and cools while flowing through the turbine. The mechanical movement produced is converted in electricity since the rotor shaft of the turbine is coupled with the shaft of the electrical generator. Afterwards, from 3 to 4, the vapour fluid cools down and condenses back to the liquid phase in the condenser heat exchanger and finally from 1 to 4, the pump forces the flow of the liquid fluid around the internal circuit and pressurizes the liquid fluid back to its initial thermodynamic state.

In addition to the organic fluid loop, there are also two circuits of hot water at low and high temperature in the liquid state. The ORC vaporization heat is released by hot water, from 5 to 6, while the condensation one heats the swimming pool water from 7 to 8. The water of the thermal source in point 6 is restored to the previous thermal conditions through the heat released by the combustion of the pellet in a vertical firetube biomass boiler.

Each component, that constitutes the cogeneration plant previously described, has been sized in such a way as to fully follow the users' requests, independently of any hybrid solutions such as the solar one shown below. The goal is indeed to create an independent system capable of providing the service regardless of atmospheric conditions. For each component installed are also reported the model names and the peculiar information necessary to simulate the operating conditions of the cogeneration plant, as follows:

- **Evaporator:**

The heat exchanger installed is the liquid evaporator SWEP B200THx110/1P-NC-M (2 1/2"+2 1/2"+2x2 1/2").

Those are the main parameter provided by the manufacturer necessary to the model the plant:

Enlargement factor	o	1.17	[-]
Channel angle of the plate	β	27.5	[°]
Longitudinal step	p_{co}	0.0046	[m]
Thickness of channels	t_c	0.00244	[m]
Entrance diameter	D_e	0.060	[m]
Plate length	L	0.450	[m]
Plate width	w	0.243	[m]
Plate area	A_p	0.1300	[m ²]
Number of plates	N_p	107	[-]

- **Turbine**

The turbine installed in the plant is the DEPRAG Turbine Generator GET11 kW.

The values under nominal conditions provided by the turbine manufacturer are the following:

Inlet pressure	P_{2n}	892.7842	[kPa]
Mass flow rate	\dot{m}_{ORCn}	0.667	[kg/s]
Inlet temperature	T_{2n}	90	[°C]
Pressure ratio	r_{pn}	3.71	[-]
Thermodynamic efficiency	$\eta_{isoturbn}$	0.8	[-]
Mechanical efficiency	η_{men}	0.88	[-]

From the data provided by the manufacturer and the experimental analyses on the component carried out by the SCIVEN company, it was also possible to obtain the pressure and thermodynamic efficiency correlations between real condition and nominal one:

$$P_2 = \frac{\dot{m}_{ORC}}{\dot{m}_{ORCn}} \cdot \sqrt{\frac{T_2 + 273.15}{T_{2n} + 273.15}} \cdot P_{2n} \quad (1)$$

$$\eta_{isoturb} = \left(-2.1122 \cdot \left(\frac{r_p}{r_{pn}} \right)^2 + 3.9773 \cdot \left(\frac{r_p}{r_{pn}} \right) - 0.8683 \right) \cdot \eta_{isoturbn} \quad (2)$$

Plotting the equation (2), a parabolic evolution of the efficiency is obtained, the maximum of which is recorded for a pressure equal to 3.5. This value will be fundamental to understand the trend of the electrical efficiency of the system, which will be shown subsequently in Chapter 4.1.

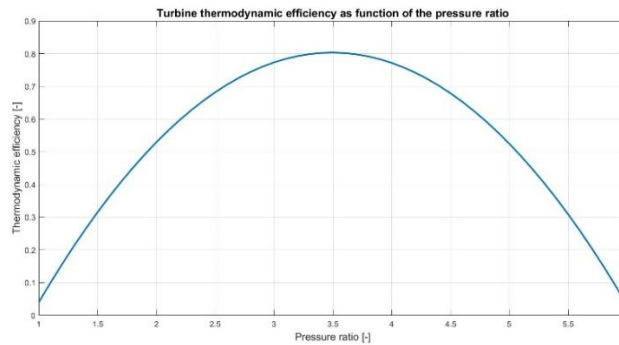


Figure 2.3 Evolution of the isentropic efficiency of the turbine as function of the pressure ratio

- **Condenser:**

The plate heat exchanger installed is the condenser KELVION BPHE GmbH GBS757M-60.

Those are the main parameter provided by the manufacturer necessary to the model the plant:

Enlargement factor	o	1.17	[-]
Channel angle of the plate	β	27.5	[°]
Longitudinal step	p_{co}	0.0046	[m]
Thickness of channels	t_c	0.00225	[m]
Entrance diameter	D_e	0.060	[m]
Plate length	L	0.460	[m]
Plate width	w	0.281	[m]
Plate area	A_p	0.1600	[m ²]
Number of plates	N_p	58	[-]

- **Recirculation pump:**

The recirculation pump used in the plant is the MPO 3R series.

According to the data provided by SCIVEN, the thermodynamic and mechanical efficiencies of the pump are in first approximation constant and equal to:

$$\eta_{iso_{pump}} = 0.98 \quad (3)$$

$$\eta_{me_{pump}} = 0.6 \quad (4)$$

- **Vertical biomass firetube boiler:**

The proposed in this thesis for the plant, chosen to cover the thermal needs required by the evaporator, is the SMART 180 kW, from the company SMART HEATING TECHNOLOGY, to create a simulation close to a real case, it was decided to use as a system input only the operational data certified by the manufacturer [37]. The main operating values from the installed wood pellets boiler, in rated and minimum conditions, are the following:

Table 2.1 Main features of the boiler SMART 180

	Rated	Minimum	
Heat capacity	186.1	48.8	[kW]
Carbon dioxide CO ₂	11.43	7.65	[%]
Exhausted gas temperature	116.1	72.4	[°C]

Finally, the knowledge of the real operational data allowed the creation of a correlation of input data, i.e. the CO₂ exiting the chimney and the temperature of the gases expelled to the chimney, with the thermal power required by the evaporator, obtainable from the cogeneration model.

Once the combustion system is defined, the attention is focused on the fuel used. The characteristics of burnt pellets come instead from the analysis carried

out by LEBS.CBE (Laboratório Especializado em Biocombustíveis Sólidos). The parameters characterizing the biofuel [38] are the following:

Table 2.2 Characteristics of the used pellet

Carbon content _(d)	49,4	% $\left[\frac{m}{m}\right]$
Oxygen content _(d)	43,7	% $\left[\frac{m}{m}\right]$
Hydrogen content _(d)	6,1	% $\left[\frac{m}{m}\right]$
Nitrogen content _(d)	0,1	% $\left[\frac{m}{m}\right]$
Ash content _(d)	0,6	% $\left[\frac{m}{m}\right]$
Moisture content _(ar)	4,8	% $\left[\frac{m}{m}\right]$
Net calorific value _(d)	19,04	$\left[\frac{MJ}{kg}\right]$

As it is possible to notice from the data reported above, the values for sulphur and chlorine content are not considered as they represent a mass percentage less than or equal to 0.01%.

Finally, it should be highlighted that, from the results obtained in the laboratory, a standardized high-quality pellet is burned, ENplus A1[®], in accordance with the requirements foreseen by the guidelines published by the European Pellet Council (EPC) and the European Biomass Association (AEBIOM) [39].

2.2 Hybrid biomass-solar plant layout and control systems

Once the biomass-powered cogeneration system has been defined, it is necessary to focus attention on hybrid layout, suggested by the design improvement results of the exergoeconomic analysis (Chapter 4.2), that reduces biomass consumption through the preheating of the fluid R245fa and the generation of DHW for showers.

The solar system simulations have been carried out with Polysun software, which unfortunately does not allow simulating phase transitions. For this reason, the control systems and the external heat exchangers have been designed in such a way as to preheat the organic fluid until the boiling temperature relative to its pressure.

The hybrid solar system was projected following the plant layout shown in Figure 2.4.

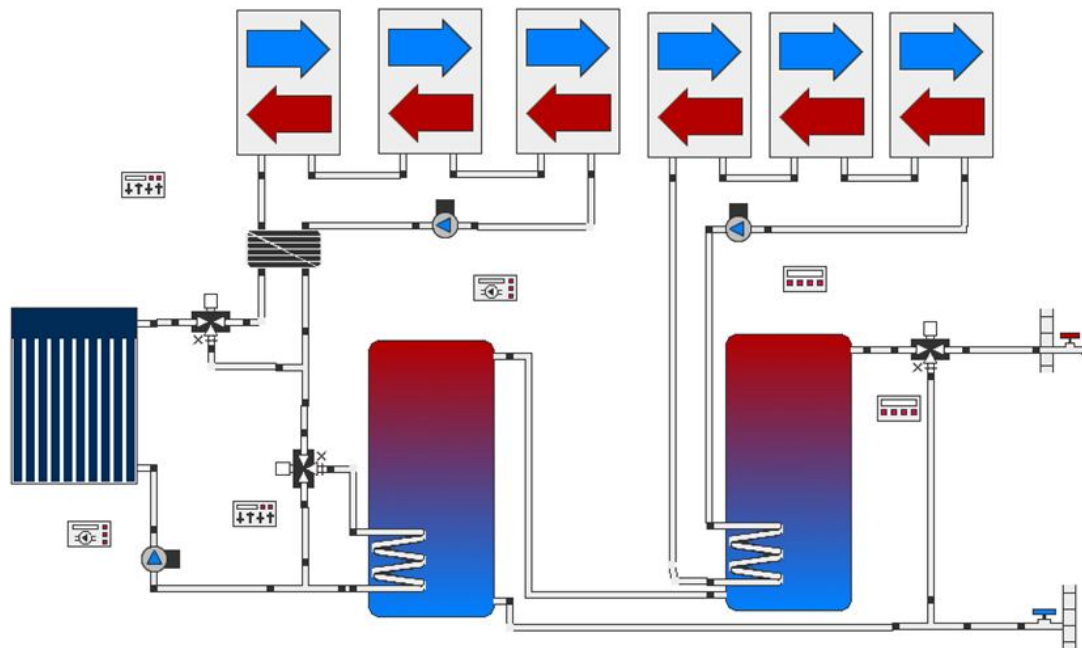


Figure 2.4 Hybrid biomass-solar plant scheme

The hybrid system, located in Coimbra (Portugal), consists of a solar circuit, a mixture of water and glycol, which can preheat both the ORC fluid and the water coming from the network. This fluid is activated if its temperature is 10 °C higher than that of the ORC fluid, while it is deactivated if it is lower than 5 °C. Since the inlet temperature of the ORC (30.7 °C) is greater than that of the network (between 11 and 15 °C), it was decided to exploit the hot source first for organic fluid and then for shower water. An external plate heat exchanger was used to preheat the ORC, while the DHW circuit was preheated and subsequently heated through coils immersed in the storage.

Not having the possibility of insert additional hot and cold sources, a series of fictitious exchangers have been inserted, as shown in the upper part of Figure 2.4. In this way it was possible to reach at each iteration, both for the ORC fluid and for the biomass heated water, the initial conditions.

To reach at most the boiling point of the ORC fluid, a three-way valve has been inserted, which reduces the mass flow rate of the solar fluid, through an energy balance. The ORC circuit pump is activated when the temperature of the solar fluid is above 10 °C, while it is switched off when it is below than 5 °C.

A second three-way valve was inserted into the solar circuit to evaluate the effectiveness of heat exchange with the first storage. If the temperature of the upper layer of the storage coil is 2 °C higher than that of the solar fluid, the fluid regularly enters the storage, otherwise it is bypassed.

2. Case studies

Finally, the hot water coming from the auxiliary circuit is activated when the temperature in the layer above the coil, of the second storage, is lower than 65 °C until 70 °C is reached in the penultimate layer (in the upper part of the second storage).

These controls allow to have different operating conditions of the solar fluid, as shown in the following figures:

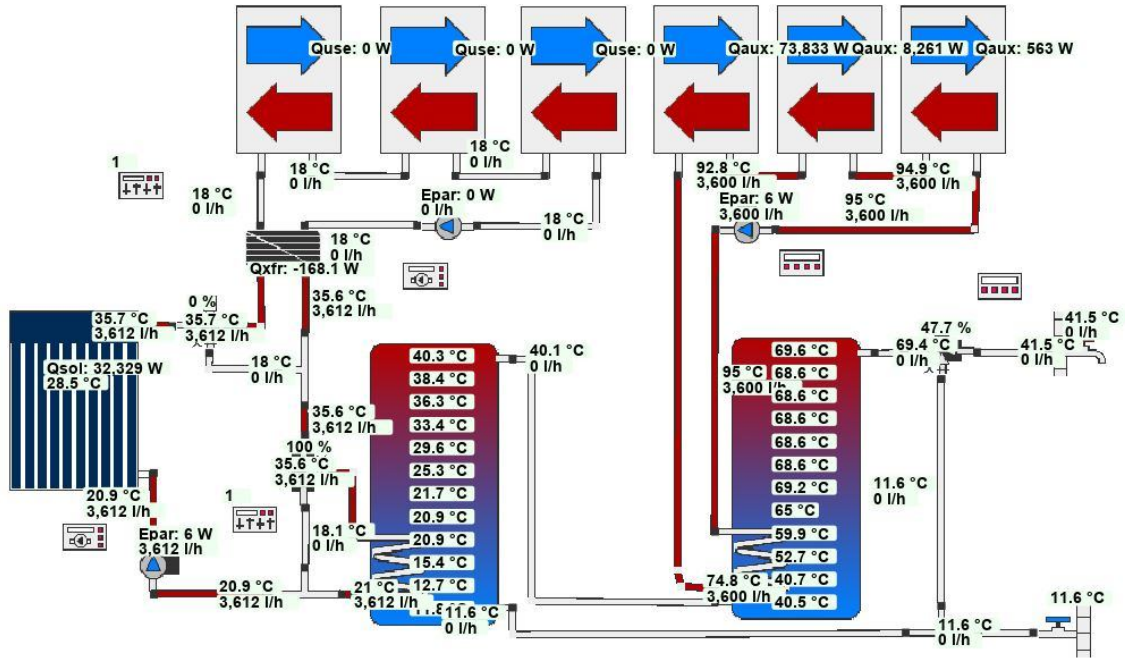


Figure 2.5 Hybrid solution, only water preheating condition

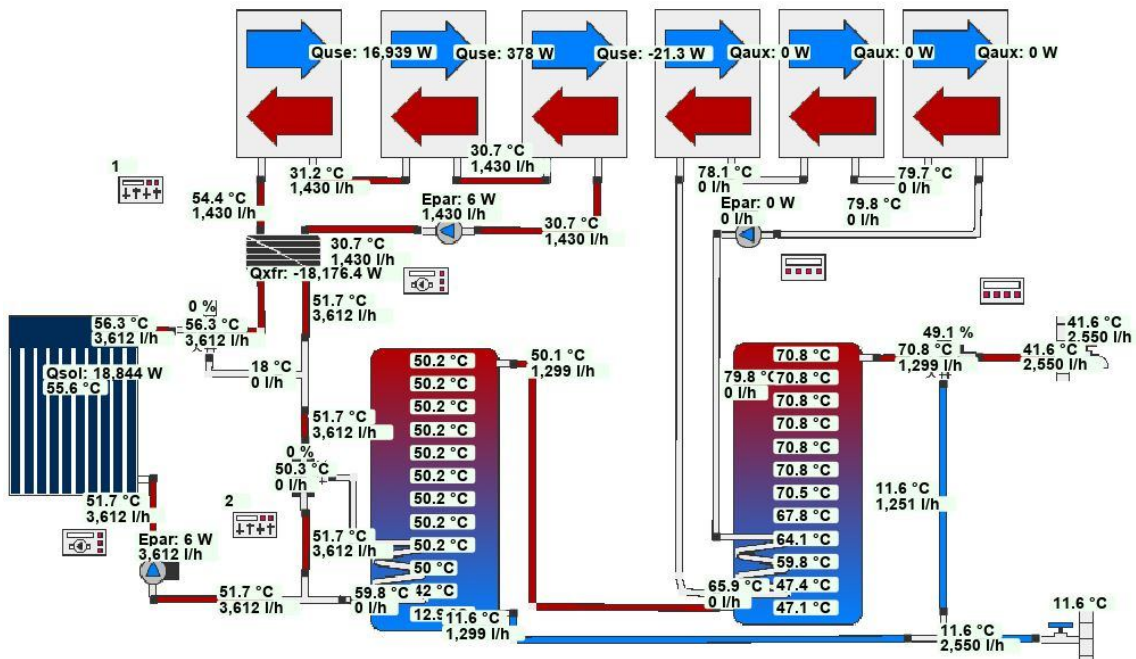


Figure 2.6 Hybrid solution, only ORC preheating condition

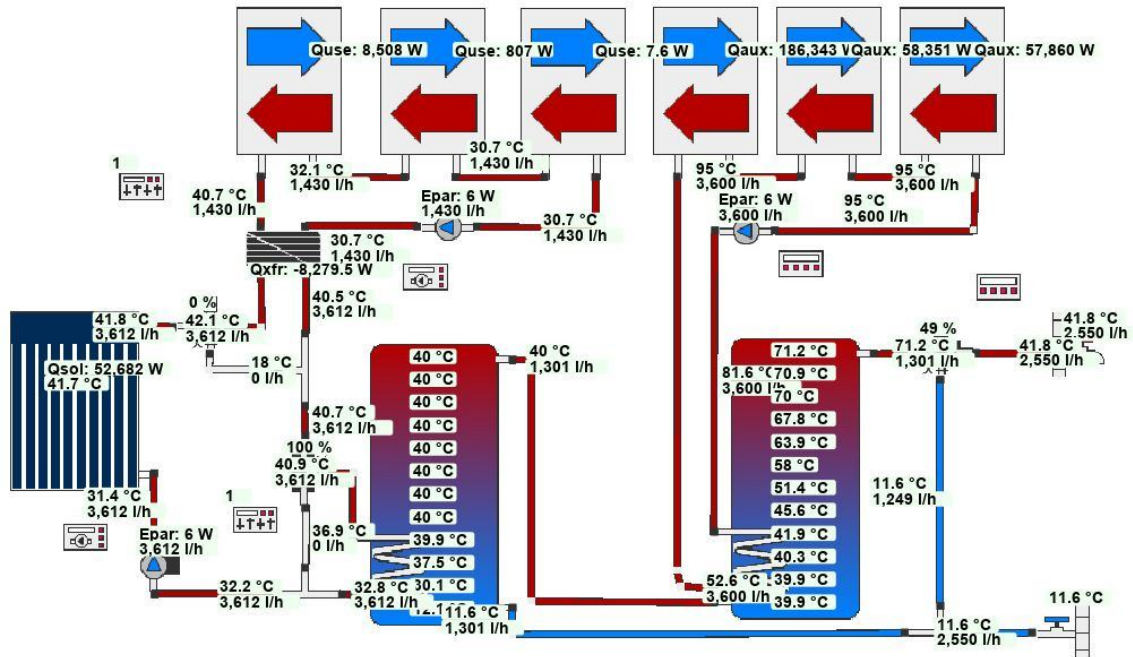


Figure 2.7 Hybrid solution, ORC and water preheating condition

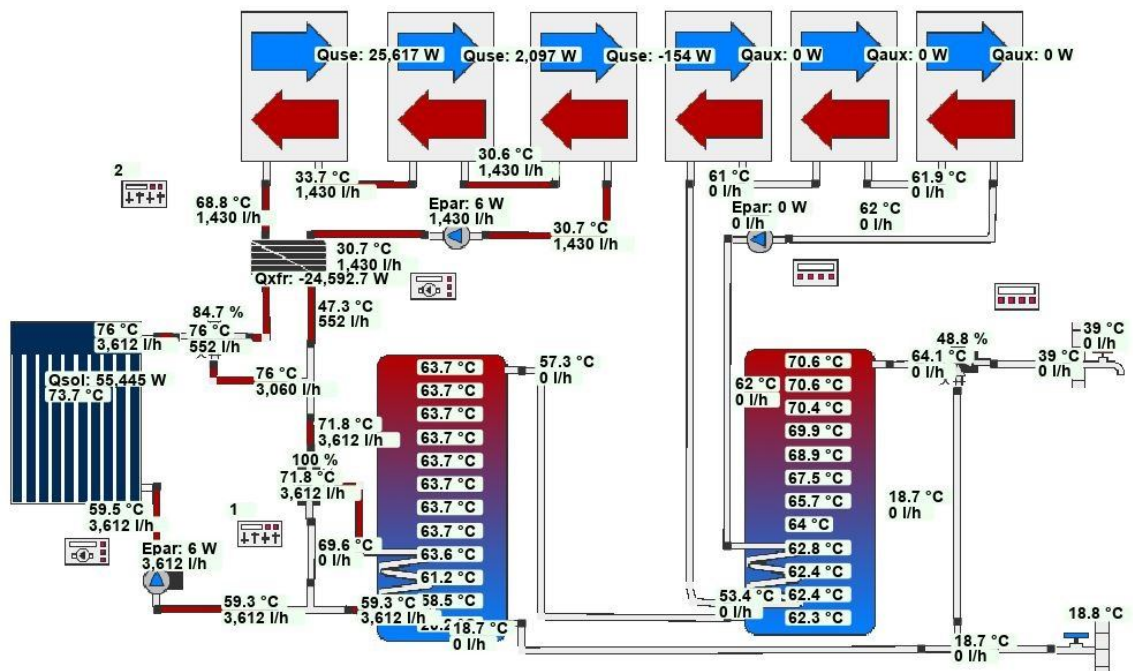


Figure 2.8 Hybrid solution, ORC and water preheating condition, with the use of the three-valve in order to reach at most the boiling point

In the condition shown in Figure 2.5, generally manifested in the morning, is noted that the solar fluid temperature is not sufficient to start the heat exchange with the ORC, however the exchange with the storage is allowed. The opposite case is shown in Figure 2.6 as heat exchange with the ORC is allowed, while the temperature difference, as previously described, is less than 2 °C with storage. In the third condition, shown in Figure 2.7, the solar fluid has such thermal energy to be able to transfer its heat to both

fluids. In the last condition, that generally occurs in summer month (Figure 2.8), the solar fluid has sufficient energy to overcome the point of boiling of the ORC, and therefore part of the fluid is bypassed to respect the software constrains.

Regarding the dimensions, the system was designed to meet the demand for domestic hot water for the showers of a sports centre with swimming pool that have an average of 250 daily users. According to the Portuguese legislation [40], for the swimming pools is expected that the shower water has an average temperature of 40 °C and an average mass flow rate of 40 litres/users, data that are in accordance with those provided by other books dealing with the same subject [41] [42].

Starting from this data, to have a storage with a volume of water equal to that required daily, has been estimated a storage volume of 10 m³, equal to the product between the daily request, referred to one average user, for the mean number of users attending the structure. Finally, to avoid the health consequences related to the legionella bacteria, following the directive of the United States Environmental Protection Agency document [43], it was decided to set the maximum temperature of the water pre-heated from solar to 70 °C.

Despite being a renewable source, the solar energy has, however, the disadvantage of not being constant neither daily nor annually. The amount of missing energy, necessary to heat the water to 70 °C, will be supplied through the hot water (95 °C) of an auxiliary heater, which corresponds to the biomass boiler described in the previous section.

Once the total storage volume and the range of temperatures were defined, to improve the efficiency of the system it was decided to split the storage into two separate units. This configuration, already widespread in the market, called the “twin-store system”, consists of the use of two different storage units: one is exclusively dedicated to solar pre-heating (first storage), while the other heat the water with the auxiliary system only when is necessary (second storage). In this way is possible to maximize the solar resource and to have better exploitation of thermal stratification. To guarantee the service to 50 users, that is the requests assumed during the peak period, it was decided to install for preheating a storage of 2 m³. Consequently, the first storage has a volume of 8 m³, which, as will be seen later in the parametric optimization phase, presents a thermal inertia that maximizes the exploitation of solar energy.

3. Methodology

3.1 Biomass plant model

3.1.1 ORC cycle model

The ORC plant simulation was developed using MATLAB and REFPROP thermodynamic database [44], by creating specific sub-models for all the main components.

To illustrate the mathematical and physical model, in addition to the fixed design parameters, the nominal condition and the relation with the operational condition of each component, described in the subchapter 2.1, it will be necessary to focus the attention on the assumption, the inputs entered, the initial guess and the outputs desired.

It should be noted that the numbering follows that adopted in Figure 2.2.

- **Assumptions**

- a) There are no pressure drops on both sides of the heat exchangers, i.e. $P_1 = P_2$, $P_3 = P_4$, $P_5 = P_6$ and $P_7 = P_8$.
- b) The heat exchangers are performing their first use and therefore the fouling factors (R_{f_h} and R_{f_c}) $\left[\frac{m^2 \cdot K}{W}\right]$ of the bathed surfaces by each fluid can be considered null as a first approximation ($R_{f_h} = R_{f_c} = 0$).

- **Fixed operation inputs**

- a) The temperature of the water entering the evaporator (T_5) is set fix and equal to 95 [°C].
- b) The temperature of the ORC working fluid exiting the evaporator (T_2) is set fix and equal to 90 [°C].
- c) The pressure of hot water at high and low temperature is set fix and equal to 300 [kPa]. From the assumption that there are no pressure drops in the heat exchangers, it follows that: $P_5 = P_6 = P_7 = P_8 = 300 [kPa]$.
- d) The minimum temperature difference in both evaporator and condenser is equal to 5 [°C].
- e) The pressure at point 4 is such that the corresponding saturation temperature is 5 [°C] above the value of T_4 .

- **Variable operation inputs (customer demand conditions)**

- a) The water temperature exiting the pool (T_7) is in the range between 25-27 [°C].

- b) The water temperature entering the pool (T_8) is in the range between 30-32 [°C].
- c) The thermal power requested by the user in the condenser ($|\dot{Q}_{cond}|$) is the range between 80-150 [kW_{th}].

- **Initial guess**

- a) The mass flow rate of the organic fluid (\dot{m}_{ORC}).
- b) The pressure exiting the turbine (P_3).
- c) The ORC temperature exiting the condenser (T_4).
- d) The water temperature exiting the evaporator (T_6).
- e) The area of the evaporator in which occurs the phase change (A_2).

- **Outputs:**

- a) The mass flow rates.
- b) The thermal power exchanged in the heat exchangers.
- c) The net work produced in the turbine and absorbed in the pump.
- d) The temperatures, the pressures and the state functions, such as enthalpies and entropies.

These outputs, both in the design and off-design conditions in all relevant points, are necessary to understand the trend of the cogeneration plant in different operating conditions.

To perform the first simulation, as initial values were chosen the ones close to a generic operational condition of the plant, i.e. $\dot{m}_{ORC} = \left(\frac{\dot{Q}_{cond}}{\dot{Q}_{cond_n}}\right) \cdot \dot{m}_{ORC_n}$ and $P_3 = 250 \text{ kPa}$ and subsequently, iteratively they will be modified to find the values as close as possible to the real ones. Indeed, to avoid problems related to cavitation, it is necessary to have the organic fluid subcooled at the condenser outlet. For this reason, several simulations have been performed to reach a temperature at point 4 five degrees lower than the saturation temperature for P_4 .

For each component, following the MATLAB model, will be highlighted the steps necessary to extrapolate the fundamental thermodynamic properties of each benchmark.

Before explaining the mathematical model in detail, a block diagram of the ORC cycle model is presented, created with the intention of facilitating the reader to understand the iterative cycles adopted.

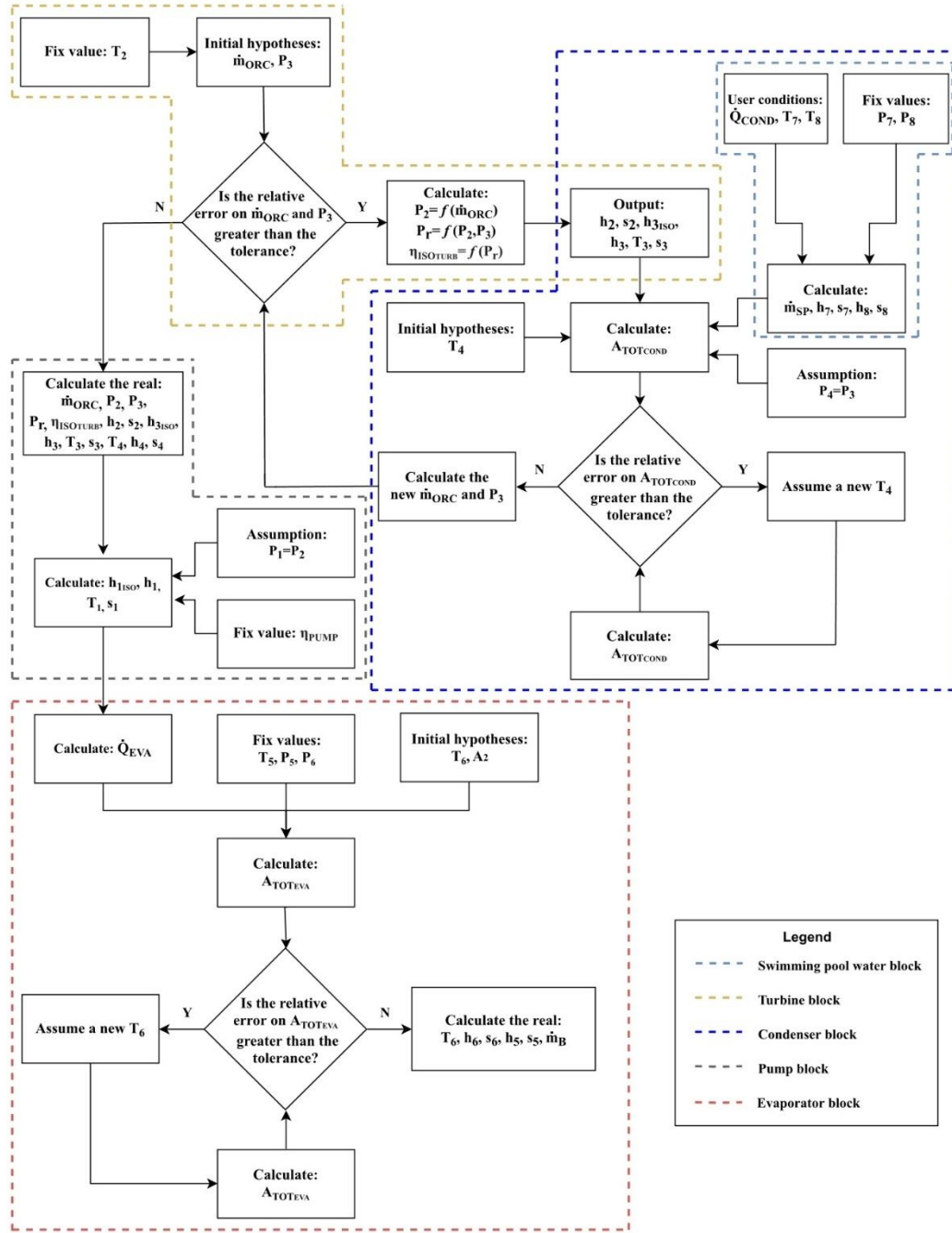


Figure 3.1 Block diagram of the ORC cycle model

❖ Swimming pool flow rate ($\dot{m}_{H_2O_{SP}}$)

The flow rate of the swimming pool is a fixed number, only function of the three variable operation inputs ($T_7, T_8, |\dot{Q}_{cond}|$). From temperatures T_7 and T_8 , provided and requested by the users respectively, note P_7 and P_8 , as they are fixed operation inputs and equal for assumption, it can be achieved the values of h_7 and h_8 .

At this point, using the equation (5), are known all the information necessary to evaluate the value of $\dot{m}_{H_2O_{SP}}$.

$$|\dot{Q}_{cond}| = \dot{m}_{H_2O_{SP}} \cdot (h_8 - h_7) \quad (5)$$

❖ The starting point of the ORC loop (Point 2)

In the motor fluid cycle, the only point where the temperature is fixed in every operating condition, due to the fixed operation inputs, is point 2 and, for this reason, it is considered as the first point of the simulation. Known the nominal parameters, the fixed temperature T_2 and the flow rate, which in the first simulation provided by the hypothesized value, using the equation (1), it is possible to obtain the pressure P_2 . Note the pressure and the temperature it is possible to obtain the enthalpy (h_2) and the entropy (s_2).

❖ Turbine submodel

Taking advantage of the hypothesis of the mass flow rate of the organic fluid (\dot{m}_{ORC}) it was possible to obtain P_2 . At this point, since P_3 has been assumed, the pressure ratio of the turbine can be calculated as $r_p = \frac{P_2}{P_3}$. Therefore, having been calculated all the unknowns of equation (2), it can be calculated the turbine's isentropic efficiency.

In general, the isentropic efficiency of a turbine is expressed as:

$$\eta_{iso_{turb}} = \frac{h_2 - h_3}{h_2 - h_{3_{iso}}} \quad (6)$$

Since the P_3 and the s_2 are already known, the $h_{3_{iso_{turb}}}$ can be derived and therefore, from the formula (6), it is possible to extrapolate the unknown h_3 . As already happened previously, note two thermodynamic properties, P_3 and h_3 , it is possible to easily calculate T_3 and s_3 .

❖ Heat exchangers submodel

In this paragraph is explained the mathematical and physical procedure of both heat exchangers, evaporator and the condenser, since the structure followed is the same.

Due to the absence of information provided by the heat exchanger manufacturer in off-design conditions, it was necessary to extrapolate these values through an iterative process.

Starting from the heat exchanger fluid ends, it was not possible to obtain the global thermal transmittance exploiting the simplified model of the logarithmic mean temperature $\left(U = \frac{\dot{Q}}{A \cdot \Delta T_{ml}}\right)$ due to the phase transition process. The heat exchange process is linked to the properties of the fluid, which vary greatly from one phase to another [45].

To cope with the large variations of the global heat transfer coefficient, note the pressures of ORC fluid, it is possible to obtain the temperature in which the phase transition occurs and to split each heat exchanger in three sub heat exchangers, connected in series, each characterized by a single condition of the fluid subjected to the phase transition, i.e. liquid, boiling and steam, as shown in Figure 3.2. This approach presented for heat exchangers, based on the identification of these different zones, area of which is a priori unknown, is called in literature the moving boundary method [46].

The three sub heat exchangers are connected in series by the fact that the temperatures exiting from an exchanger correspond to the temperatures entering the next. From this, it can be deduced that for each heat exchanger there are 3 different physical zones (I, II, III), which for simplicity will be mentioned with the subscript i. Moreover, from this subdivision can be defined, for each fluid, the 4 remarkable points that demarcate the ends of different zones, indicated with subscript j.

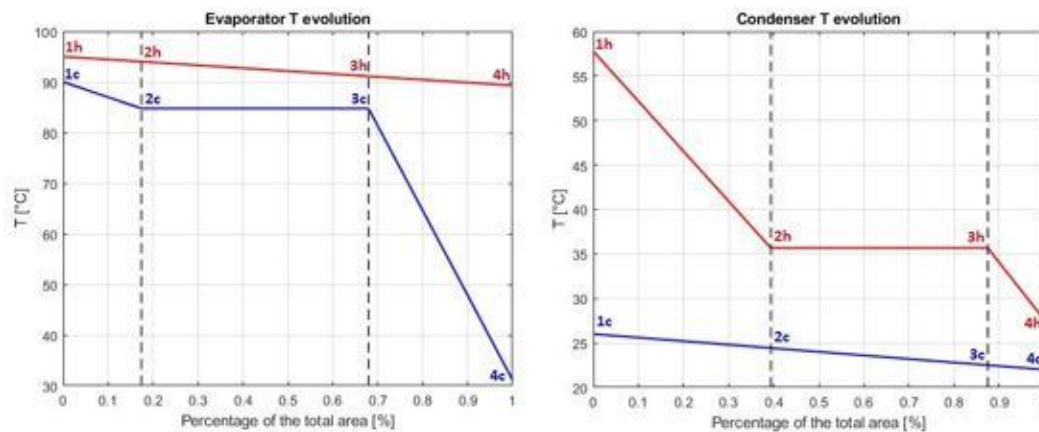


Figure 3.2 Moving boundaries principle in heat exchangers: evaporator (left), condenser (right)

To recapitulate are known:

- T_2 and T_5 because they are fixed operation inputs;
- T_7 and T_8 as they are variable operation inputs;
- T_1 and T_3 from energy balances to the pump and the turbine, as shown in the respective sections;
- T_4 and T_6 through the hypothesized value.

Since are known the four temperatures at the extremes of the three sub-heat exchangers, on the side where the phase transition occurs, and the two temperatures at the extreme of the heat exchanger, on the opposite side, it is possible to calculate the temperatures of the single-phase fluid in the ends of the intermediate zone through an energy balance. In fact, by equalizing the modules of the thermal power exchanged in both parts of each zone ($|\dot{Q}_{h_i}| = |\dot{Q}_{c_i}|$) it is possible to obtain:

$$\dot{m}_h \cdot |h_{h_i} - h_{h_{i+1}}| = \dot{m}_c \cdot |h_{c_i} - h_{c_{i+1}}| \quad (7)$$

Equation (7) has only one unknown if it would be applied where 3 extreme temperatures and the respective enthalpies are already known. Applying (7) first in the zone I or III and subsequently, in zone II, it is possible to calculate the missing enthalpies and therefore the respective temperatures from the inverse formula, since the pressure is known.

Once all the temperatures at the end of each zone are calculated, the mean logarithmic temperature is obtained applying stepwise, in three zones of the heat exchanger, the following formula:

$$\Delta T_{ml_i} = \frac{\Delta T_{1_i} - \Delta T_{2_i}}{\ln\left(\frac{\Delta T_{1_i}}{\Delta T_{2_i}}\right)} \quad (8)$$

At this point, since the ends temperatures of each sub-heat exchanger are entirely known and the properties for both sides of the generic sub-heat exchanger are approximately constant, it is possible to estimate the value of the global heat transfer coefficient (U_i) in zone i, neglecting the conductive thermal resistance of the plates, through the formula:

$$U_i = \frac{1}{\frac{1}{h_{h_i}} + R_{f_h} + R_{f_c} + \frac{1}{h_{c_i}}} \quad (9)$$

Following the moving boundary approach, adopted by Ziviani et al. [47] and widely described in the recent ORC article published by Dickes et al. [48], several convective coefficients can be determined by applying a set of correlation for each phase of the fluid and then compared with the experimental one. For every side of each zone, the suitable convective coefficients are the ones which provide as output the simulated temperature, at the extremes of the heat exchanger, closer to the experimental ones.

In this thesis, to compute the convection coefficients at the hot (h_{h_i}) and cold (h_{c_i}) surfaces of the heat exchangers in the various zones, since the heat exchangers

analyzed are compact plate type and the fluid adopted is the pentafluoro propane, it was decided to follow the semi-empirical approach investigated by Santos et al. [49].

For each heat exchanger were computed different convection coefficients, through the empirical correlations of Muley and Manglik [50], Thonon [51], Maslov and Kovalenko [52], Kumar [53] and Wanniarachchi et al. [54] for homogeneous fluids, and of Yan et al. [55] and Han et al. [56] for fluids subjected to phase change.

From these empirical models, different convection coefficients were obtained. From their combination, for each side and zone of the heat exchanger in different operating conditions, it was possible to calculate various global heat transfer coefficients and compare them with those obtained in experimental tests.

In the specific plate compacted heat exchangers, it emerged that the best correlation is provided by Maslov and Kovalenko [52] and Thonon [51] for homogeneous fluids and Han et al. [56] for fluids subjected to phase change. The details on the implementation in each zone of these correlations will take place in the section dedicated to the evaporator and condenser sub-models. In this section are briefly introduced the correlations of empirical models that best approximate real conditions.

As an assumption, if is not specified differently, the properties of each fluid are computed at the mean fluid temperature in the zone.

$$\left\{ \begin{array}{l} \mu = \frac{\mu_j + \mu_{j+1}}{2} \\ c_p = \frac{c_{p_j} + c_{p_{j+1}}}{2} \\ k = \frac{k_j + k_{j+1}}{2} \\ Pr = \frac{Pr_j + Pr_{j+1}}{2} \end{array} \right. \quad (10)$$

The formulas that often occur in all models are related to the calculation of the Prandtl number (Pr), the mass flow rate per unit cross-section area (G), the Reynolds number (Re) and the Nusselt number of convection (Nu).

$$\left\{ \begin{array}{l} Pr = \frac{c_p \cdot \mu}{k} \\ G = \frac{\dot{m}}{N_p \cdot t_c \cdot W} \\ Re = \frac{G \cdot D_h}{\mu} \\ Nu = \frac{D_h \cdot h}{k} \end{array} \right. \quad (11)$$

After introducing the features common to the models, now are treated in detail the formulas and parameters that are specific to each model.

Maslov and Kovalenko [52] correlation:

$$\left\{ \begin{array}{l} C_1 = 0.78 \\ C_2 = 0.5 \\ Re' = Re \\ Nu = C_1 \cdot Re'^{C_2} \cdot Pr^{\frac{1}{3}} \end{array} \right. \quad (12)$$

Thonon [51] correlation:

$$\left\{ \begin{array}{l} C_1 = 0.2946 \\ C_2 = 0.7 \\ Re' = Re \\ Nu = C_1 \cdot Re'^{C_2} \cdot Pr^{\frac{1}{3}} \end{array} \right. \quad (13)$$

Han et al. [56] correlation for condensation:

In this model the μ and k used are related only in the liquid phase.

$$\left\{ \begin{array}{l} C_1 = 11.22 \cdot \left(\frac{p_{co}}{D_h}\right)^{-2.83} \cdot \left(\frac{\pi}{2}\right) \cdot \left(\frac{\beta \cdot \pi}{180}\right)^{-4.5} \\ C_2 = 0.35 \cdot \left(\frac{p_{co}}{D_h}\right)^{0.23} \cdot \left(\frac{\pi}{2}\right) \cdot \left(\frac{\beta \cdot \pi}{180}\right)^{1.48} \\ G' = G \cdot \left(1 + x_m \cdot \left(\frac{\rho_l}{\rho_v^{0.5}} - 1\right)\right) \\ Re' = \frac{G' \cdot D_h}{\mu_l} \\ Nu = C_1 \cdot Re'^{C_2} \cdot Pr^{\frac{1}{3}} \end{array} \right. \quad (14)$$

Han et al. [56] correlation for evaporation:

In this model the μ and k used are related only in the liquid phase.

$$\left\{ \begin{array}{l} C_1 = 2.81 \cdot \left(\frac{p_{co}}{D_h}\right)^{-0.041} \cdot \left(\left(\frac{\pi}{2}\right) \cdot \left(\frac{\beta \cdot \pi}{180}\right)\right)^{-2.83} \\ C_2 = 0.746 \cdot \left(\frac{p_{co}}{D_h}\right)^{-0.082} \cdot \left(\left(\frac{\pi}{2}\right) \cdot \left(\frac{\beta \cdot \pi}{180}\right)\right)^{0.61} \\ G' = G \cdot \left(1 + x_m \cdot \left(\frac{\rho_l}{\rho_v^{0.5}} - 1\right)\right) \\ Re' = \frac{G' \cdot D_h}{\mu_l} \\ Bo = \frac{\dot{m}}{G' \cdot A_i} \\ Nu = C_1 \cdot Re'^{C_2} \cdot Bo^{0.3} \cdot Pr^{0.4} \end{array} \right. \quad (15)$$

By entering the values of the Nusselt numbers obtained from the correlations ((12), (13), (14) and (15)) in the Nusselt number of convection (11), it is finally possible to obtain the convection coefficients for each side of the sub-heat exchanger. These values, inserted in the equation (9), provide as output the global heat transfer coefficient (U_i) in each zone.

Once obtained for each zone the mean logarithmic temperature and the global heat transfer coefficient (U_i), from equations (8) and (9), it is finally possible to obtain the area corresponding to each sub-heat exchanger (A_i).

$$A_i = \frac{|\dot{Q}_i|}{U_i \cdot \Delta T_{ml_i}} \quad (16)$$

The final step is related to the comparison between the real area of the heat exchanger and the sum of the three areas of the sub exchangers in series.

$$\frac{A_{real} - \sum_{i=1}^3 A_i}{A_{real}} \quad (17)$$

If the relative error (17) is greater than the set tolerance, it means that the error is not acceptable and therefore the hypothesized parameters must be modified to reach convergence.

❖ Condenser submodel

Once all the thermodynamic properties of points 3, 7 and 8 are known, through the initial hypothesis on T_4 and applying the steps described in the heat exchangers sub-model section, it is possible to calculate the exact values of T_4 and \dot{m}_{ORC} initially hypothesized.

From the pressures and temperatures in points 3 and 4, it is possible to obtain h_3 and h_4 . Then, based on the thermal power requested by the user in the condenser \dot{Q}_{cond} , which is a variable operation input, the new \dot{m}_{ORC} is obtained as:

$$\dot{m}_{ORC} = \frac{|\dot{Q}_{cond}|}{h_3 - h_4} \quad (18)$$

The new \dot{m}_{ORC} , applied in the equation (7), provides the unknown temperatures of the intermediate section, through which the mean logarithmic temperature differences (ΔT_{ml_i}) and the thermal power exchanged ($|\dot{Q}_i|$) of each sub condenser can be calculated.

Applying the semi-empirical approach described by Santos et al. [49], the best correlations to obtain the convection coefficients (h_i) in the condenser are:

- a) Maslov and Kovalenko [52] correlation for: $h_{h_I}, h_{h_{III}}, h_{c_I}, h_{c_{II}}, h_{c_{III}}$.
- b) Han et al. [56] correlation for condensation for: $h_{h_{II}}$.

From this convection coefficients are evaluated the values of the global heat transfer coefficients (U_i) (9).

Finally, by applying the equation (16), the area corresponding to each sub condenser (A_i) is obtained. If the relative error (17) is greater than the set tolerance, it means that the error is not acceptable and therefore the hypothesized parameter (T_4), and consequently, the motor fluid mass flow rate (\dot{m}_{ORC}), must be modified ($T_{4_{new}}$ and $\dot{m}_{ORC_{new}}$) to reach convergence.

❖ **Convergence of motor fluid mass flow rate (\dot{m}_{ORC}) and turbine outlet pressure (P_3)**

To create a model that has physical meaning it is necessary to set two controls.

It is noted that the flow rate of the organic fluid used in the turbine sub-model ($\dot{m}_{ORC_{old}}$) is different from that obtained in the condenser sub-model ($\dot{m}_{ORC_{new}}$). For this reason, the calculations described above will be performed iteratively, replacing $\dot{m}_{ORC_{old}}$ with $\dot{m}_{ORC_{new}}$, until the relative error (19) becomes less than the imposed tolerance.

$$\frac{\dot{m}_{ORC_{new}} - \dot{m}_{ORC_{old}}}{\dot{m}_{ORC_{new}}} \quad (19)$$

Through the determination of the correct \dot{m}_{ORC} , the corresponding real values of P_2 (1), $\eta_{iso_{turb}}$ (2) and the consequents thermodynamic properties of points 3 and 4.

Meanwhile all the simulation is performed in an iterative way to reach the convergence of \dot{m}_{ORC} , the pressure P_3 is also modified iteratively, to reach about 5 [°C] of subcooling in point 4 and thus avoid cavitation problems in the pump.

Replacing P_3 with $P_{3_{sat_{sub}}}$, i.e. the one corresponding to the saturation pressure 5 [°C] greater than the T_4 , found at the end of the iteration of the condenser sub-model, was noted that the model required considerable computational efforts to converge.

Therefore, to obtain a convergent result, the pressure of the previous cycle P_{3old} was mediated with the new one P_{3new} . The coefficients used to obtain the pressure for the new iteration were obtained through a parametric analysis in all the condenser operation condition (Figure 3.3 and Figure 3.4). In the final model were chosen the coefficients, closest to the new pressure obtained, that had the minimum computational cost.

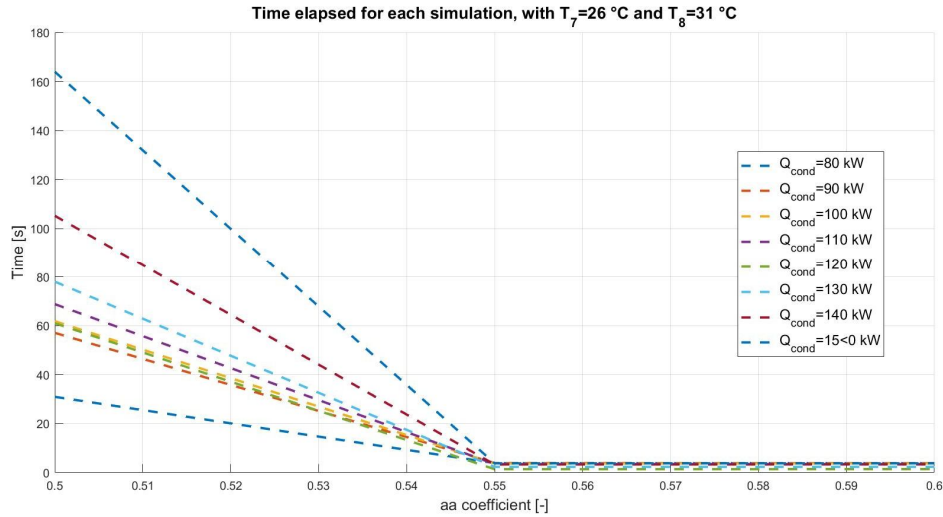


Figure 3.3 Time elapsed during simulation with variable condenser power

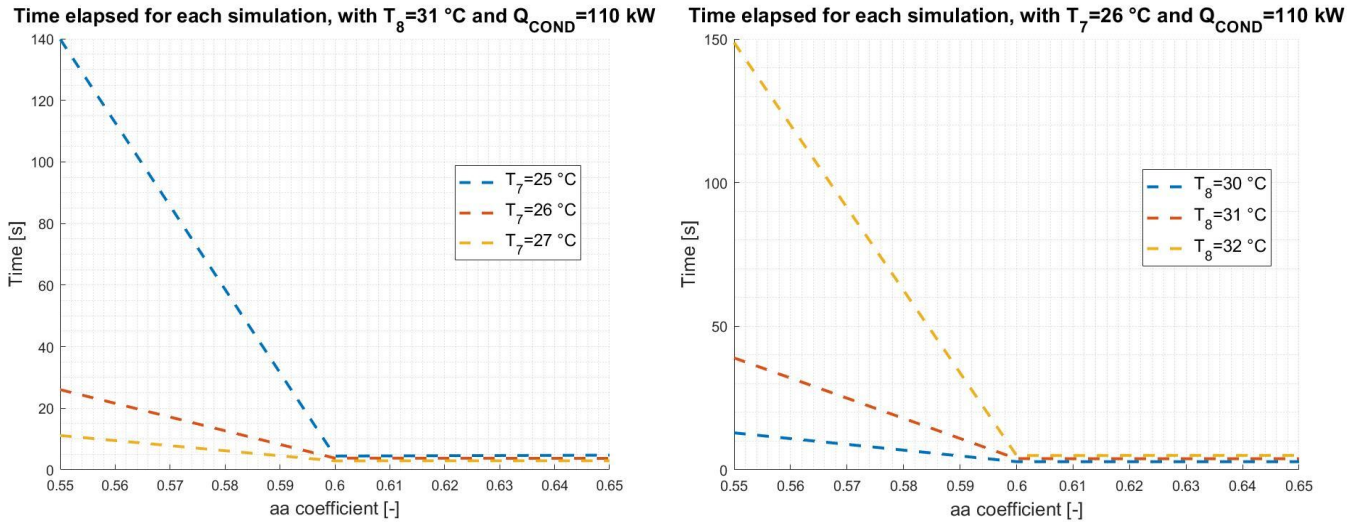


Figure 3.4 Time elapsed during simulation with variable condenser temperature inlet (Left); Time elapsed during simulation with variable condenser temperature outlet (Right)

$$P_{3new} = 0.6 \cdot P_{3old} + 0.4 \cdot P_{3sat_sub} \quad (20)$$

The calculations described above will be performed iteratively, replacing P_{3old} with P_{3new} , until the relative error (21) becomes less than the imposed tolerance.

$$\frac{P_{3sat_sub} - P_{3old}}{P_{3sat_sub}} \quad (21)$$

All calculations so far described are carried out until the convergence of both \dot{m}_{ORC} and P_3 is reached.

At the end of the iterative loops the values of \dot{m}_{ORC} , P_3 and T_4 , initially unknown and therefore hypothesized, are known and equal to $\dot{m}_{ORC_{new}}$, P_{3sat} , T_{4new} .

Finally, from the knowledge of T_4 and P_4 , which for the hypothesis is supposed to be equal to P_3 , are obtained h_4 and s_4 .

❖ Pump submodel

In analogy to the mathematical procedure that took place in the turbine, note the initial conditions the value of the isentropic efficiency of the pump, it is possible to calculate the outlet conditions of the pumps.

$$\eta_{isopump} = \frac{h_{1iso} - h_4}{h_1 - h_4} \quad (22)$$

Since the P_1 , which for the hypothesis is supposed to be equal to the calculated P_2 , and the s_4 are already known, the h_{1iso} can be derived and therefore, from the formula (22), it is possible to extrapolate the unknown h_1 . As already happened previously, note two thermodynamic properties, P_1 and h_1 , it is possible to easily calculate T_1 and s_1 .

❖ Evaporator submodel

Once all the thermodynamic properties of points 1, 2 and 5 are known, through the initial hypothesis on T_6 and applying the steps described in the heat exchangers sub-model section, it is possible to calculate the exact values of T_6 and $\dot{m}_{H_2O_B}$.

From the pressures and temperatures in points 1, 2, 5 and 6 it is possible to obtain the corresponding enthalpies.

Then, based taking advantage of the \dot{m}_{ORC} , previously calculated, it is possible to know the amount of thermal power required in the evaporator ($|\dot{Q}_{eva}|$).

$$|\dot{Q}_{eva}| = \dot{m}_{ORC} \cdot (h_2 - h_1) \quad (23)$$

Finally, through the energy balance applied in the whole evaporator (7), the $\dot{m}_{H_2O_B}$ is calculated.

The $\dot{m}_{H_2O_B}$, applied in the equation (7), first in the zone I or III and subsequently in zone II, provides the unknown temperatures of the intermediate section, through which the mean logarithmic temperature differences (ΔT_{mli}) and the thermal power exchanged ($|\dot{Q}_i|$) of each sub evaporator can be calculated.

Adopting the semi-empirical approach described by Santos et al. [49], the best correlations to obtain the convection coefficients (h_i) in the evaporator are:

- a) Maslov and Kovalenko [52] correlation for: $h_{h_I}, h_{h_{II}}, h_{h_{III}}, h_{c_I}$.
- b) Han et al. [56] correlation for evaporation: $h_{c_{II}}$.
- c) Thonon [51] correlation for: $h_{c_{III}}$.

In this model, following the steps the equation (15), it was used in the first simulation an hypothesized area and afterwards the new area obtained at the end of each loop (16).

From this convection coefficients are evaluated the values of the global heat transfer coefficients (U_i) (9).

Finally, by applying the equation (16), the area corresponding to each sub condenser (A_i) is obtained. If the relative error (17) is greater than the set tolerance, it means that the error is not acceptable and therefore the hypothesized parameter (T_6) must be modified until the convergence is reached. At the end of the iterations, the exact value of T_6 is available and consequently the one of $\dot{m}_{H_2O_B}$.

3.1.2 Vertical biomass firetube boiler model

To perform a complete analysis from the plant, it is also necessary to estimate the mass flow rate of pellets to be burned.

This sub-chapter will show the procedure followed to estimate the required mass flow rate of fuel and the properties of the hot flue gases needed to satisfy the thermal demand required by the evaporator, calculated in the ORC model. Known the characteristics of the combustion chamber and the fuel used, listed in section 2.1, following the previous scheme adopted, it is considered appropriate to describe the model focusing initially the attention on the assumptions, the simplifications adopted, the inputs entered and the outputs desired.

- **Assumptions**

- a) The combustion is complete, therefore the unburnt products, as they represent only 0.6% of the total burnt biomass [38], in first approximation are neglected.
- b) In the combustion reaction, for simplicity of calculation, are considered only the reactants with a weight percentage greater than or equal to 0.01%.

- **Fixed operation inputs**

- a) The characteristics of the pellets are those mentioned in subchapter 2.1.
- b) The temperature of combustion air (T_{air}) is set fix and equal to 16.1 [°C], according to the average annual temperature of Coimbra [57], that is the city in which the plant the system is supposed to be installed.
- c) The relative humidity of the air ($H_2O_{a_{rel_{hum}}}$) is set fix and equal to 0.6, according to the average values recorded in the mechanical engineering department of Coimbra.

d) The boiler pressure is assumed as fix value equal to 101.325 [kPa].

- **Variable operation inputs (customer demand conditions)**

- a) The thermal power exchanged in the evaporator ($|\dot{Q}_{eva}|$) is obtained from the ORC cycle model (23).
- b) The water mass flow rate $\dot{m}_{H_2O_B}$ of the hot source is the one estimated in the evaporator sub-model.
- c) The operating values of the boiler are illustrated in subchapter 2.1.

- **Initial guess**

- a) The products of combustion are assumed, at the beginning of the stoichiometric balance, all in the vapour state.

This hypothesis is mandatory and needs to be verified to safeguard the ducts from the corrosion. The fuel, even though in small quantities, has percentages of sulphur and chlorine which, reacting with water in the liquid state, could generate acids that would limit the operating life of the components.

- **Outputs:**

- a) The mass flow rates of burnt biomass (\dot{m}_{BIO}) and hot gases at the exit of the chimney (\dot{m}_{GAS}).
- b) The adiabatic flame temperature.
- c) The temperatures, the pressures and the state functions, such as enthalpies and entropies of significant thermodynamic points.

❖ **Combustion chamber sub-model**

The sub-model of the combustion chamber is based on the oxidation of the fuel. The mass balance of the real and complete combustion (24) starts from the determination of the molar fractions of the elements of the reactants. To perform a thorough investigation, it was decided to account in this model also the humidity of the reagents.

Since for the pellet are known the mass fractions per mass unit of the main elements of which the pellet is composed, can be evaluated the respective mole fractions through the ratio between mass fractions and the correspondent molar masses. The chemical formula of the fuel adopted in the analysis, considering 1 kg of biomass, is therefore $C_{0.0412}O_{0.0273}H_{0.061}N_{0.0007}$ more a “x” moles of incombustible Ash, the mass fraction of which represents 0.6%.

The extrapolation of water molar fraction in the vapour state contained in the air takes place instead through the knowledge of temperature and relative humidity of the air, defined by the fixed operation inputs. Starting from the defined temperature, was estimated the saturation pressure of the air, which, multiplied by the relative humidity of the air, finally provide the partial pressure of the water contained in the air. Reminding that the air has been considered an ideal gas, the molar fraction of water contained in the air was obtained, exploiting the Dalton law of partial pressures, through the ratio between partial pressure and atmospheric pressure.

Once the molar fractions of reagents have been defined, knowing the amount of carbon dioxide in the dry fumes through the operating values supplied by the manufacturer, the moles of reagents and products unknown can be derived through simple stoichiometric balances.

$$\begin{aligned} x \cdot (C + H + N + O + H_2O_b) + air \cdot (O_2 + 3.76 \cdot N_2 + H_2O_a) \\ = CO_{2g} \cdot CO_2 + N_{2g} \cdot N_2 + H_2O_g \cdot H_2O + O_{2g} \cdot O_2 \end{aligned} \quad (24)$$

From the equation (24) it is noted that there are five unknowns ($x, air, N_{2g}, H_2O_g, O_{2g}$), while the equations obtainable from the mass balances of the elements are only four. For this reason, an auxiliary equation (25) has been applied which considers the mass balance of dry gasses.

$$CO_{2g} + O_{2g} + N_{2g} = 1 \quad (25)$$

After this calculation, the moles of reagents (n_r) and products (n_p) obtained have been reported per kmol of fuel. Defined reagents and products for a kmol of fuel ($\bar{x}_r = \frac{n_r}{x}$ and $\bar{x}_p = \frac{n_p}{x}$), adding algebraically the moles of the products, the total mass of the gases for a kmol of fuel at the outlet is obtained (\bar{x}_{gas}), which, inserted in the equation (26) provides as a result the partial pressure (P_p) of the elements constituting the exhaust gas.

$$P_p = \frac{\bar{x}_p}{\bar{x}_{gas}} \cdot P_{boiler} \quad (26)$$

At this point in the calculation, to validate the initial hypothesis, according to which the water of the gases is only in the vapour state, it is necessary to compare the dew point temperature of the water in the gas with the temperature at the exit of the chimney. From one error message, placed as a control in the code, it emerges that the condensation does not occur in any operating condition.

Once the moles of the individual combustion products per unit of biomass have been established, the molar and mass fractions of the exhaust gas components can also be easily established.

Currently, completed the mass balance, the energy balance can be set up. The energy conservation equation, considering a combustion in the permanent regime, of which the changes in kinetic and potential energies are negligible, can be written as:

$$Q_{in} + W_{in} + \sum_{r=1}^N n_r \cdot \bar{h}_r = Q_{out} + W_{out} + \sum_{p=1}^M n_p \cdot \bar{h}_p \quad (27)$$

Since most steady-flow combustion processes do not involve any work interactions or heat inputs, through those simplifications the equation (27) can be rewritten for obtaining the energy balance for a typical steady-flow combustion process [58]

$$Q_{out} = \sum_{r=1}^N n_r \cdot \bar{h}_r - \sum_{p=1}^M n_p \cdot \bar{h}_p \quad (28)$$

Dividing the equation (28) for the total mole of the fuel and making explicit the total enthalpy (in the contribution related to the formation enthalpy of the compound, from its elements, and the specific change in the state between the standard state and the state of interest) it is finally possible to find the energy realised by the combustion of one kmol of fuel:

$$\bar{q}_{out} = \sum_{r=1}^N \bar{x}_r \cdot [\bar{h}_{f_r}^0 + (\bar{h}(T_r) - \bar{h}^0(T_{ref_r}))] - \sum_{p=1}^M \bar{x}_p \cdot [\bar{h}_{f_p}^0 + (\bar{h}(T_p) - \bar{h}^0(T_{ref_p}))] \quad (29)$$

Where the formation enthalpies of CO₂, H₂O_l and H₂O_g have been taken from the tabulated data in [59], while the one of the biomass has been calculated starting from the LHV provided by experimental results [38]. The values of enthalpy at the reference, reagent inlet and product outlet temperature were instead calculated using the results provided by the NASA thermodynamic database of the software EES (Engineering Equation Solver) [60].

Finally, the energy obtained per unit of mole can be converted into energy per unit of mass. Dividing the power required by the evaporator by the energy per unit of mass and knowing the humidity of the real biomass, the real mass flow rate of the fuel is calculated in the specific operating condition. At the same time, the corresponding combustion air is defined by the product between the mass flow rate of the biomass and the air to fuel ratio, which can be obtained from the stoichiometric balance.

In addition, the mass flow rate of the gas at the chimney is determined through a mass balance, i.e. the mass flow rate of the products is set equal to the mass flow rate of the reactants. The detailed mass flow rate of each gasses is defined trough the mass fractions previously obtained.

Lastly, the determination of the adiabatic flame temperature, i.e. the temperature that would be achieved by the products, is iteratively obtained through the energy balance between reagents and products (30).

$$\sum_{r=1}^N \bar{x}_r \cdot [\bar{h}_{f_r}^0 + (\bar{h}(T_r) - \bar{h}^0(T_{ref_r}))] = \sum_{p=1}^M \bar{x}_p \cdot [\bar{h}_{f_p}^0 + (\bar{h}(T_{flame}) - \bar{h}^0(T_{ref_p}))] \quad (30)$$

After this final step, all the mass flow rates, temperatures and partial pressures, in the thermodynamically significant points, for each reactant and product are known. Therefore, using the REFPROP thermodynamic database [44], the corresponding enthalpies and entropies could be easily evaluated.

3.2 Exergy and exergoeconomic analysis

The performance of an energy system is generally determined by applying the first principle of thermodynamics. The energy conservation law, however, allows the evaluation of the energy efficiency only in quantitative terms, so it is inadequate to distinguish the different qualities of energy that cross the boundaries of the system since this method does not provide as output any information about the quantity and location of thermodynamic irreversibilities [61]. Another limitation linked to the simple application of the first principle of thermodynamics is that it does not allow to determine the cost of the useful product per unit of energy since a process of allocation of operating and investment costs is not implemented. To solve these problems and to have a broader view of the plant, in the following thesis will be implemented an exergetic and exergoeconomic analysis on the entire cogeneration plant.

3.2.1 Exergy analysis

Exergetic analysis provides a deep level of plant investigation, as it allows to estimate in which component the greatest irreversibilities occur. The quality of energy, degraded during the conversion process from an ordered to a disordered one, is determined by the simultaneous application of the first and second law of thermodynamics, i.e. through enthalpy and entropy balances [61]. From the application of this new model, which has stimulated considerable interest in the scientific community in recent decades, it is possible to define the work through the thermodynamic status function called exergy.

Exergy represents the maximum available energy of a system that is in a specific thermodynamic state compared to a reference one. In other words, exergy provides information on the capability of a given system, that is in thermodynamic and chemical disequilibrium compared to a reference system, to produce useful work [62].

Combining the first two principles of thermodynamics, the exergetic balance for a generic component is defined as:

$$\sum_{k=1}^{n_k} \left(1 - \frac{T_0}{T_k}\right) \cdot \dot{Q}_k + \sum_{i=1}^{n_i} \dot{E}_i = \left(\frac{dA}{dt}\right)_{cv} + \dot{W} + \sum_{j=1}^{n_j} \dot{E}_j + \dot{I} \quad [W] \quad (31)$$

where the terms, in order of appearance, accounts the exergy associated the k^{th} heat transfer process, the one of the i^{th} stream of matter entering the control volume, the time rate of variation of internal exergy, the mechanical work exchanged and, the exergy of the j^{th} stream of matter exiting the control volume and, lastly, the exergy destruction rate, also called in literature irreversibility.

In the current thesis is hypothesized that the components work in steady-state conditions and are considered adiabatic with the external environment, so the equation (31) is simplified in:

$$\sum_{i=1}^{n_i} \dot{E}_i = \dot{W} + \sum_{j=1}^{n_j} \dot{E}_j + \dot{I} \quad [W] \quad (32)$$

The exergy of the generic mass flow rate that crosses the boundary could be evaluated as the sum of physical, chemical, potential and kinetic exergy.

$$\dot{E} = \dot{E}_{ph} + \dot{E}_{ch} + \dot{E}_{pot} + \dot{E}_{kin} \quad [W] \quad (33)$$

In the following thesis, potential and kinetic exergy will be neglected.

Physical exergy is defined as the maximum amount of the work obtainable from the initial state of the stream, defined in the thermodynamic analysis, to the restricted dead state, that is the condition of mechanical and thermal equilibrium, therefore the system and the environment have same pressure and temperature. It is defined as:

$$\dot{E}_{ph} = \dot{m} \cdot [(h - h_0) - T_0 \cdot (s - s_0)] \quad [W] \quad (34)$$

where \dot{m} is the mass flow rate, h and h_0 are the specific enthalpies of the substance in the initial and in the restricted dead state, T_0 is the dead state temperature and finally s and s_0 represent the specific entropies of the substance respectively in the initial and in the restricted dead state.

According to the general approach followed by several studies, [63] [64] [65] [66] [67], the reference of dead state, of solid, liquid and gaseous compound analysed, was set equal to 25°C and 1 atm.

Chemical exergy is instead defined as the maximum amount of the work obtainable from the restricted dead state of the stream to the dead state, that represents the condition of chemical equilibrium.

The value per unit of mole related to a gas mixture is calculated by:

$$\dot{E}_{ch} = \sum_k x_k \cdot e_{ch} + R \cdot T_0 \cdot \sum_k x_k \cdot \ln x_k \quad [W] \quad (35)$$

where x_k is the molar fraction of the generic element or compound of the mixture, while R is the universal gas constant.

Chemical exergy of reference substances was taken from [63], instead regarding the standard molar chemical exergy of pure organic compounds, the literature review revealed the lack of disclosure of detailed information. To fill this gap in the various articles analysed, it is considered useful to cite the article by Gharagheizi et al. which has values of 133 different organic fluids [64]. These parameters referred to a dead state with $T_0 = 298.15$ K and $p_0 = 1$ atm, can also be corrected in function the reference temperature, using the equation proposed by Abam et al. [68]. Unfortunately, the fluid treated in the following thesis, R245fa, is not present in the list of fluids previously mentioned. Therefore, following the exergoeconomic analysis conducted on this fluid, it emerges that the reference state is the same as that of the gases present in the air, but the standard molar chemical exergy of the R245fa has not been taken into consideration [65] or has been considered equal to zero [66]. Confirmation of this approach comes from the study conducted by Chen et al. [67], which states that the chemical energy of R245fa is equal to zero due to the absence of chemical reactions in the atmosphere.

To conclude the collection of the specific chemical exergy data, it was also necessary to compute the term related to the biomass. The evaluation of this parameter, generally complex due to the application of Szargut and Styrylska's methods, could be simplified through the application of the formula proposed by G. Song et al. [69]. The simplification introduced by this new method, validated with 86 varieties of biomass, is the calculation of the specific chemical exergy of biomass taking advantage of the ultimate analysis data plus ash content, namely mass concentrations of the major elements of the biomass [38], as follows:

$$e_{ch_{bio}} = 1812.5 + 295.606 \cdot C + 587.354 \cdot H + 17.506 \cdot O + 17.735 \cdot N + 95.615 \cdot S - 31.8 \cdot ASH \quad \left[\frac{kJ}{kg} \right] \quad (36)$$

Through the simple product between the result of (36) and the mass flow rate of the pellet, calculated in the thermodynamic analysis, it is possible to have the exergy associated with the stream related to the biomass.

Once a preliminary data collection, necessary for the evaluation of the exergies of all the streams, has been carried out, it is essential to univocally represent the system, through the creation of the incidence matrix, represented with the letter A of dimensions [n x m],

3. Methodology

the rows of which [n] represent the physical components and the columns [m] the flows. In this matrix, the generic elements a_{ij} assume a value of +1 if the flow j^{th} enters the subsystem i^{th} , -1 if the flow leaves the subsystem and 0 if there is finally no direct physical relationship between the two [70]. The incidence matrix, which represents the analysed system, is available in Table 3.1. It should be noted that the numbering follows that adopted in Figure 2.2.

Table 3.1 Incidence matrix A

	ORC ₁	ORC ₂	ORC ₃	ORC ₄	HW _{in}	HW _{out}	PW _{in}	PW _{out}	Air	P	GAS _{out}	Em ₁	Em ₂
	E1	E2	E3	E4	E5	E6	E7	E8	E9	E10	E11	E12	E13
CC	0	0	0	0	-1	1	0	0	1	1	-1	0	0
EVA	1	-1	0	0	1	-1	0	0	0	0	0	0	0
TURB	0	1	-1	0	0	0	0	0	0	0	0	-1	-1
COND	0	0	1	-1	0	0	1	-1	0	0	0	0	0
PUMP	-1	0	0	1	0	0	0	0	0	0	0	0	1

At that point, in the case of steady-state operation, it will be possible to describe the balance of exergy as follow:

$$A \cdot \dot{E} = \dot{I} \quad [W] \quad (37)$$

where the values of the unknown column vector \dot{I} , of dimensions [n], represent the exergies destroyed in the unit i^{th} due to internal irreversibility.

At that point, it could be also computed the relative ratio of exergy destruction of a component to the total irreversibility of the system as:

$$I_n = \frac{\dot{I}}{\dot{I}_{tot}} \cdot 100 \quad [\%] \quad (38)$$

Finally, exploiting the definitions of fuel and product, which will be illustrated in the next section (Table 3.2), the exergetic efficiency of each component was calculated through the following formula:

$$\varepsilon = \frac{E_{fuel}}{E_{product}} \cdot 100 \quad [\%] \quad (39)$$

3.2.2 Exergoeconomic analysis

To perform an analysis that allows analysing simultaneously exergetic results with economic ones, it was decided to follow the F-P-L-I method, proposed for the first time by Lozano and Valero [70]. Due to the vastness of the method adopted, it will be divided

into three sections, to highlight the input data and the intermediate steps necessary for the extrapolation of the economic exergo parameters.

❖ Exergy cost E^* and unit exergetic cost k^* of streams

The first output of this methodology is the column vector of exergy cost of a stream, E^* , of dimension [m], that is defined as the exergy of a stream plus all the irreversibilities that are generated in the process of its production. The analysis of exergy cost is based on the principle of the cost formation process, that accounts and allocates, within the plant, the exergy destruction of a certain component. The procedure aims to determine the quantity of energy request to product each stream.

The cost allocation analysis starts from the definition of the exergy cost as a conservative property of the system. Once the irreversibility is generated in a component, it is distributed in the outlet streams in the component and then passes in the successive components. This concept, converted into matrix form, can be expressed using the incidence matrix as:

$$A \cdot E^* = 0 \quad [W] \quad (40)$$

However, it is possible to notice that are necessary auxiliary equations since the n equations available are less than the m unknowns. The determination of those additional equations, equal to the number of fluids minus the number of components, occurs through the application of four rules, generally called in the literature P1, P2, P3, P4.

The propositions related to those rules arises since each unit of the plant has a specific productive function, so for each component it can be clearly indicated which resources or fuel (F) have been consumed to obtain a product (P) and, therefore, determine the losses (L) associated with the conversion process. Loss flows are those that, being released into the external environment, leave the unit and the plat and are not subsequently used, because the exploitation process is not technologically mature, it is expensive compared to gains or simply there is no interest to be used.

According to rule P1 the exergy cost of sources, that comes from the external ambient, is set equal to the exergy of the stream ($E = E^*$), so its unit of exergy cost is equal to one; contrarily the P2 rule states that discharges are considered equal to zero for allocating the entire cycle costs only to the final useful products ($E^* = 0$).

The application of the first two rules makes possible to obtain, for the case study under investigation, four auxiliary equations, defined in the matrixial form as:

$$\alpha_e \cdot E^* = \omega \quad [W] \quad (41)$$

where ω is set equal to the exergy in the application of the first rule, to zero in the second one.

3. Methodology

Lastly, according to P3 and P4 rule, if the components have a fuel defined as a difference of streams or the components produce more than one product, the streams and the products considered have the same unit of exergy cost $\left(\frac{E_n^*}{E_n} = \frac{E_m^*}{E_m} \rightarrow -\left(\frac{E_n^*}{E_m^*}\right) \cdot E_m + E_n = 0\right)$.

The equations obtained through the last two rules are expressed in matrixial form as:

$$\alpha_x \cdot E^* = 0 \quad [W] \quad (42)$$

To facilitate the reading, following these definitions, was built the Table 3.2, which subdivides the fluids that interact with the components according to their use and highlight the four rules with the green, red, blue and yellow colours respectively.

Table 3.2 Plant fuel, product and discharges definition that highlight the application of the four rules (benchmarks related to Figure 2.2)

	Fuel	Products	Discharges
CC	E9+E10	E5-E6	E11
EVA	E5-E6	E2-E1	
TURB	E2-E3	E12+E13	
COND	E3-E4	E8-E7	
PUMP	E13	E1-E4	

The procedure shown allows finally to create a fully defined problem, expressed in matrix form as:

$$\begin{bmatrix} A_C \\ \alpha_e \\ \alpha_x \end{bmatrix} \cdot E^* = \begin{bmatrix} 0 \\ \omega \\ 0 \end{bmatrix} \rightarrow A_C \cdot E^* = Y_e \quad [W] \quad (43)$$

where the cost matrix A_C is the combination of the three matrices that define the equations of the problem, while the vector of external assessments Y_e contains the know terms of the problem. Both the cost matrix and the vector of external assessment are reported in Appendix A. The column vector of exergy costs E^* is thus obtained as:

$$E^* = A_C^{-1} \cdot Y_e \quad [W] \quad (44)$$

In the end, to determine the amount of exergy used to produce a unit of product, for each stream was calculated the unit exergetic cost k^* , which is mathematically expressed as:

$$k_n^* = \frac{E_n^*}{E_n} \quad [-] \quad (45)$$

❖ Economic parameters

The choice to invest in whatever type of system is mainly related to economic aspects since high costs wouldn't make the plant profitable for the investor. Therefore, the main goal of a production process is the minimization of the production cost for a unit of product generated. The price of the product is determinate from the simultaneous combination of operative (OPEX) and initial investment (CAPEX) cost. It is also briefly mentioned that for a more in-depth analysis maintenance costs could also be included, which in the present discussion for simplicity and lack of information, available in the literature and from the company, will be neglected. From this double source of prices, it is deduced that the optimal value is given by a correct balance between the efficiency of the thermodynamic processes involved and the purchase cost of the component. This is the main reason that makes necessary an estimation of the price per unit of fuel and the initial costs related to the plant construction.

Regarding the price of pellets per unit of mass, bought by SCIVEN company, is $140 \frac{\text{€}}{\text{ton}}$, a value in accordance with average prices in the European market [71].

The capital cost estimation was determined instead following the methodology provided by the NETL [72]. The procedure consists in split out the capital cost in different levels, to evaluate the total price starting from the initial costs of the component. As a first step, for all the components of the plant was established the Bare Erected Cost (BEC), which account the purchasing costs. In this thesis were used the data provided by the CEO of SCIVEN, that are summarized in Table 3.3

Table 3.3 Plant components BEC

Components	BEC [€]
Biomass Boiler [SMART 180 kW]	44,000.00 €
Evaporator [SWEP B200THx110/1P-NC-M (2 1/2"+2 1/2"+2x2 1/2")]	500.00 €
Turbine [DEPRAG Turbine Generator GET11 kW]	30,000.00 €
Condenser [KELVION BPHE GmbH GBS757M-60]	350.00 €
Pump [MPO 3R series]	800.00 €

Following the average values proposed by NETL, to evaluate the Engineering, Procurement and Construction Cost (EPCC), so additional cost related to the design, sizing and the choosing process of the equipment, the values of BER have been increased by 10%. Then for the determination of the Total Plant Cost (TPC), that includes project and process contingencies (costs that are not simple to be estimated previously, but that can occur with unexpected problems), the values of EPCC have been increased by 20%, since it is a small pilot plant not currently available on the Portuguese market. Finally, the Total Overnight Cost (TOC), that accounts other

3. Methodology

owners cost, was set equal to 15% more than the EPCC, in accordance with the average parameters provided by NETL.

The TASC (Total As-Spent Cost) was considered equal to the TOC value because the plant requires short installation times and the risk connected with the investment is rather low, due to the ratio equity debt, following described, and then the main products of the plant, electricity and hot water, will always require by the structure. The investment cost of the entire plant results equal to 114,836.70 €.

To account the whole plant lifetime, it is also necessary to consider a discount rate, which can scale in time in a uniform series the present value of the components. The discount factor may be considered equal to the Weighted Average Cost of Capital (WACC), which is given by the following equation:

$$WACC = K_e \cdot \frac{E}{E + D} + K_d \cdot \frac{D}{E + D} \quad [\%] \quad (46)$$

where E and D represent respectively the equity and the debt of the investment, which were considered equal to 25% and 75% respectively to have a low-risk investment, while K_e and K_d refer to the cost of equity and debt.

The cost of equity is generated by two contributions, i.e. R_f , that is the risk-free interest, which is considered as the national government bond at a short time, and an additional premium, that account the small stock premium due to reduced liquidity, R_s , and the Equity Market Risk Premium (EMRP) that accounts the average interest that is obtainable investing in the market multiplied by β , a coefficient which considers the specific sector of the market:

$$K_e = R_f + premium = R_f + R_s + \beta \cdot EMRP \quad [\%] \quad (47)$$

The values adopted during this economic analysis to obtain K_e are: $R_f = 0.51\%$ [73] [74], $R_s = 0$ because the investment is supposed made by a not-small investor; $\beta = 1$ and $EMRP$ equal to 5.75% for the European market [75].

On the other hand, the cost of equity is generated by the sum of two other contributions, i.e. the Interest Rate Swap (IRS), that is the general reference cost of debt, and a spread that is the increase of interest depending on the capability of the investor to return the capital.

$$K_d = IRS + spread \quad [\%] \quad (48)$$

The values adopted during this economic analysis to obtain K_e are: IRS at 10 years equal to 0.19% [76], according to data published by the European Banking Federation, and spread equal to 1%.

Applying the formulas (47) and (48), it is obtained $k_e = 6.26\%$ and $k_d = 1.19\%$, which inserted in the (46) give as result $WACC = 2.4575\%$.

Starting from these economic and financial considerations, the annuity cost of a component is obtained by multiplying TOC of each component by the Discount Rate Factor (DRF), a value that considers both cost capital and the plant lifetime, expressed as:

$$DRF = \frac{(WACC + 1)^n \cdot WACC}{(WACC + 1)^n - 1} \quad [\%] \quad (49)$$

With a precautionary period of life of the plant (n) guaranteed by the company, equal to 20 years, is obtained a $DRF = 6.389\%$.

Summarizing, the annuity of the n^{th} component is:

$$Annuity_n = TOC_n \cdot DRF \quad \left[\frac{\text{€}}{\text{year}} \right] \quad (50)$$

Therefore, could be also considered the availability factor (AF), that represents the fraction of time of the year for which the system is working, considering planned and not planned stops in the productivity. The Availability Factor suggested by the company for this plant is equal to 0.57, which represent around 5000 hours per year.

The cost rate is obtained by dividing the Annuity over the Availability Factor, considering the change in the units of measure of time from year to second:

$$Z_n = \frac{Annuity_n}{AF} \cdot \frac{1}{31536000} \quad \left[\frac{\text{€}}{\text{s}} \right] \quad (51)$$

❖ Exergo economic cost C and unit exergo economic cost c

The results obtained in the exergy analysis refer only to physical quantities, without estimate a monetary cost for both resources and products. A competitive plant needs to be analysed in the process of cost formation, to understand the final cost of products and eventually try to improve the plant by reducing the main sources of these costs.

The exergoeconomic cost of a flow ($C_{OUT,i}$) could be defined as the combination of the exergetic cost of the processed flow ($C_{IN,i}$) and the cost rate of the component (Z), that in mathematical form is expressed as:

$$\sum_{i=1}^n C_{IN,i} + Z = \sum_{i=1}^n C_{OUT,i} \quad \left[\frac{\text{€}}{\text{s}} \right] \quad (52)$$

Applying the balance equation (52) for all the component involved during the process, the problem could be represented in matricial form:

$$\begin{bmatrix} A_C \\ \alpha_e \\ \alpha_x \end{bmatrix} \cdot C = \begin{bmatrix} -Z \\ \omega_e \\ 0 \end{bmatrix} \quad \begin{bmatrix} \text{€} \\ \text{S} \end{bmatrix} \quad (53)$$

where the first square matrix is equal to the one adopted in equation (43), instead Z is the cost rate of the components and ω_e is the cost of input and output resources, the values of which followed the proposition of P1, P2, P3 and P4 rules, previously illustrated. The only input value set different from zero was the cost of the pellet, because the combustion air and the inlet water were considered available for free [77]. Regarding the output resource, the exhausted gas combustion, it was set equal to zero, because is assumed that any CO₂ taxation was applied.

Finally, applying the inverse formula of the equation (53), could be calculated the vector of the exergoeconomic costs C .

Dividing for each steam the exergoeconomic obtained for the relative exergy, it also established the unit exergoeconomic cost c :

$$c_n = \frac{C_n}{E_n} \quad \begin{bmatrix} \text{€} \\ \text{MWh} \end{bmatrix} \quad (54)$$

3.2.3 Design improvement and optimization

The obtained values are useful to compute some exergo-economic parameters which highlight in which part of the plant there are the main contributions to the cost and their source, i.e. the irreversibilities associated to the process or the high cost of the component.

For this purpose, it is necessary to define the exergoeconomic unit cost of resources and products for the different components. Considering the productive structure of the represented previously, 5 different definitions (D) are available for the exergoeconomic unit cost of resources and products [70]:

- D1: if the fuel or the product is equal to a physical flow, its exergoeconomic unit cost is the same obtained through (54), so $c_f = c_i$ and $c_p = c_i$.
- D2: if the fuel is defined as the difference between two flows, its exergoeconomic unit cost is the same of the unit exergoeconomic cost obtained through (54) of one of the two streams, since they have the same value, so $c_f = c_i = c_{i+1}$.
- D3: if the fuel is defined as the sum of two physical flow, its exergoeconomic unit cost is defined as:

$$c_f = \frac{c_i \cdot E_i + c_{i+1} \cdot E_{i+1}}{E_i + E_{i+1}} \quad \begin{bmatrix} \text{€} \\ \text{MWh} \end{bmatrix} \quad (55)$$

- D4: if the product is defined as the difference of two physical flow, its exergoeconomic unit cost is defined as:

$$c_p = \frac{c_i \cdot E_i - c_{i+1} \cdot E_{i+1}}{E_i - E_{i+1}} \quad \left[\frac{\text{€}}{\text{MWh}} \right] \quad (56)$$

- D5: if the product is defined as the sum between two flows, its exergoeconomic unit cost is the same obtained through (54) of one of the two streams, since they have the same value, so $c_p = c_i = c_{i+1}$.

To facilitate the reading, following these new definitions, as happened in the previous chapter, was built the Table 3.4, which subdivides the fluids, that interact with the components, according to their use and highlight the five definitions mentioned with the blue, red, yellow, green and grey colours respectively.

Table 3.4 Plant fuel, product and discharges definition that highlight the application of the five definitions (benchmarks related to Figure 2.2)

	Fuel	Products	Discharges
CC	E9+E10	E5-E6	E11
EVA	E5-E6	E2-E1	
TURB	E2-E3	E12+E13	
COND	E3-E4	E8-E7	
PUMP	E13	E1-E4	

For each component also the Relative Cost Difference (r_i) is expressed, a parameter that represents the increase of the products unit cost per unit cost of resources:

$$r_i = \frac{c_{p_i} - c_{f_i}}{c_{f_i}} \quad [\%] \quad (57)$$

Components with higher relative cost difference are the ones which have a higher cost increase inside them, so are the ones for which an improvement could be obtained.

The cost increase is generated by the irreversibility or the cost of the component. For establish which is the main source, is introduced the Exergoeconomic Factor (f):

$$f = \frac{Z_i}{Z_i + CD_i} \quad [\%] \quad (58)$$

where Z_i is the sum of the cost rate of the component and CD_i is the cost associated with the exergy destruction. This last term is the product of the irreversibilities associated with the component times the unit cost of its resource

$$CD_i = c_{f_i} \cdot \dot{I}_i \quad \left[\frac{\text{€}}{\text{s}} \right] \quad (59)$$

Components with the exergoeconomic factor near to one are the ones which require a reduction of costs, contrary the ones near to zero are the ones which require a thermodynamic improvement.

3.3 Hybrid biomass-solar plant model

Once all the considerations relating to the biomass-powered cogeneration plant model have been completed, will now be shown in detail the assumptions and the steps that allowed to obtain the optimized hybrid solar model.

The layout and control systems of the plant are accurately described in chapter 3.3, was analysed assuming that the ORC fluid entering the external exchanger had a mass flow rate of about 0.503 kg/s, in the thermodynamic conditions of 30.7 °C and 673 kPa. Starting from the fluid pressure, the boiling temperature of 73.77 °C was obtained through a database [78]. These values are those recorded at the pump output of the ORC circuit in the intermediate operating conditions of the range analysed in the Matlab model, i.e. $T_7 = 26$ °C, $T_8 = 31$ °C and $|\dot{Q}_{cond}| = 110$ kW_{th}. In such a way it is possible to compensate in a first approximation, with a single constant value, the thermodynamic fluctuations to which the cogeneration cycle is subjected.

Furthermore, since the R245fa fluid was not included in the list provided by the software, each property of the working fluid used has been entered manually between the inlet and the boiling point, in accordance with EES [60], SWEP [78], ASHRAE [79] and fluid seller [80] database, as shown in Table 3.5.

Table 3.5 ORC fluid inputs required by the software

R245fa properties	
Relative molar mass $\left[\frac{g}{mol}\right]$	134.05
Heat capacity $\left[\frac{J}{kg \cdot K}\right]$	1385.6
Thermal conductivity $\left[\frac{W}{m \cdot K}\right]$	0.080096
Density $\left[\frac{kg}{m^3}\right]$	1266.2
Cinematic viscosity $\left[\frac{m^2}{s}\right]$	0.000233

All the properties of the fluid R245fa refer to the average data between the inlet and the boiling temperature, at an absolute pressure of 6.73 bar.

Once the plant structure, operating conditions and control dynamics have been established, the design phase focuses on the solar panel, in particular in the determination of the optimal area, the angle of installation and the orientation. In the following thesis

two different thermal solar panel technologies have been investigated, namely the vacuum tube and the flat plate.

Both panel technologies were initially investigated in the conditions in which there was a greater probability of being close to the optimal point, i.e. a tilt angle equal to the latitude of the studied location ($\beta = 40.12^\circ$) and a south-facing orientation ($\gamma = 0^\circ$).

The panels used in the simulations were chosen from the catalogue proposed by the software and their main characteristics are shown in Table 3.6.

Table 3.6 Main features of solar thermal panels investigated

	Vacuum tube	Flat plate
Name	AR 20	WTS-F2 K6
Manufacturer	Baxi Group	Max Weishaupt GmbH
Absorber area [m ²]	2.15	2.33
Aperture area [m ²]	2.15	2.33
Gross area [m ²]	2.77	2.51
η_0 [-]	0.768	0.826
$a_1 \left[\frac{W}{m^2 \cdot K} \right]$	1.292	2.965
$a_2 \left[\frac{W}{m^2 \cdot K^2} \right]$	0.0053	0.036

Regarding the flow rate of the solar thermal system, for the production of domestic hot water, the common rule of thumb suggests to have between 30 and 50 $\left[\frac{1}{h \cdot m_{\text{panel}}^2} \right]$ [41]. In the following thesis was adopted a specific flow rate of 40 $\left[\frac{1}{h \cdot m_{\text{panel}}^2} \right]$.

For the area of the coil immersed in the first storage it is instead suggested to have between 0.2 and 0.4 [m²] per unit of solar panel area [42]. In the following thesis was simulated a coil that had 0.2 [m²] per unit of solar panel area.

Finally, it was decided to size the external plate heat exchanger for each simulation in which the collector area varied. Using the advanced calculation tool offered by SWEP [78], each heat exchanger has been designed with a solar fluid temperature higher than 10 °C compared to that of the ORC fluid, which corresponds to the heat exchange activation point. Having defined the characteristics of the two fluids, the change in the exchanger was linked to the modification of the mass flow rate of the solar circuit.

For both types of panels was noted that the heat exchanger B25T is suggested in the whole range analysed, shown in the results section and that includes the optimal point. The features of the established model are reported in Table 3.7.

3. Methodology

Table 3.7 Geometric characteristics of the heat exchanger B25T [81]

B25T plate heat exchanger [81]	
Length [mm]	119
Height [mm]	526
Width [mm]	$4+2.25 \cdot (\text{Number of plates})$

Therefore, following this approach, in each simulation the transfer capacity, the number of plates and therefore also the thickness were simply changed.

As previously anticipated, in solar thermal installations one of the crucial points in the design phase is the choice of the optimal area of the solar collectors.

Following the technical tips of the Planning and Installing Solar Thermal Systems manual, it was decided to use solar fraction (SF) and system efficiency (SE) as indicators for the optimization. These parameters make possible to determine an ideal trade-off between primary energy savings and investment costs respectively [42].

The solar fraction is described as the ratio of solar heat yield to the total energy requirement for hot water heating, in accordance with formula (60):

$$SF = \frac{Q_s}{Q_s + Q_{aux}} \cdot 100 \quad (60)$$

where Q_s is the solar heat yield and Q_{aux} is the auxiliary heating requirement, both expressed in kWh . Consequently, the higher the solar fraction, the lower the amount of backup energy required for auxiliary heating. The extreme case refers to $SF = 100\%$ where no external energy is required.

The system efficiency is instead defined as the ratio of solar heat yield to the global solar irradiance on the absorber surface in a pre-established period, for example one year, as expressed in

$$SE = \frac{\dot{Q}_s}{E_G \cdot A} \cdot 100 \quad (61)$$

where \dot{Q}_s is the solar heat yield in one year $\left[\frac{kWh}{year}\right]$, E_G is the total yearly solar irradiance $\left[\frac{kWh}{year}\right]$ and A is the absorber surface area $[m^2]$.

From the comparison of the formula (60) with the (61), appear clear that there is a relation of the two coefficients. The system efficiency is higher at a lower solar fraction, that is when the solar water heater size is smaller than the domestic hot water demand. If the solar fraction is increased by increasing the collector area, the system efficiency is reduced, therefore every further kilowatt-hour gained becomes more expensive [42]. The

opposite trend of these two variables, that is at the base of the optimization of the total area of the solar collectors, can be seen in Figure 3.5:

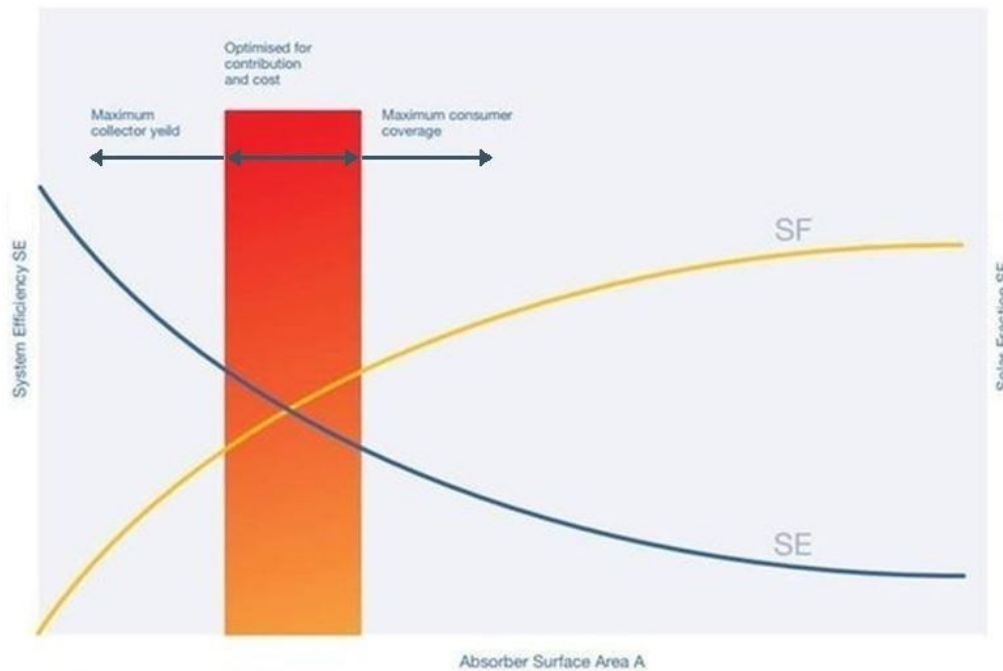


Figure 3.5 Definition of the optimal area through the solar factor and the system efficiency [82]

Following this approach, the area of the panels was modified and, consequently, the external heat exchangers and the area of the solar coil inside the first storage. The parameters entered in the exchanger of the ORC circuit, resulting from the sizing with the tool offered by SWEP [78], are briefly reported in Table 3.8, for both technologies, as a function of the units installed and the relative area.

Table 3.8 Relation between the area of the collector and the external heat exchanger

Number of units	Vacuum tube			Flat plate		
	Absorber area [m^2]	Transfer capacity [$\frac{W}{K}$]	Heat exchanger plates	Absorber area [m^2]	Transfer capacity [$\frac{W}{K}$]	Heat exchanger plates
30	64.5	2746.8	22	69.9	2891.2	24
35	75.25	3004.9	26	81.55	3148.8	28
40	86	3148.8	28	88.54	3238.4	30
42	90.3	3238.4	30	93.2	3345.3	32
45	96.75	3345.3	32	104.85	3552.4	36
50	107.5	3552.4	36	116.5	3728.4	40
55	118.25	3728.4	40	128.15	3895.5	44
60	129	3895.5	44	139.8	4060	48

Subsequently, an optimization analysis was conducted on the optimal area, both for tilt angle and orientation, in order to maximize the solar factor. The tilt angle was investigated in the range between 0° and 90° , while the orientation compared to the south was analysed between -45° and 45° . To obtain the optimal solar factor value through the

3. Methodology

variation of the two independent variables, the numerical method of the *Quadratic approximation* was adopted. The extreme and intermediate values are approximated with a parabola, the coefficients of which are used to find the optimal value ($\beta_{\text{opt}} = -\frac{b}{2a}$ when $\gamma = \text{constant}$ and $\gamma_{\text{opt}} = -\frac{b}{2a}$ when $\beta = \text{constant}$). The procedure was applied until values of the solar factor obtained changing variables become about constant.

Finally, once was decreed the optimal area of solar collectors, their inclination and orientation, the optimal area of the second storage coil was also found with parametric analysis.

4. Results

4.1 Biomass plant results

In this chapter the main thermodynamic results of the cogeneration plant will be shown, focusing on their evolution, in the whole range of thermal power and temperatures, to understand which are the operative points with best performances.

For a first analysis it was decided to set the difference in temperature of the pool water, between the input and output of the condenser, equal to 5 degrees Celsius. By varying the inlet temperature in the power range, three different curves were obtained, which were studied in terms of electrical and thermal efficiency.

Moreover, it is important to highlight that markers have been inserted in each graph to represent the operational condition of the condenser, from 80 kW to 150 kW with a discretization of 10 kW each.

Regarding electrical efficiency, shown in Figure 4.1, a parabolic trend can be seen for each condition, with a maximum power between 130 kW and 140 kW required from the condenser.

It's clear, from this first graph, that the efficiencies differences are minimal around the optimal point, while there is an absolute difference of about 0.45% in the minimum required power condition. This result is remarkable since at the same thermal power, with a simple adjustment of the inlet temperature, it is possible to have a relative increase in electrical efficiency of 15.2%.

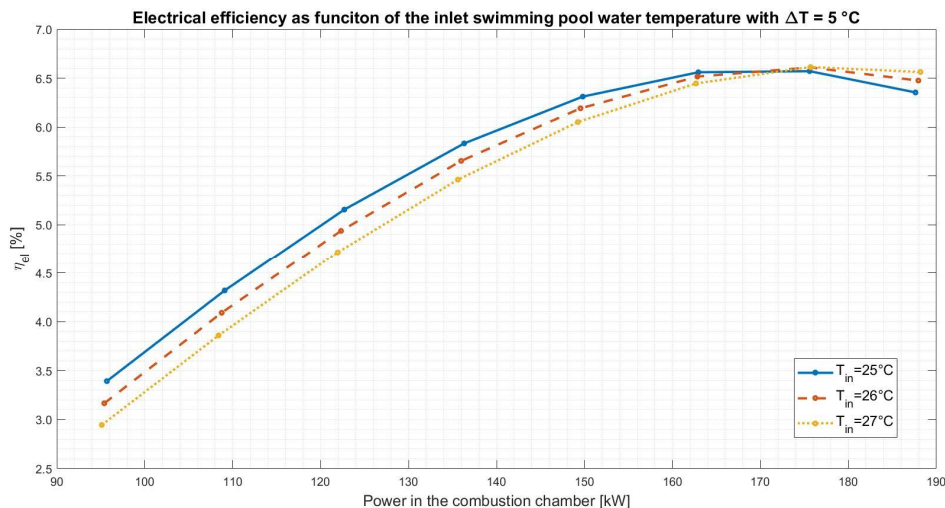


Figure 4.1 Evolution of electrical efficiency with different temperatures of pool water inlet

Since the operating condition with a condenser inlet temperature of 25 °C is the one with the highest electrical efficiency at low thermal power, while it is the worst at maximum power, and the opposite case occurs if the temperature is 27 °C, it was decided to proceed by investigating the cause of this trend.

4. Results

The explanation of this maximum efficiency inversion is mainly related to the constraint of the pressure reached at the turbine outlet, which has been imposed in the model to avoid the presence of condensation in the recirculation pump.

The electrical efficiency of the plant was considered as the ratio between the net electricity produced by the plant and the energy released by the pellet combustion. Since in the various operating conditions in the condenser the electrical consumption of the pump is minimal, for the explanation of the trend of electrical efficiency in qualitative terms, only the electric current trend produced by the turbine will be analysed.

Neglecting, in first approximation, the electric current consumed by the pump, the electrical efficiency can be calculated as:

$$\begin{aligned}\eta_{el} &= \frac{P_{el,net}}{LCV \cdot \dot{m}_{bio}} \approx \frac{P_{el,turb}}{LCV \cdot \dot{m}_{bio}} = \frac{\eta_{m,turb} \cdot P_{m,turb}}{LCV \cdot \dot{m}_{bio}} = \frac{\eta_{m,turb}}{LCV} \cdot \frac{\dot{m}_{ORC}}{\dot{m}_{bio}} \cdot (h_2 - h_3) \\ &= \frac{\eta_{m,turb}}{LCV} \cdot \frac{\dot{m}_{ORC}}{\dot{m}_{bio}} \cdot \eta_{iso,tub} \cdot (h_2 - h_{3,iso})\end{aligned}\quad (62)$$

Since the efficiency of the conversion of the mechanical energy of the turbine into electrical is constant, and the combustible remains unchanged, the only significant terms are the mass flow rate ratio and the isentropic efficiency of the turbine.

$$\eta_{el} = f\left(\frac{\dot{m}_{ORC}}{\dot{m}_{bio}}, \eta_{iso,tub}\right)\quad (63)$$

The trend of these main parameters is shown in Figure 4.2.

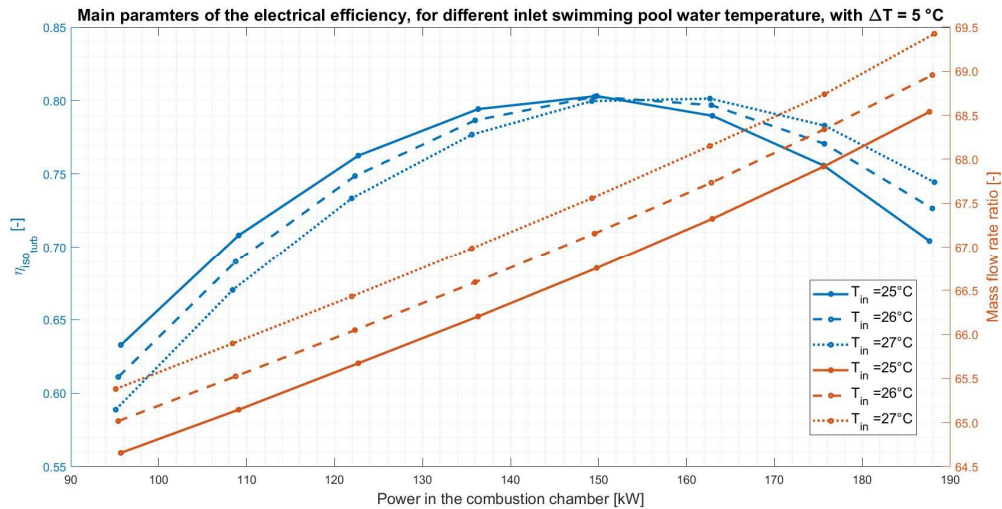


Figure 4.2 Evolution of the isentropic efficiency of the turbine and of the ratio between the mass flow rates with different pool water inlet temperatures

It is immediately clear that the electrical efficiency follows the same trend as the isentropic efficiency of the turbine, the maximum point of which, however, is shifted to the right, due to the monotonous increase in the mass flow rate ratio.

Therefore, to better understand the cause of the inversion of the operating condition that guarantees the maximum electrical efficiency, before and after the maximum point, for the same power conditions, the evolution of pressure ratio has been reported.

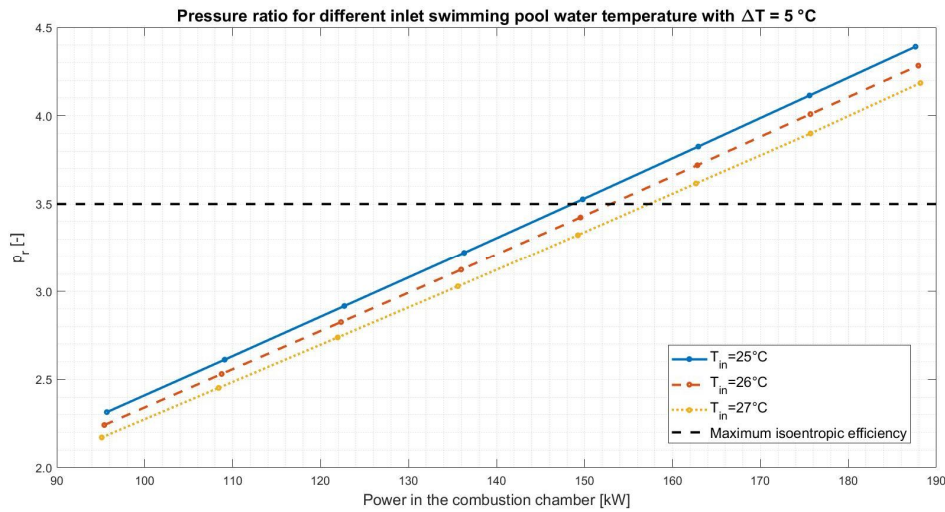


Figure 4.3 Evolution of the pressure ratio with different pool water inlet temperatures

The pressure ratio is always higher for a lower pool water inlet temperature, due to the constraints imposed on the heat exchanger to avoid condensation in the turbine. In this case, for low thermal powers there will be a better isentropic efficiency up to the optimal p_r , equal to 3.5 (Figure 2.3). Once this point of optimal efficiency is exceeded, it begins to decline (Figure 2.3).

On the other hand, for higher input temperatures, with the same thermal power, as the optimum point of the pressure ratio has not been reached, the isentropic efficiency of the turbine and also the electrical efficiency both increase, until they reach the optimal p_r .

The evolution of the electrical efficiency shown in Figure 4.1, as just demonstrated in physical terms, constitutes an excellent starting point for regulating the plant since, for the same thermal power transferred to the pool water, there will be a greater production of electricity.

An example of implementing this control at high power can be the application of a valve that mixes the just heated water (T_8) with the condenser inlet water (T_7) to raise its temperature. For low powers, instead, it is advisable to activate the system when the swimming pool water temperature (T_7) reaches the lowest acceptable level.

Similar conditions are recorded if the water inlet temperature at the condenser is fixed and the output changes parametrically. In fact it is noted that, before the optimal point, there is a greater electrical efficiency with low differences in the temperature of the pool water, whereas exceeding the optimum, the greater efficiency is maintained by higher differences in temperature.

4. Results

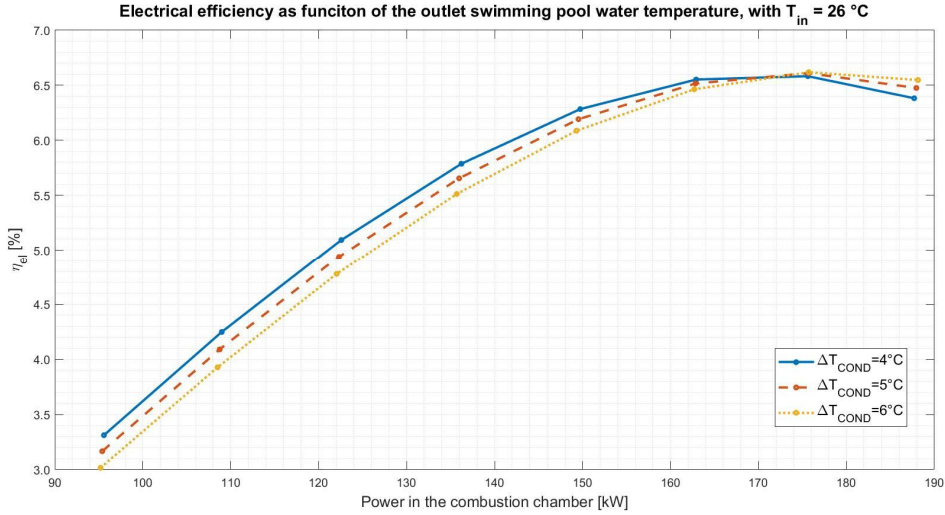


Figure 4.4 Evolution of the electrical efficiency with different variations of pool water temperature

Therefore, a table that summarizes the condenser water control strategy to optimize the electrical efficiency of the system is presented.

Table 4.1 Condenser pool water regulation strategy required to optimize the electrical efficiency of the plant

Fix parameter	Optimal pool water temperature regulation in the condenser	
	$ \dot{Q}_{COND} < 140\text{ [KW]}$	$ \dot{Q}_{COND} \geq 140\text{ [KW]}$
ΔT	minimum T_{in}	maximum T_{in}
T_{in}	minimum ΔT	maximum ΔT

From the complete analysis of the entire range for each possible linear combination between the input and output temperature of the condenser, it emerges that the effect of temperature input has a greater effect on the electrical efficiency of the system compared to the temperature difference of the water to the condenser. For this reason, both of these extreme cases will be shown.

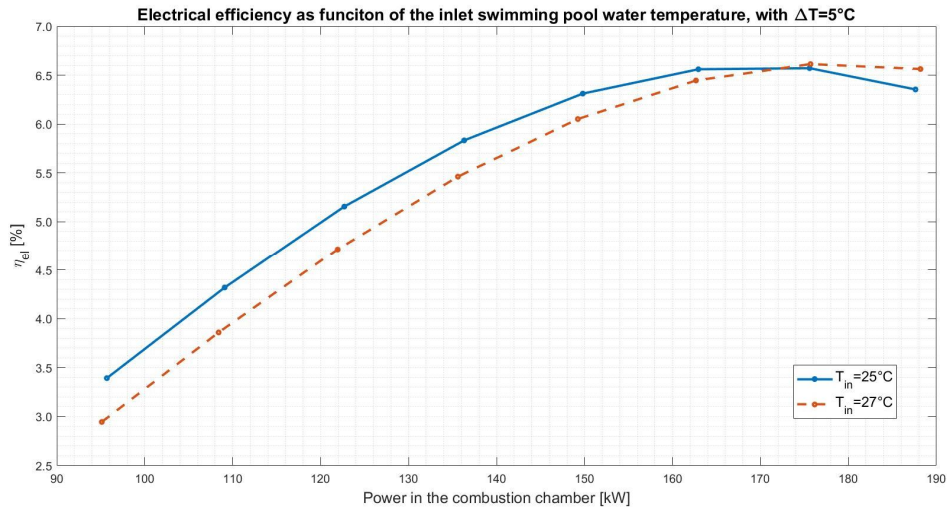


Figure 4.5 Extreme cases of electrical efficiency recorded in the range analyzed in the condenser

Comparing the curves of Figure 4.5, it appears clear that, with a simple adjustment of the water inlet temperature to the condenser, it is possible to increase, in absolute terms, the electric efficiency of 0.45% and 0.21% respectively for low and high powers required in the condenser.

Through the suggested regulation (Table 4.1), the net electric power produced records, for low thermal demands, an increase of 16%, i.e. from 2.8 kW to 3.25 kW, while for high powers there is an increase of 3.6%, i.e. from 11.92 kW to 12.35 kW.

As regards to the thermal efficiency, there is an opposite trend compared to that of the electrical one.

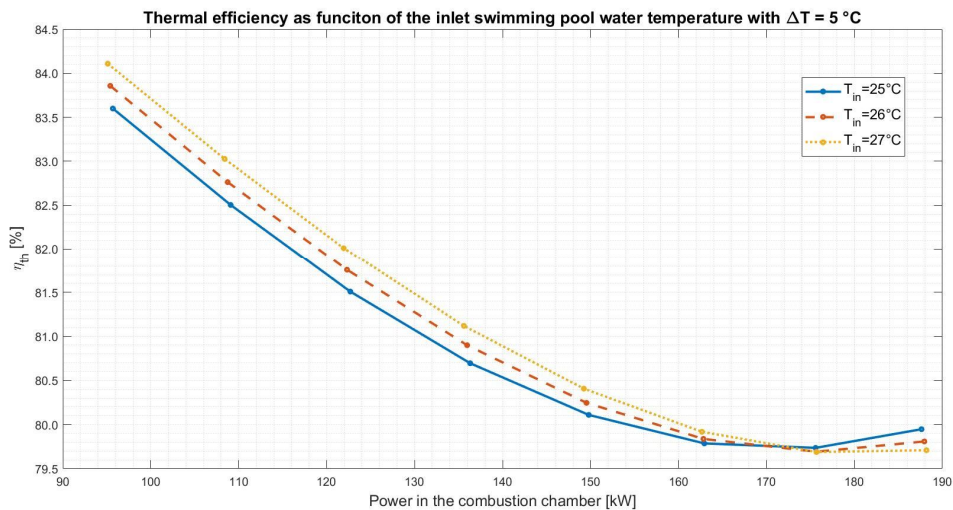


Figure 4.6 Evolution of thermal efficiency with different temperatures of pool water inlet

4. Results

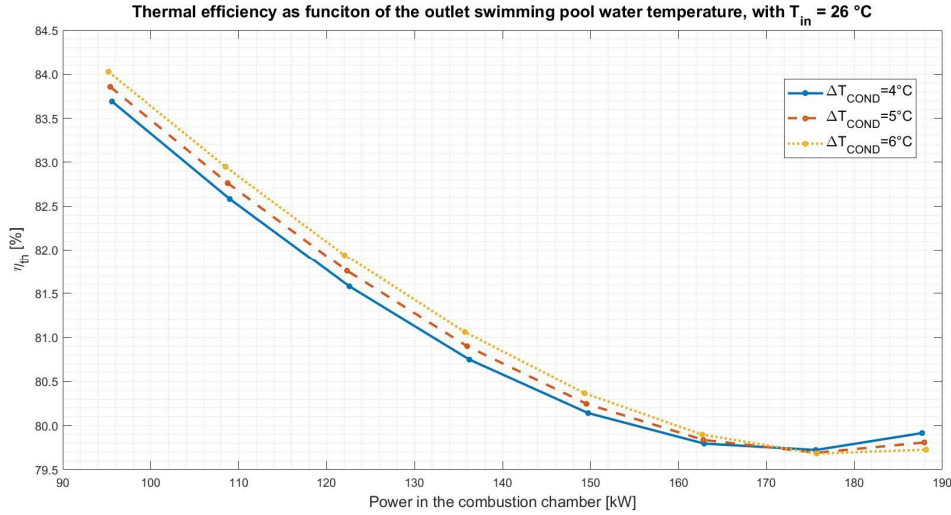


Figure 4.7 Evolution of the thermal efficiency with different variations of pool water temperature

The explanation of this trend, which is closely related to the thermal one, can take place by focusing on the thermal efficiency formula:

$$\eta_{th} = \frac{\dot{Q}_{cond}}{LCV \cdot \dot{m}_{bio}} \quad (64)$$

The thermal power of the biomass released in the combustion chamber, that is the denominator of formula (64), is necessary for both the production of thermal and electric power. However, with the same condenser power required, it is possible to increase the electric power by simply adjusting the water temperature to the condenser, as previously explained. Therefore, in stationary conditions, the increase in electrical power will be offset by a greater quantity of burnt pellets. The consequence is a reduction in thermal efficiency.

Finally, having defined the thermal and the electrical efficiencies of the cogeneration plant (η_{CHP_H} and η_{CHP_E}), the Primary Energy Savings (PES) was calculated as the last parameter. It represents the relative saving of primary energy achievable by a cogeneration plant compared to separate plants for the production of thermal energy and electricity [83]. In accordance with the EU directive [84], it was evaluated using the formula (65):

$$PES = \left(1 - \frac{1}{\frac{\eta_{CHP_H}}{\eta_{REF_H}} + \frac{\eta_{CHP_E}}{\eta_{REF_E}}} \right) \cdot 100 \quad (65)$$

For the reference efficiencies (η_{REF_H} and η_{REF_E}), those previously applied in studies conducted on small Portuguese CHP systems were used [85]. Specifically, 0.9 was used as the harmonized efficiency reference value for separate production of heat (η_{REF_H}) (considering that the thermal energy produced is in the form of hot water from a natural gas boiler produced before 2016 [86]), while 0.445 was assumed as the harmonized efficiency reference value for separate production of electricity (η_{REF_E}) (considering that

the electrical energy is produced in a natural-gas fuelled power plant built before 2012 and an aggregated correction factor that includes the climatic specificities and the grid losses for low-voltage level end-users [86]).

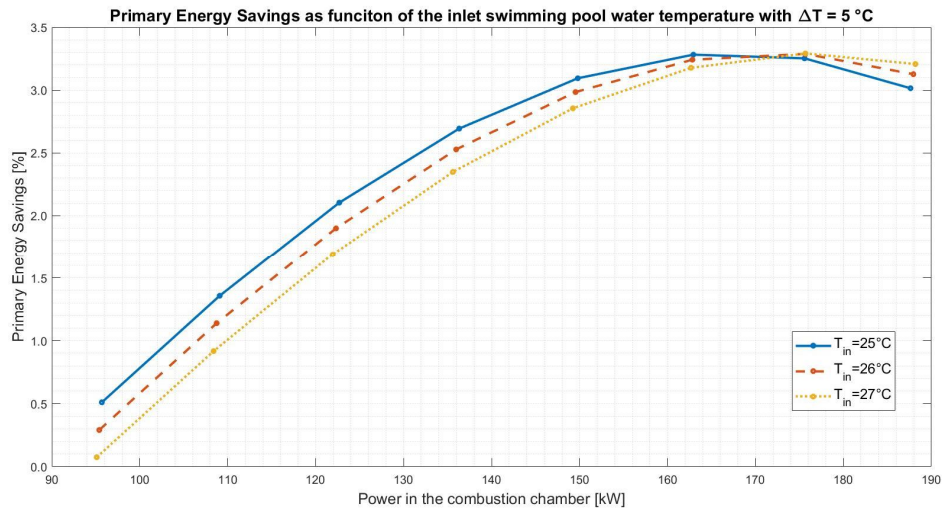


Figure 4.8 Evolution of Primary Energy Savings with different temperatures of pool water inlet

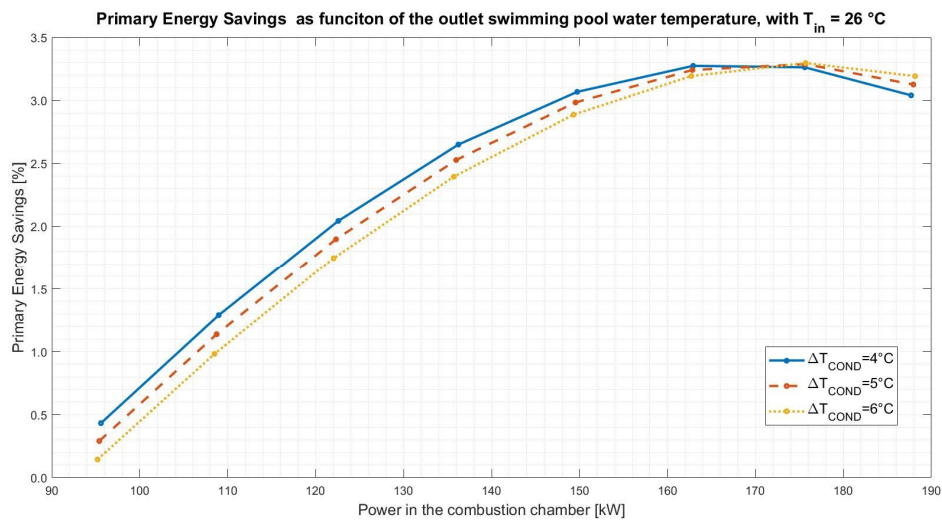


Figure 4.9 Evolution of Primary Energy Savings with different variations of pool water temperature

Through Figure 4.8 and Figure 4.9, it is clear that, in the various operating conditions of the condenser, the evolution of the primary energy savings follows the one of the electrical efficiency of the system (Figure 4.1 and Figure 4.4). Therefore maximizing the efficiency of the plant, at the same time the PES is also maximized.

4. Results

In conclusion, it is suggested to adopt the regulation proposed in Figure 4.5 since, with the same thermal power released by the condenser, the excess energy released in the combustion chamber is completely transformed into electrical energy.

Once the maximum production conditions of the plant have been defined (Figure 4.5), the thermodynamic results in the benchmarks obtained in the simulations of the model explained in Chapter 3.1 are now shown.

Starting from the huge amount of data obtained, linked to the combinations of the three variable condenser ranges (Chapter 3.1.1), it was decided to show only the maximum electrical efficiency condition (Case I), the condition adopted in Chapter 3.3 in the hybrid solution (Case II) and another two noteworthy conditions of the exergoeconomic analysis (Cases III and IV).

The conditions of the condenser in these case studies of the plant (Figure 2.2), are shown in Table 4.2.

Table 4.2 Operating conditions of relevant case studies

Case	\dot{Q}_{COND} [kW]	T_7 [°C]	T_8 [°C]
I	140	26	32
II	110	26	31
III	150	25	32
IV	150	27	30

Table 4.3 Temperatures and pressures recorded in the benchmarks of relevant case studies

T [°C]	Case				P [kPa]	Case			
	I	II	III	IV		I	II	III	IV
T_1	32.5	30.7	32.6	31.5	P_1	897	673	969	960
T_2	90.0	90.0	90.0	90.0	P_2	897	673	969	960
T_3	56.6	63.9	55.2	55.4	P_3	228	216	229	221
T_4	32.2	30.7	32.3	31.2	P_4	228	216	229	221
T_5	95.0	95.0	95.0	95.0	P_5	300	300	300	300
T_6	89.9	74.6	90.1	89.7	P_6	300	300	300	300
T_7	26.0	26.0	25.0	27.0	P_7	300	300	300	300
T_8	32.0	31.0	32.0	30.0	P_8	300	300	300	300
T_9	16.1	16.1	16.1	16.1	P_9	101	101	101	101
T_{10}	16.1	16.1	16.1	16.1	P_{10}	101	101	101	101
T_{11}	113.8	100.9	117.8	117.7	P_{11}	101	101	101	101

Table 4.4 Mass flow rates recorded in the benchmarks of relevant case studies

Mass flow rate $\left[\frac{kg}{s}\right]$	Case			
	I	II	III	IV
$\dot{m}_{ORC} = (\dot{m}_1, \dot{m}_2, \dot{m}_3, \dot{m}_4)$	0.670	0.503	0.724	0.717
$\dot{m}_{H_2O_B} = (\dot{m}_5, \dot{m}_6)$	7.297	1.393	8.041	7.404
$\dot{m}_{H_2O_{SP}} = (\dot{m}_7, \dot{m}_8)$	5.583	5.264	5.127	11.963

$\dot{m}_{AIR} = (\dot{m}_9)$	0.100	0.087	0.104	0.104
$\dot{m}_{BIO} = (\dot{m}_{10})$	0.010	0.008	0.010	0.010
$\dot{m}_{EG} = (\dot{m}_{11})$	0.110	0.094	0.114	0.114

Table 4.5 Main results obtained in the relevant case studies

Parameter	Case			
	I	II	III	IV
Q_{CC} [kW]	175.70	135.97	188.10	187.77
Q_{EVA} [kW]	153.10	118.68	163.83	163.55
P_{elTURB} [kW]	11.84	7.79	12.53	12.28
Q_{COND} [kW]	140.00	110.00	150.00	150.00
P_{elPUMP} [kW]	0.21	106.48	0.25	0.25
P_{elNET} [kW]	11.63	7.69	12.28	12.04
η_{el} [%]	6.62	5.65	6.53	6.41
η_{th} [%]	79.68	80.90	79.75	79.88
PES [%]	3.296	2.528	3.178	3.066

These thermodynamic results, besides giving a clear overview of some relevant conditions of the plant, will be extremely useful for the last exergoeconomic considerations discussed in Chapter 4.2.

Finally, after an accurate processing of the data obtained in all combinations of condenser powers and temperatures, tables have been drawn up which show the operating range of all the system's parameters. These data provide useful information for sizing other plant components, not considered in this thesis, such as pipes, and to develop future analyses, such as thermomechanical resistance.

Table 4.6 Range of temperatures and pressures recorded in all the simulations

T [°C]	Range	\dot{Q}_{COND} [kW]	T_7 [°C]	T_8 [°C]	P [kPa]	Range	\dot{Q}_{COND} [kW]	T_7 [°C]	T_8 [°C]
T_1	Min. 28.3 Max. 33.0	80 150	25 27	30 32	P_1	Min. 460 Max. 972	80 150	25 27	30 32
T_2	Min. 90 Max. 90	All the conditions			P_2	Min. 460 Max. 972	80 150	25 27	30 32
T_3	Min. 55.1 Max. 76.4	150 80	27 27	32 32	P_3	Min. 199 Max. 232	80 150	25 27	30 32
T_4	Min. 28.2 Max. 32.7	80 150	25 27	30 32	P_4	Min. 199 Max. 232	80 150	25 27	30 32
T_5	Min. 95 Max. 95	All the conditions			P_5	Min. 300 Max. 300	All the conditions		
T_6	Min. 57.4 Max. 90.2	80 150	25 27	30 32	P_6	Min. 300 Max. 300	All the conditions		
T_7	Min. 25 Max. 27	User condition			P_7	Min. 300 Max. 300	All the conditions		
T_8	Min. 30 Max. 32	User condition			P_8	Min. 300 Max. 300	All the conditions		

4. Results

T_9	Min. 16.1 Max. 16.1	All the conditions			P_9	Min. 101 Max. 101	All the conditions		
T_{10}	Min. 16.1 Max. 16.1	All the conditions			P_{10}	Min. 101 Max. 101	All the conditions		
T_{11}	Min. 87.5 Max. 117.9	80	27	32	P_{11}	Min. 101 Max. 101	All the conditions		

Table 4.7 Range of mass flow rates recorded in all the simulations

Mass flow rate $\left[\frac{kg}{s}\right]$	Range	\dot{Q}_{COND} [kW]	T_7 [°C]	T_8 [°C]
$\dot{m}_{ORC} = (\dot{m}_1, \dot{m}_2, \dot{m}_3, \dot{m}_4)$	Min. 0.344 Max. 0.726	80 150	25 27	30 32
$\dot{m}_{H_2O_B} = (\dot{m}_5, \dot{m}_6)$	Min. 0.531 Max. 8.223	80 150	25 27	30 32
$\dot{m}_{H_2O_{SP}} = (\dot{m}_7, \dot{m}_8)$	Min. 2.734 Max. 11.963	80 150	25 27	32 30
$\dot{m}_{AIR} = (\dot{m}_9)$	Min. 0.070 Max. 0.104	80 150	27 27	32 32
$\dot{m}_{BIO} = (\dot{m}_{10})$	Min. 0.005 Max. 0.010	80 150	27 27	32 32
$\dot{m}_{EG} = (\dot{m}_{11})$	Min. 0.075 Max. 0.114	80 150	27 27	32 32

Table 4.8 Range of the main thermodynamic results evaluated in all the simulations

Parameter	Range	\dot{Q}_{COND} [kW]	T_7 [°C]	T_8 [°C]
Q_{CC} [kW]	Min. 95.11 Max. 188.18	80 150	27 27	32 32
Q_{EVA} [kW]	Min. 83.16 Max. 163.90	80 150	27 27	32 32
P_{elTURB} [kW]	Min. 2.84 Max. 12.60	80 150	27 27	32 32
Q_{COND} [kW]	Min. 80.00 Max. 150.00	User condition		
P_{elPUMP} [kW]	Min. 0,04 Max. 0.25	80 150	27 27	32 32
P_{elNET} [kW]	Min. 2.80 Max. 12.35	80 150	27 27	32 32
η_{el} [%]	Min. 2.95 Max. 6.62	80 140	27 26	32 32
η_{th} [%]	Min. 79.68 Max. 84.11	140 80	26 27	32 32
η_{TOT} [%]	Min. 86.27 Max. 87.06	150 80	27 27	32 32
PES [%]	Min. 0.07 Max. 3.30	80 140	27 26	32 32

From the tables shown above, some interesting results can be extracted, such as the maximum pressure recorded in the ORC circuit, equal to 9.72 in the benchmarks 1 and 2. Moreover, the combustion chamber is correctly dimensioned, since the maximum power required is lower than 190 kW, and the minimum nominal power of the turbine never reaches values below 2 kW, in order to prevent low electrical efficiencies.

Regarding the mass flow rates, for the simulated ranges, a pellet consumption between 5 and 10 $\left[\frac{g}{s}\right]$ was obtained, while regarding the boiler water and the ORC fluid, a mass flow was estimated proportional to the heat output required from the condenser, between 0.53 and 8.22 $\left[\frac{kg}{s}\right]$ and between 0.34 and 0.73 $\left[\frac{kg}{s}\right]$ respectively. Finally, the pool water flow rate is variable between 2.73 and 11.96 $\left[\frac{kg}{s}\right]$, depending on the temperature range requested by the user.

In conclusion, from the thermodynamic point of view, there is a considerable reduction in electrical efficiency for low condenser powers due to a low-pressure ratio and, for the same condenser power, it is suggested to adopt the temperature regulation, proposed in Table 4.1, to optimize global plant production.

4.2 Exergy and exergoeconomic results

In this subchapter will be shown the main results of the exergetic analysis related to the operating conditions that maximizes electrical efficiency. Subsequently, through the optimization phase, will be analysed the costs for exergetic units produced, associated to the whole operative range of the condenser, in order to find where the minimum value occurs, and finally will be identified, through the design improvement phase, which part of the process needs a design variation in order to improve the system.

❖ Exergy and exergoeconomic analysis

As anticipated, are now shown the main exergetic and exergoeconomic results obtained with the model described in Chapter 3.2, related to the case of greater electrical efficiency of the plant (Case I of Table 4.2).

4. Results

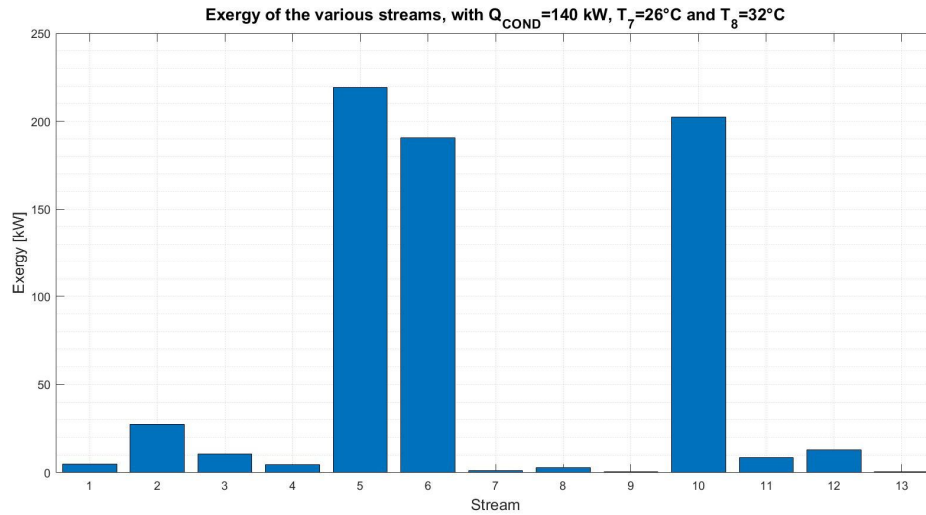


Figure 4.10 Exergies of the streams in the operating condition that provides the greatest electrical efficiency of the system

It should be noted that the major exergies are recorded respectively for the fifth stream, i.e. hot water at 95 °C, for the tenth, i.e. the pellet to be burned and the sixth, i.e. the hot water exiting the evaporator. Comparing the exergy of the pellet (E_{10}) with the increase in exergy of the hot water that crosses the evaporator ($E_5 - E_6$), it is already evident that the least efficient component of the exergetic system is the combustion chamber. Furthermore, focusing attention on the ORC fluid (streams 1, 2, 3 and 4), as expected, the increase in exergy is recorded after the pump and the evaporator, while the decrease after the turbine and condenser outlet.

By processing these data, within the equations (39) and (37), it is also possible to determine where are recorded the major irreversibilities and the exergetic efficiency of the components, values of which are shown in Figure 4.11 and Figure 4.12.

Irreversibility of the components [%]

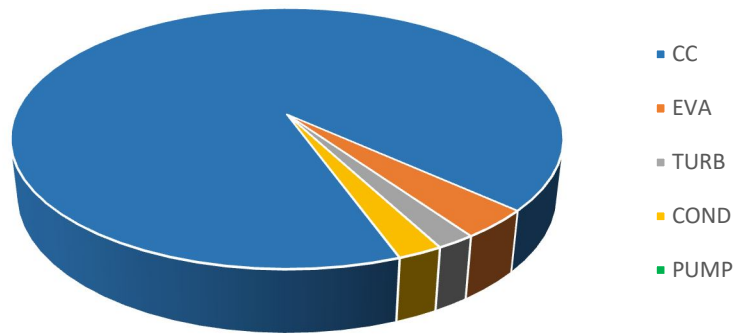


Figure 4.11 Irreversibilities of the components in the operating condition that provides the greatest electrical efficiency of the system

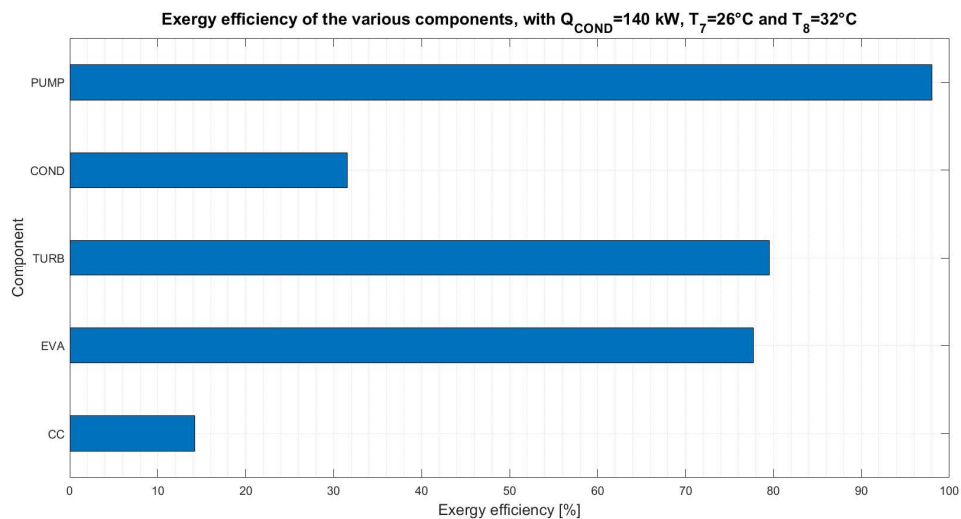


Figure 4.12 Exergy efficiency of the components in the operating condition that provides the greatest electrical efficiency of the system

From the point of view of the exergetic efficiency (Figure 4.12), the most performing component is the pump ($\epsilon_{\text{PUMP}} = 98\%$), followed by the turbine ($\epsilon_{\text{TURB}} = 79.55\%$) and the evaporator ($\epsilon_{\text{EVA}} = 77.69\%$), while the least efficient are the combustion chamber ($\epsilon_{\text{CC}} = 14.23\%$) and the condenser ($\epsilon_{\text{COND}} = 31.56\%$).

Since the lower efficiency is recorded in the first conversion process, due to a hot resource at relatively low temperatures, the element with greater irreversibility is the combustion chamber ($I_{\text{CC}} = 92.25\%$), followed by the evaporator ($I_{\text{EVA}} = 3.59\%$), the condenser ($I_{\text{COND}} = 2.23\%$), the turbine ($I_{\text{TURB}} = 1.93\%$) and finally from by the pump, the irreversibility of which is almost zero ($I_{\text{PUMP}} \approx 0\%$) (Figure 4.11).

4. Results

As expected, there was therefore an opposite trend between the one recorded for the exergetic efficiency and that one of the irreversibility.

Having reached this point, it is now possible to obtain and show the exergy cost of each stream.

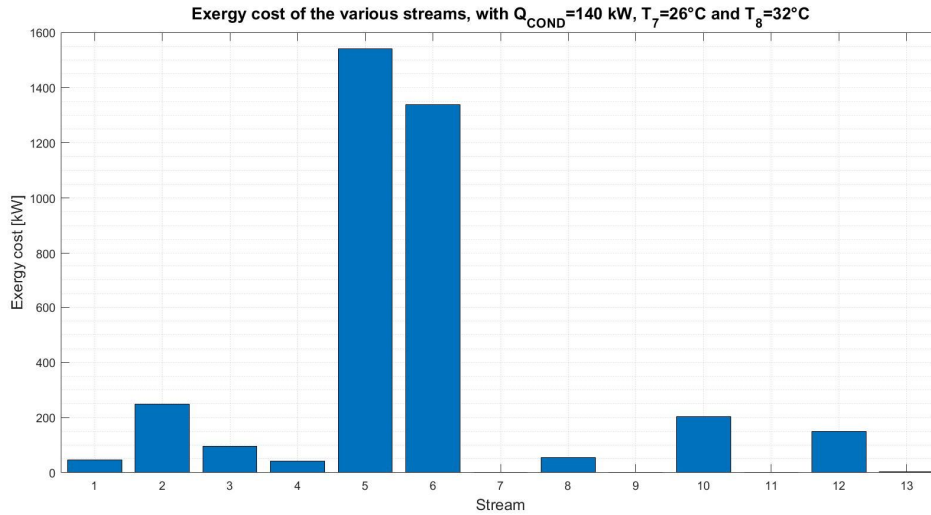


Figure 4.13 Exergy cost of the streams in the operating condition that provides the greatest electrical efficiency of the system

The exergetic cost, by definition, considers the exergy of the stream plus the irreversibilities generated through an allocation process. Therefore, streams 5 and 6 are those with the greatest exergetic cost, since they are those with the greatest exergetic content and those that interact with the most irreversible component.

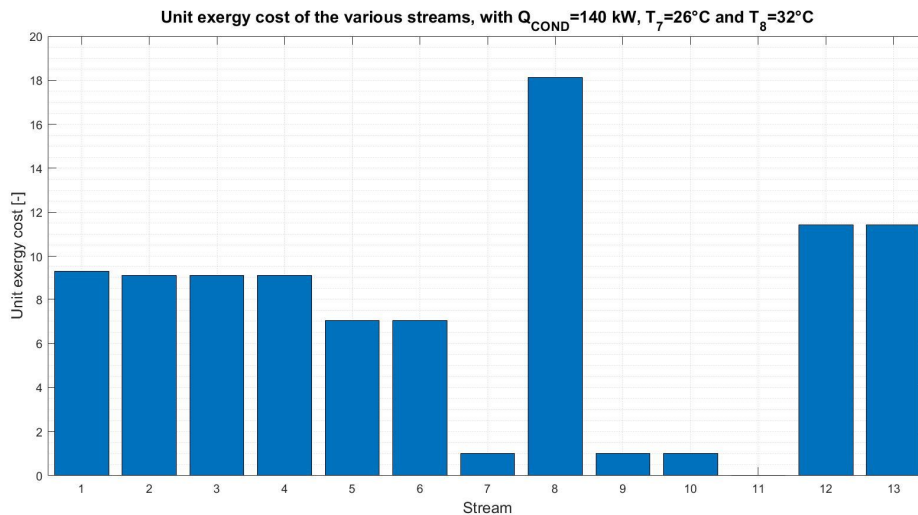


Figure 4.14 Unit exergy cost of the streams in the operating condition that provides the greatest electrical efficiency of the system

From the calculation of the unit exergy cost, for definition, a unitary value was obtained for the input streams in the control volume, ie. the incoming water (k_7^*),

the air (k_9^*) and the pellet (k_{10}^*), a zero value for the discharges, i.e. The exhaust gases (k_{11}^*).

For each intermediate product of the process there is an increase in the unit exergy cost. In fact, the one related to the boiler water ($k_5^* = k_6^* = 7.03$) is less than that of the ORC cycle ($k_1^* = 9.26$ and $k_2^* = k_3^* = k_4^* = 9.08$), which, in turn, is smaller than that of the mechanical product ($k_{12}^* = k_{13}^* = 11.42$). From this concatenation, the highest value is recorded for the last useful product, the thermal product of the pool water ($k_8^* = 18.12$).

In terms of energy costs, the stream with the highest cost is the pool water exiting the condenser.

Going back to the exergoeconomic considerations, Figure 4.15, it is also noted that the exergo economic cost has the same trend of the exergy cost.

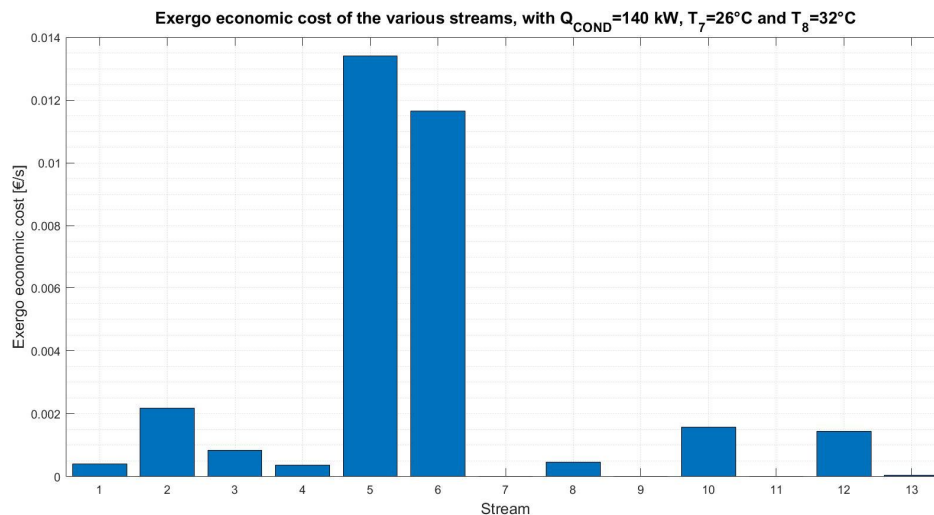


Figure 4.15 Exergo economic cost of the streams in the operating condition that provides the greatest electrical efficiency of the system

Obviously, the stream 5 has the greatest cost as it is generated in the component with the highest investment cost and moreover it requires, to be generated, the consumption the pellet, that is the only operational cost of the plant.

In conclusion, is shown the main result of this analysis, namely the unit of exergo economic cost.

4. Results

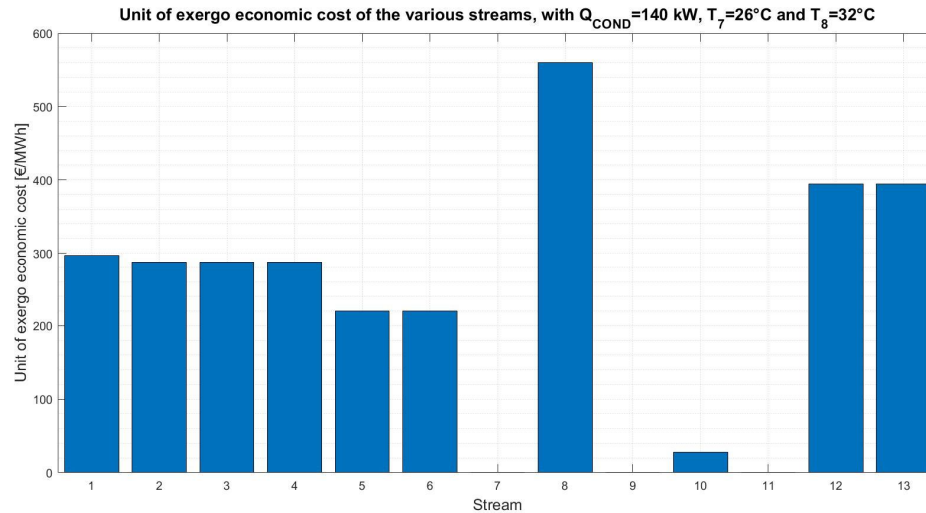


Figure 4.16 Unit of exergo economic cost of the streams in the operating condition that provides the greatest electrical efficiency of the system

Also in this case there is a close correlation between the exergetic (Figure 4.13) and exergoeconomic trends (Figure 4.16).

For each intermediate stream, in fact, there is an increase in the cost, passing from the initial $28 \left[\frac{\text{€}}{\text{MWh}} \right]$ of the pellet, until reach $412.88 \left[\frac{\text{€}}{\text{MWh}} \right]$ for the mechanical product and $576.23 \left[\frac{\text{€}}{\text{MWh}} \right]$ for the thermal product.

After having analysed in detail, for only one particular operating condition on the condenser, the energy and exergoeconomic values of the various streams and components, now more general considerations are shown. The new considerations that will be discussed are related exclusively to the exergoeconomic results of the plant products (mechanical and thermal), in the entire range of operating conditions of the condenser, in order to discover the optimal operative situation.

❖ Optimization

In the following paragraph the unit of exergo economic cost of the mechanical and thermal product will be investigated, as a function of the condenser parameters, according to the range reported in Chapter 3.1.1.

Due to the considerable amount of operating conditions, it was decided to analyze the costs of mechanical exergy following the approach used in the analysis of electrical efficiency. Therefore, for the first analysis, it was decided to set the difference in temperature of the pool water, between the input and output of the condenser, equal to 5 degrees Celsius.

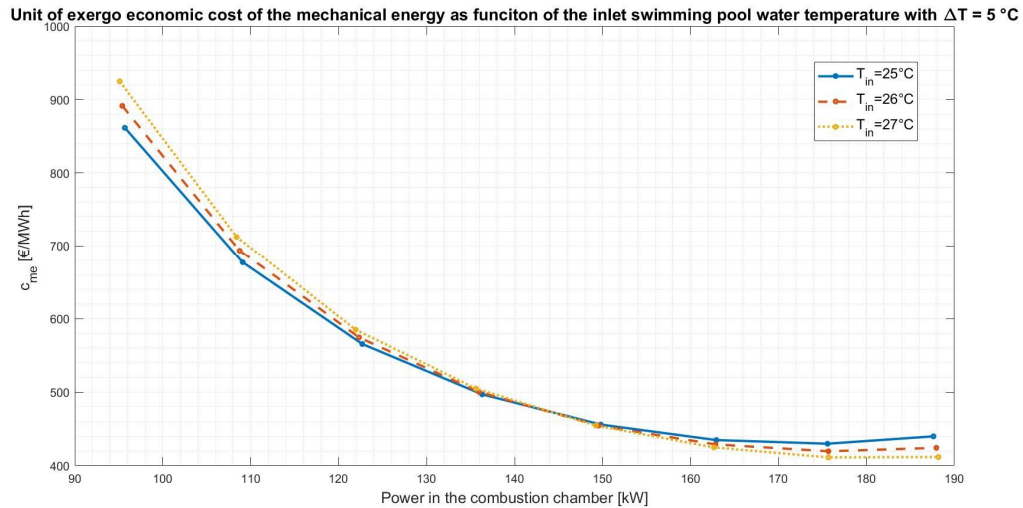


Figure 4.17 Evolution of the unit of exergo economic cost of the mechanical product with different inlet pool water temperatures

It is noted that all the cost curves for exergetic units of Figure 4.17 have a decreasing evolution as the thermal power required by the condenser increases. To understand in detail the trend of this curve it is necessary to analyze the equation from which it was generated:

$$c_{me} = c_{12} = \frac{C_{12}}{E_{12}} \quad \left[\frac{\text{€}}{\text{MWh}} \right] \quad (66)$$

From the analysis of the results it is noted that, by increasing the power required in the condenser, there is a small increase in the exergo economic cost (C_{12}) and a considerable increase in the exergy produced (E_{12}).

In fact, in the thermodynamic results section (

Table 4.8), it has been shown that by increasing the load in the condenser, also the mechanical power generated, and consequently the electrical one, increases. Furthermore, it should be remembered that the mechanical efficiency increases for low thermal loads on the condenser with low inlet pool water temperatures, while for high thermal loads with high inlet water temperatures in the condenser (Figure 4.1).

From the combination of these two effects, as shown in Figure 4.17, to reduce the cost of the energy produced, it is suggested to operate, whenever possible, at high thermal powers and with high temperatures of the water entering the condenser. If, on the other hand, the user requires low thermal powers, it is suggested to have the minimum water temperature at the condenser inlet.

In conclusion, the strategy to minimize the cost of the mechanical exergy unit is similar to that adopted to maximize electrical efficiency.

4. Results

These considerations are the same if the water inlet temperature is kept fixed at the condenser and the thermal power and temperature required by the user are parametrically varied (Figure 4.18).

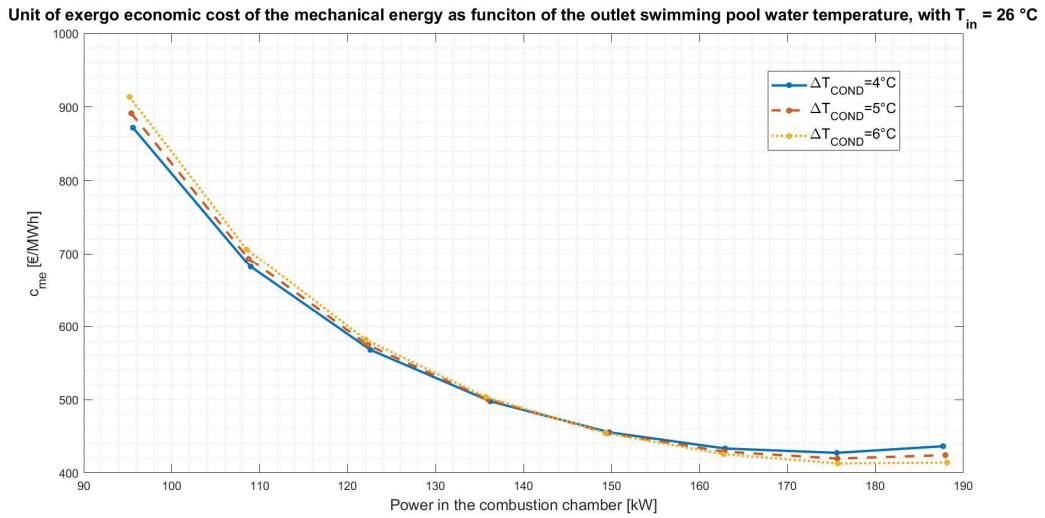


Figure 4.18 Evolution of the unit of exergo economic cost of the mechanical product with the same inlet and different outlet of pool water temperature

For the entire range of condenser temperatures, are reported, as in the case of the turbine efficiency, the extreme cases of the cost per unit of exergy of the mechanical product are reported.

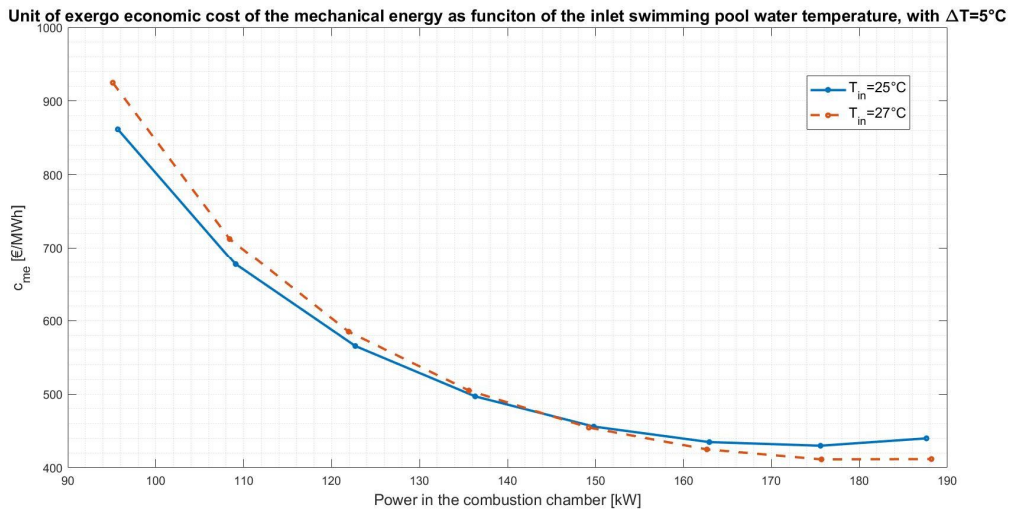


Figure 4.19 Extreme cases of the unit of exergo economic cost of the mechanical product recorded in the range analyzed in the condenser

The best regulation requires a condenser water inlet temperature equal to $25\text{ }^{\circ}\text{C}$ for low thermal loads ($Q_{COND} \leq 120\text{ kW}$) and $27\text{ }^{\circ}\text{C}$ for the high ones ($Q_{COND} > 120\text{ kW}$). Therefore, fixed at $5\text{ }^{\circ}\text{C}$ the increase in the heated pool water temperature, there will be a saving of the unit cost of the mechanical exergy equal to 63.4 and $28.2 \left[\frac{\text{€}}{\text{MWh}} \right]$ respectively to the two extreme thermal loads.

However, the most interesting result of the following analysis is in the calculation of the unit exergo economic cost of the thermal product of the cogeneration plant.

It was considered useful to report the equation that determined the trends of the figures shown below:

$$c_{th} = c_8 = \frac{C_8}{E_8} = \frac{C_8}{e_8 \cdot \dot{m}_8} \quad \left[\frac{\text{€}}{\text{MWh}} \right] \quad (67)$$

Also in this case it was decided to start the result presentation by setting the difference in temperature of the pool water, between the input and output of the condenser, equal to 5 degrees Celsius.

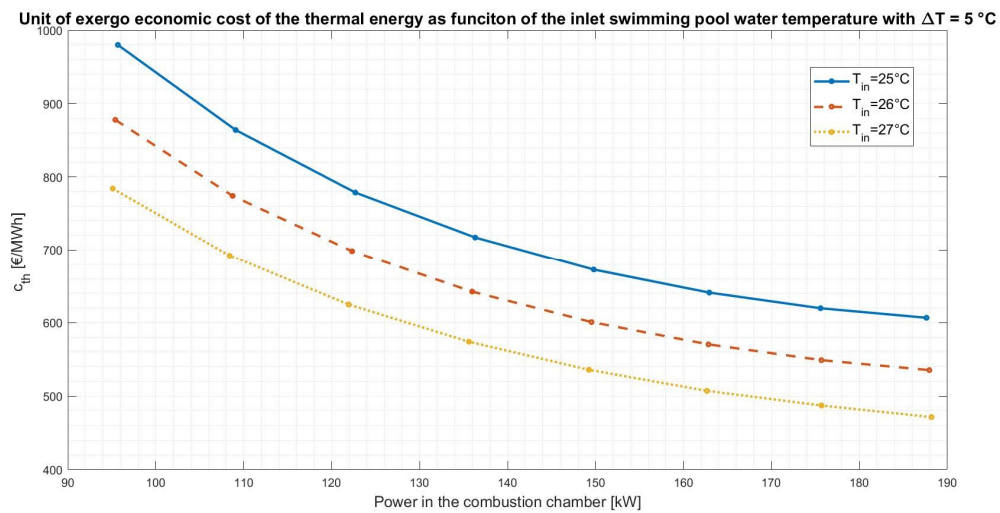


Figure 4.20 Evolution of the unit of exergo economic cost of the thermal product with different temperatures of pool water inlet

The trend of the curves in Figure 4.20 is related through the denominator of (69). Obviously, for all temperatures, the decreasing evolution is recorded as grow the required load on the condenser, due to the exergy increase in the benchmark 8.

In the case of Figure 4.20, with the same load at the condenser, there will be the same water mass flow rate, since the difference in temperature of the pool water at the ends of the condenser is the same.

The parameter that has the greatest variation in the equation (67) is therefore the exergy per unit of mass of the flow 8 (e_8), which rises by increasing the outlet temperature.

Therefore, to minimize the unit cost of the thermal exergetic unit produced, with the same water thermal variation and mass flow rate at the extremes of the condenser, it is necessary to have the highest outlet water temperature in the condenser.

4. Results

Finally, the opposite case is shown, that is the one with a fix outlet water temperature in the condenser, so a fix exergy per unit of mass (e_8), while is changed parametrically the temperature of the pool water entering the condenser and, consequently, the mass flow rate.

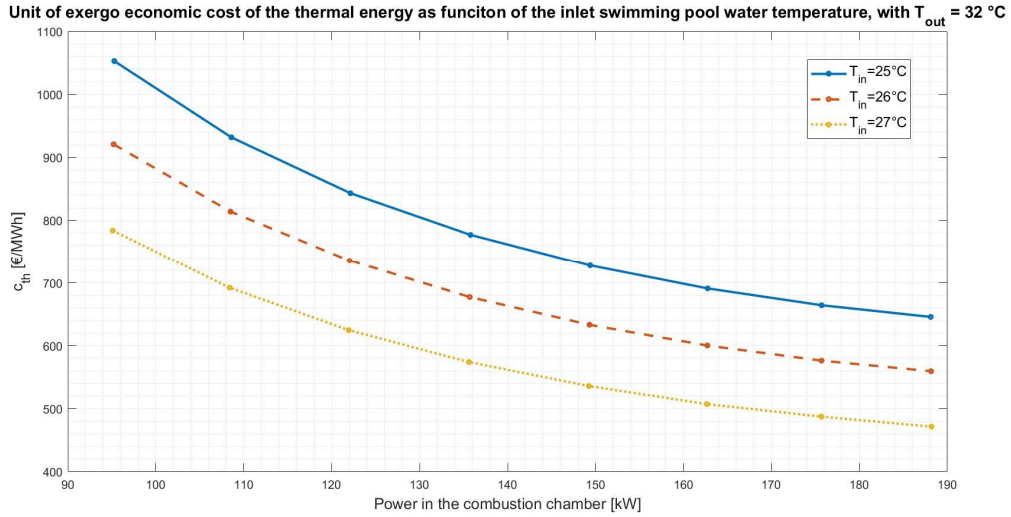


Figure 4.21 Evolution of the unit of exergo economic cost of the thermal product with the same outlet and different inlet of pool water temperature

The trend of Figure 4.21 is similar to that of Figure 4.20 since, also in this case, in the range of temperatures and thermal powers analyzed, there are minimal exergoeconomic costs variations compared to the exergy of the outlet pool water of the condenser. To better illustrate the concept related to this trend, in Figure 4.22 have been represented the terms used in equation (67).

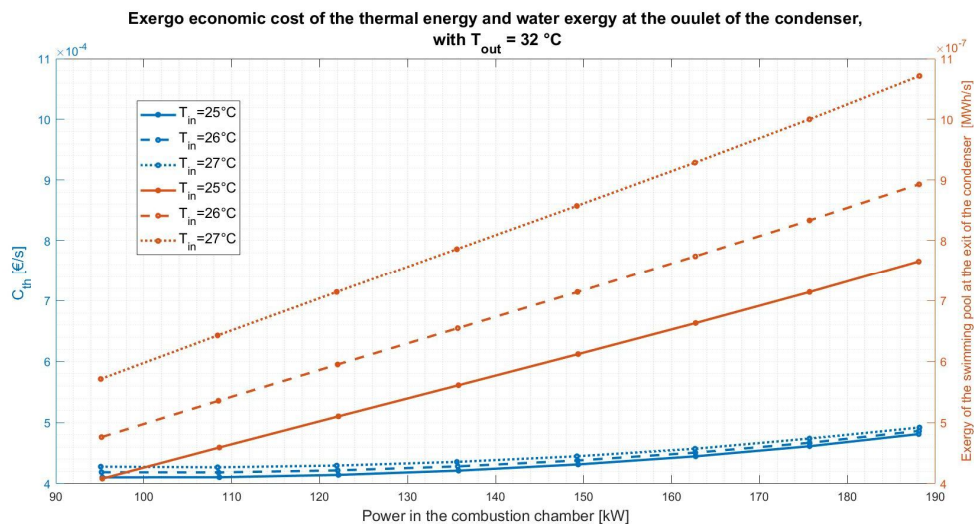


Figure 4.22 Evolution of the exergo economic cost of the thermal product and the outlet water condenser exergy with different pool water inlet temperatures

At the same thermal capacity requested from the condenser, there is greater exergy of the pool water exiting from the condenser where there will be a greater temperature difference between inlet and outlet. The exergy per unit of mass (e_8)

remains constant, since in the following parametric analysis the outlet temperature remains fixed ($T_{out} = T_8 = 32\text{ }^\circ\text{C}$), while the mass flow rate (\dot{m}_8) varies in relation to the temperature difference.

It was therefore understood that, to minimize the unit of exergo economic cost of the thermal product, it is necessary to maximize the outlet temperature of the condenser, in order to have large exergies per unit of mass (e_8), and to minimize the variation of water temperature at the condenser ends, to maximize the mass flow rate (m_8).

The analysis of the entire temperature range showed that the greatest effect is found for the temperature difference. It was considered useful for the readers to show the extreme cases of the unit of exergo economic cost, of the cogeneration thermal product, related to the more and less favorable condition.

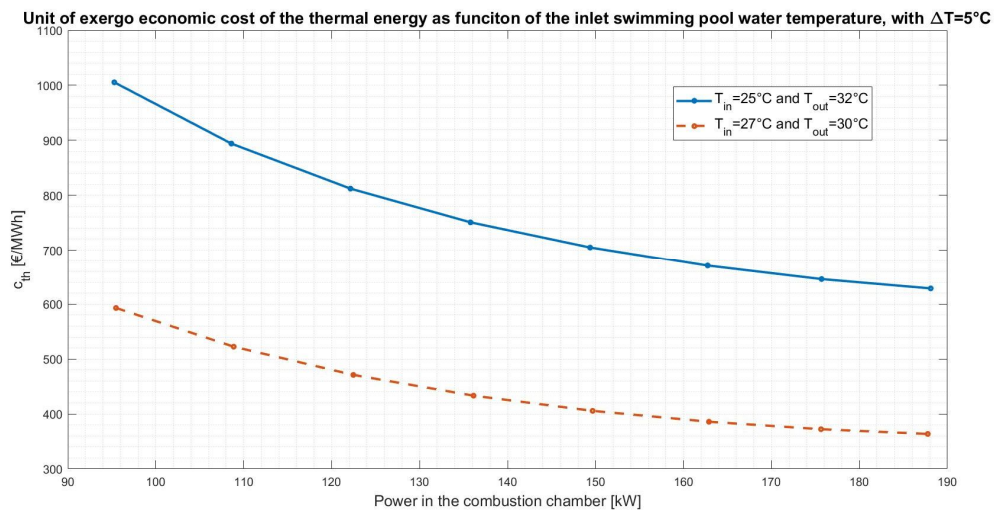


Figure 4.23 Extreme cases of the unit of exergo economic cost of the thermal product recorded in the range analyzed in the condenser

The optimization of operating conditions has shown that for the thermal product there is a single pair of temperatures at the ends of the condenser ($T_{in} = T_7 = 27\text{ }^\circ\text{C}$ and $T_{out} = T_8 = 30\text{ }^\circ\text{C}$) that minimizes the unit of exergo economic cost.

In this condition, there is a cost per exergetic unit variable from $621\left[\frac{\text{€}}{\text{MWh}}\right]$, in the case where $\dot{Q}_{COND} = 80\text{ [kW]}$, to $373\left[\frac{\text{€}}{\text{MWh}}\right]$, in the case where $\dot{Q}_{COND} = 150\text{ [kW]}$. In the optimal condition of temperatures there is a 40% reduction in the cost per produced exergetic unit between the maximum and the minimum load required on the condenser.

Moreover, if the condenser does not work in the ideal temperature condition ($T_{in} = T_7 = 27\text{ }^\circ\text{C}$ and $T_{out} = T_8 = 30\text{ }^\circ\text{C}$), the cost per exergetic unit could increase considerably, even double in the worst case ($T_{in} = T_7 =$

25°C and $T_{out} = T_8 = 32^\circ\text{C}$). In fact, for this last condition, there is a cost per exergetic unit variable from 1052 $\left[\frac{\text{€}}{\text{MWh}}\right]$ (for $\dot{Q}_{COND} = 150 [\text{kW}]$) to 645 $\left[\frac{\text{€}}{\text{MWh}}\right]$ ($\dot{Q}_{COND} = 80 [\text{kW}]$).

In conclusion, from the regulation point of view, the costs per unit of mechanical exergy produced do not vary considerably, while they change extremely per unit of thermal exergy.

Furthermore, considering that the maximum mechanical nominal power produced is two orders of magnitude smaller than the required thermal load in the condenser, following optimization of the exergoeconomic costs in the entire condenser range, it is suggested to work as much as possible at low water flow rates of the swimming pool, high outlet temperatures and high thermal power ($T_{in} = T_7 = 27^\circ\text{C}$ and $T_{out} = T_8 = 30^\circ\text{C}$).

❖ Design improvement

Finally, to conclude the exergoeconomic analysis, was also investigated what change could be made in order to have a better plant performance. The results shown below, obtained following the methodology illustrated in Chapter 3.2.3, refer to the condition that minimizes the cost of the thermal product ($T_{in} = T_7 = 27^\circ\text{C}$ and $T_{out} = T_8 = 30^\circ\text{C}$).

In this section only the relevant results of the exergoeconomic analysis will be shown and discussed, i.e. the cost rate relative to each component (Z + CD), the relative cost difference (r_i) and the exergo economic factor (f), while the unit cost of resources and product will be shown in Appendix B.

Table 4.9 Cost rate of components and cost rate of irreversibility for all components, with $T_{in} = T_7 = 27^\circ\text{C}$ and $T_{out} = T_8 = 30^\circ\text{C}$

\dot{Q}_{COND}	CC	EVA	Z+CD		
			TURB	COND	PUMP
80	0.0009775	0.0003317	0.0004092	0.0002896	$4.646 \cdot 10^{-6}$
90	0.0010751	0.0003352	0.0003927	0.0002838	$4.685 \cdot 10^{-6}$
100	0.0011731	0.0003423	0.0003766	0.0002817	$4.736 \cdot 10^{-6}$
110	0.0012548	0.0003528	0.0003694	0.0002831	$4.801 \cdot 10^{-6}$
120	0.0013485	0.0003667	0.0003790	0.0002879	$4.881 \cdot 10^{-6}$
130	0.0014386	0.0003851	0.0004128	0.0002964	$4.982 \cdot 10^{-6}$
140	0.0015230	0.0004138	0.0004757	0.0003084	$5.111 \cdot 10^{-6}$
150	0.0015879	0.0005256	0.0005700	0.0003242	$5.278 \cdot 10^{-6}$

Table 4.10 Relative cost differences for all components, with $T_{in} = T_7 = 27^\circ\text{C}$ and $T_{out} = T_8 = 30^\circ\text{C}$

\dot{Q}_{COND}	r_i				
	CC	EVA	TURB	COND	PUMP
80	14.133	0.434	0.887	2.402	0.284
90	14.808	0.381	0.649	2.348	0.255
100	16.228	0.344	0.504	2.305	0.226
110	18.767	0.319	0.421	2.278	0.199
120	23.301	0.302	0.385	2.268	0.173
130	32.262	0.293	0.388	2.276	0.150
140	55.398	0.295	0.431	2.303	0.128
150	74.569	0.376	0.514	2.347	0.110

Table 4.11 Exergoeconomic factor for all components, with $T_{in} = T_7 = 27^\circ\text{C}$ and $T_{out} = T_8 = 30^\circ\text{C}$

\dot{Q}_{COND}	f				
	CC	EVA	TURB	COND	PUMP
80	0.243	0.008	0.396	0.007	0.929
90	0.221	0.008	0.412	0.007	0.921
100	0.202	0.008	0.430	0.007	0.911
110	0.189	0.008	0.438	0.007	0.899
120	0.176	0.007	0.427	0.007	0.884
130	0.165	0.007	0.392	0.006	0.866
140	0.156	0.007	0.340	0.006	0.844
150	0.150	0.005	0.284	0.006	0.818

From a first analysis of the plant, Table 4.9, it emerges that combustion chamber (CC) is the component that has the greatest cost rate contribution, followed by the turbine (TURB), the evaporator (EVA) and the condenser (COND). This is due to the fact that these are the components with the highest investment cost and where the greatest irreversibilities are recorded. Consequently, a negligible contribution is recorded for the circulation pump (PUMP).

Moreover the combustion chamber, in addition to having the highest cost rate, is the component from which the greatest improvement could be obtained since it has a relative cost difference significantly higher than the others (Table 4.10).

Finally, once it was defined that the combustion chamber is the component on which to act to improve the plant, the exergoeconomic factor was analyzed to understand the implementation that had to be performed. Since the exergoeconomic value of the combustion chamber has a value closer to zero than unity, the necessary action to be done is to improve the thermodynamic efficiency of the plant. One suggestion that came from the interpretation of this parameter is,

for example, to increase the temperature of the hot water entering the evaporator. However, if for the company is mandatory to respect the constraint on the temperature of the water reached in the combustion chamber, i.e. below the boiling point, it would be suggested to reduce the thermal load exchanged in the evaporator. In fact, the main result of Table 4.11 is that for low thermal loads required by the condenser, and therefore also in the combustion chamber, the exergoeconomic factor increases. So, to improve the efficiency of the whole plant, it would be necessary to reduce the amount of pellets burned. To guarantee, to the users, the same thermal power released to the pool water, part of the energy released by the combustion of the pellet could be replaced with that generated by a different renewable source. Since the temperature range reached by the R245fa fluid at the pump outlet (T_1) is compatible with a preheating through solar thermal energy (Table 4.6), an innovative hybrid solar system solution was designed and designed. Therefore, in the final part of the result of this thesis the thermodynamic results related to this improvement will be shown.

4.3 Hybrid biomass-solar plant results

Once the energy, exergetic and exergoeconomic considerations of the biomass-powered cogeneration plant have been completed, the main energy results related to the design improvement, suggested in Chapter 4.2, will now be shown. The layout and the model of this improved design are those described in Chapter 2.2 and Chapter 3.3 respectively.

Before introducing the results of the models described in Chapter 3.3, it is considered necessary to briefly introduce the “base case”. This scenario occurs in the event that the hybrid system for heating the shower water did not exist, so all the thermal energy required by the shower come from the boiler water. The thermal energy that needs to be realised by the boiler, to supply the same amount of water annually, could be calculated through the formula:

$$Q_{DHW_{BIO}} = \frac{\dot{m}_{DHW} \cdot c_p \cdot (T_{net} - T_{DHW}) \cdot 365}{3600} \quad \left[\frac{KWh}{year} \right] \quad (68)$$

where \dot{m}_{DHW} is the daily mass flow rate consumed for shower ($10000 \frac{kg}{day}$), c_p is the specific heat of the water ($4,186 \frac{KJ}{kg \cdot K}$), T_{net} is the temperature of the water net (13 °C), while T_{DHW} is the temperature of the domestic hot water (40 °C).

From this fast calculation it can be deduced that the absence of a hybrid system would lead, in first approximation, to a request of thermal energy coming from the combustion of biomass equal to 114592 kWh.

Returning to the main case studies, the first significant result of the hybrid system sizing process, described in Chapter 3.3, was the definition of the optimal area of the solar collectors. As can be seen in Figure 4.24, for vacuum panels was obtained an area of 90.3 m², which corresponds to a solar factor of 70.6%, while for flat panels an area was achieved of 88.54 m², which corresponds to a solar factor of 65.6%. From these values it can be deduced that it is necessary to install 42 vacuum panels in the first case and 38 flat panels in the second one.

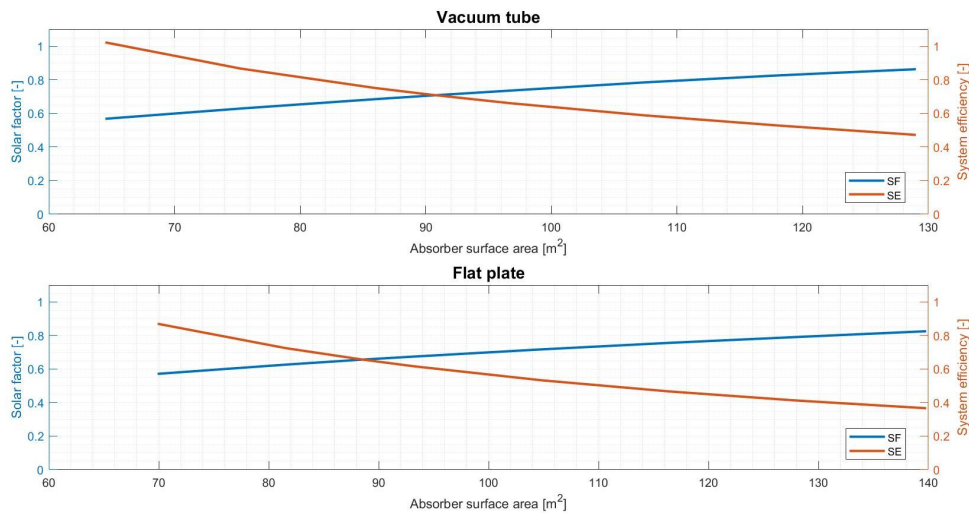


Figure 4.24 Relationship between SF and SE in the analysed cases

As expected, the optimum point of vacuum technology has a solar factor greater than the flat panel, as it has higher performance at high temperatures per unit area. However, for the same area of the absorber, the differences of the SF are not so marked, compared to the general cases, since the plant configuration favours a rapid removal of the energy absorbed by the panel. In fact, the thermal energy of the solar medium is transferred to a fluid with a fixed temperature and to low temperature storage with considerable inertia. This means that the average temperature of the panel is lowered, and the efficiency of the flat plate is favoured rather than the vacuum tube. All this is confirmed by the average annual temperature of the collector during the operations, which is approximately the same, i.e. 43.8 °C for the vacuum tubes and 41.7 °C for the flat plates.

On the chosen area, for both technologies, was also investigated the range in which occurs the optimal tilt angle and the orientation, respect south, the results of which are shown in Table 4.12.

Table 4.12 Result of tilt angle and orientation optimization

	Vacuum panel		Flat plate	
	Minimum	Maximum	Minimum	Maximum
Orientation [°]	0	-1.83	0	- 4.17
Tilt angle [°]	36.94	38.33	37.14	37.93
SF [%]	70.6		65.6	

4. Results

The minimum increments recorded in the solar factor, in the case with the angles optimized compared to those hypothesized, are due to the choices of the initial angles, i.e. the tilt angle equal to the latitude of the investigated location ($\beta = 40.12^\circ$) and a south-facing orientation ($\gamma = 0^\circ$). From the comparison of the two technologies, as expected, the variations in angles have a greater effect on the flat plate as it is a technology with lower efficiency.

Finally, with the aim of giving an overview of the plant, for both technologies are reported the main characteristics of the plant, optimized also through parametric analyses.

Table 4.13 Main plant features of the two optimized solar technologies

	Vacuum panel	Flat plate
Solar panel name	AR 20	WTS-F2 K6
Solar panel absorber area [m ²]	90.3	88.54
Solar panel aperture area [m ²]	116.34	95.38
Installed solar panel unit	42	38
Tilt angle [°]	38.33	37.93
Orientation [°]	0	0
External heat exchanger name	B25T*30	B25T*30
External heat exchanger plates	30	30
External heat exchanger transfer capacity $\left[\frac{W}{K}\right]$	3238.4	3238.4
First storage volume [m ³]	8	8
Solar loop coil [m ²]	18.06	17.71
Second storage volume [m ³]	2	2
Auxiliary system loop coil [m ²]	1	1.5

Through the various measures adopted during optimization, a solar factor of 70.9% is reached for the vacuum panels and 65.9% for the flat panels.

These will be the two definitive options, on which the economic analyses will be conducted and from which the useful thermal parameters will be extracted to define which of the two solutions is the best.

Under these operating conditions there is a net annual consumption of electricity, for the operation of pumps and control systems, equal to 38.6 kWh_{el} for the plant with vacuum panels and 36 kWh_{el} for that with flat plates.

To better understand the operating temperature ranges within a week, are also reported in the following figures the temperatures recorded at the output of the solar collectors and the temperatures in the highest and lowest layer of the first storage. The first and twenty-sixth week of the year were chosen as a reference for the winter and summer period.

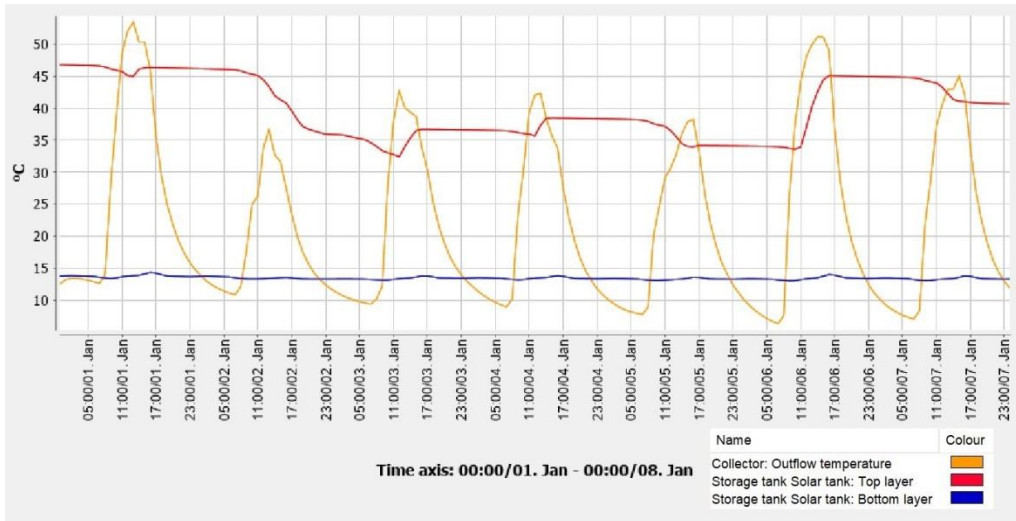


Figure 4.25 Vacuum tube, temperature evolution first week

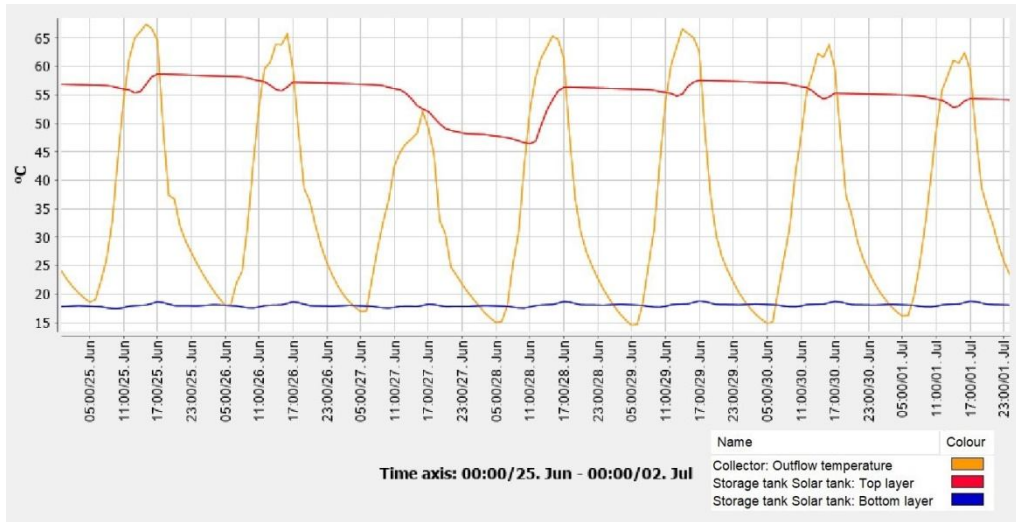


Figure 4.26 Vacuum tube, temperature evolution twenty-sixth week



Figure 4.27 Flat plate, temperature evolution first week

4. Results

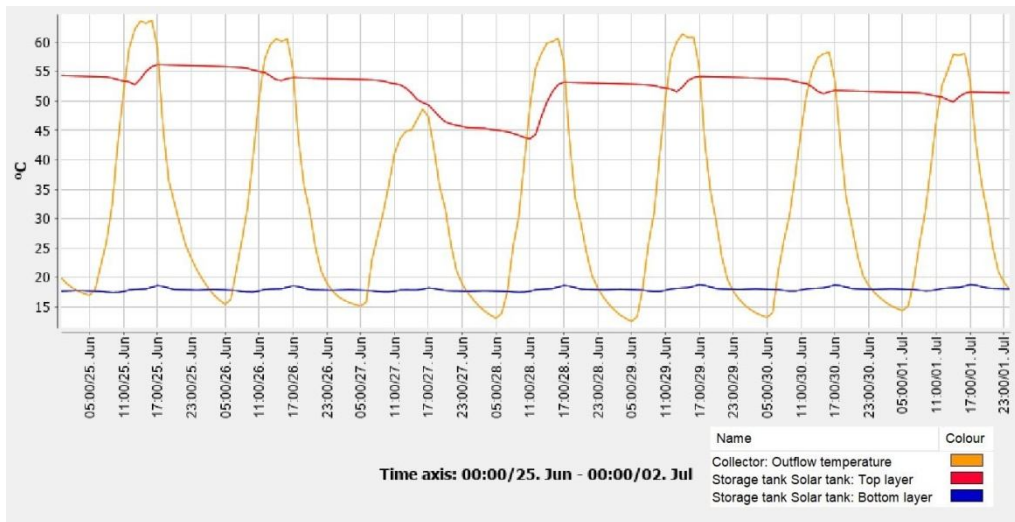


Figure 4.28 Flat plate, temperature evolution twenty-sixth week

From these figures it is noted that the temperature of the solar fluid, at the outlet of the vacuum absorber panel (Figure 4.25 and Figure 4.26), has higher values than those of the flat panel (Figure 4.27 and Figure 4.28). Specifically, in the winter and summer reference week respectively, the maximum peaks reached by the vacuum panel were 54 °C and 67 °C, while for the flat plate the values of 50 °C and 64 °C were recorded. The relatively low temperature of the vacuum panel outlet and the proximity of the recorded temperatures on the flat plate, follow the same trend that was recorded for the average annual temperatures during operational conditions. The vacuum panel, in fact, absorbs more solar energy than the other technology, however also releases it quite quickly, so the fluid returns to the solar panel in a thermodynamic condition close to that recorded in the flat plate.

The temperature of the lowest layer is mainly linked to the temperature of the water entering the network, therefore the temperature variations are more related to the season rather than to the technology adopted. Therefore, in both cases, was recorded in the lower layer a temperature of around 14 °C in winter and 17 °C in summer.

Finally, an appreciable result is the temperature of the water contained in the first storage, which with the vacuum tubes in winter records a temperature between 46 °C and 33 °C, while in summer between 59 °C and 46 °C. Similar results were recorded for flat plates, i.e. a temperature between 45 °C and 32 °C in winter, while between 56 °C and 44 °C in summer. These values make appreciable the greater performance of vacuum panels, because temperatures were recorded in the top of a thermally stratified of a 8 cubic meter tank.

Once the considerations on the recorded temperatures are over, three graphs are now proposed which show, in sequence, through the Sankey flows, the thermal flows of the base case and those obtained from the simulations of the two hybrid configurations, DHW side.

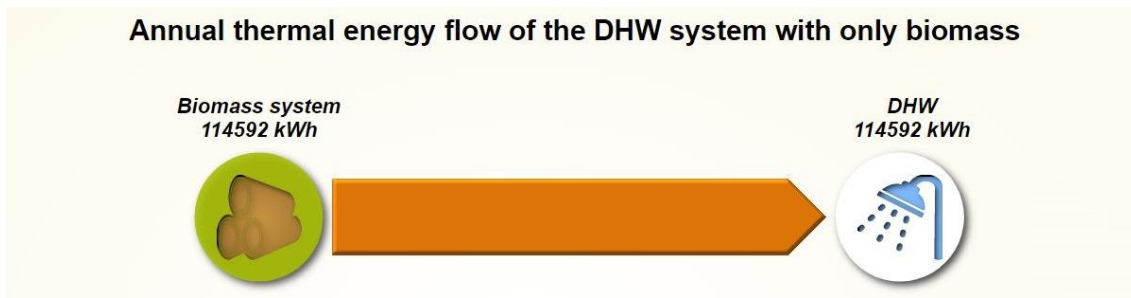


Figure 4.29 Annual thermal energy flow of a biomass system, for heating 10000 litres/day

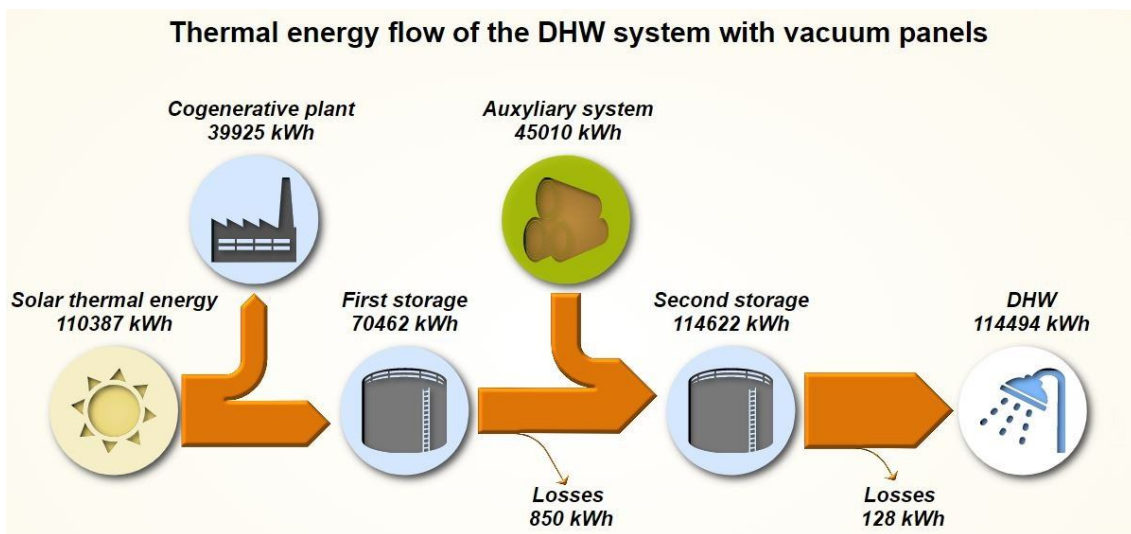


Figure 4.30 Annual thermal energy flow of a hybrid solar plant, with vacuum panels (absorber area of 90.3 m²), for heating 10000 litres/day

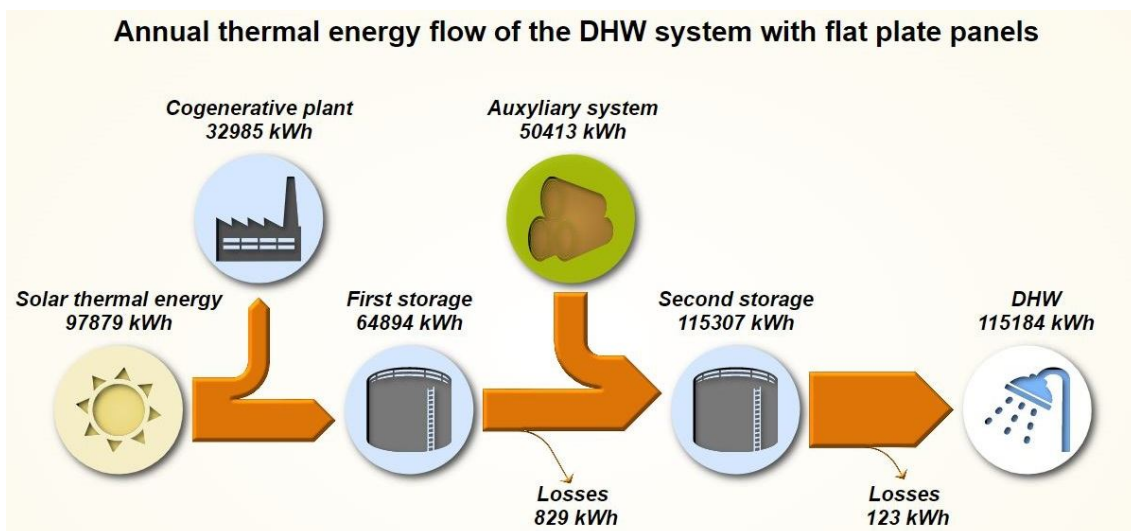


Figure 4.31 Annual thermal energy flow of a hybrid solar plant, with flat plate panels (absorber area of 88.54 m²), for heating 10000 litres/day

As can be seen in the figures above, the solar plant is able to transfer each year to the systems 110387 kWh_{th} and 97879 kWh_{th} in the case of vacuum tube and flat plate panels

4. Results

respectively. Although both technologies have a similar absorber area, it is necessary to highlight that, thanks to the best performance, vacuum tubes capture and transfer an additional 12500 kWh each year. This extra thermal energy guarantees considerable savings for the plant as it reduces the demand for biomass to be burned. About 55% of this surplus is mainly removed from the cogeneration plant, while the remaining part reduces the required auxiliary energy consumption.

The cogeneration plant is able to absorb more energy each year with the vacuum tube rather than the flat plate, 39925 kWh_{th} instead of 32985 kWh_{th}, due to the higher temperature of the solar fluid entering the external exchanger.

In addition to the greater heat exchange with the organic fluid, the vacuum panels configuration is also able to release even more energy at the first storage, 70462 kWh_{th} instead of 64894 kWh_{th} of the flat plate case. This translates into lower energy consumption of the auxiliary plant, with a consumption of 45010 kWh_{th} instead of 50413 kWh_{th}.

Finally, the minimal energy variations in the second storage between the two proposed solutions are due to the control dynamics, which activate the auxiliary systems until the set point conditions are respected.

In Table 4.14 is summarized, starting from the base case, the thermal energy from biomass that is both saved and consumed.

Table 4.14 Analysis of thermal flows, coming from the combustion of biomass, saved thanks to the hybrid system

	Vacuum tube	Flat plate
Energy saved thanks to the solar system (base case) [kWh _{th}]	114592	114592
Energy transferred to the cogeneration plant [kWh _{th}]	39925	32985
Energy supplied by the auxiliary system [kWh _{th}]	-45010	-50413
Difference between energy saved and energy consumed [kWh_{th}]	109507	97107

Thanks to the hybrid system, a thermal flow equal to the base case is saved. Considering that the cogeneration plant is powered exclusively by biomass, all the solar energy absorbed in the external exchanger is a gain. The only energy consumption is related to the auxiliary plant, which is activated to reach the set point levels.

Considering that the manufacturer of pellet boilers, described in Chapter 2.1, guarantees a thermal conversion efficiency of 94.5% [37], the amount of primary energy saved each year thanks to the hybrid plant is equal to 115880 kWh for the vacuum tube configuration and 102758 kWh for the flat plate.

This primary energy, converted through the calorific value of the used pellet (Table 2.2), corresponds to an amount of pellets saved annually equal to 21.91 tons in the case of the vacuum tube and about 19.43 tons in the case of the flat plate.

The annual saving of pellets, in addition to representing a considerable environmental advantage, as the amount of particulate matter and of monoxides released into the atmosphere is reduced, allows reducing the operating costs.

❖ Economic comparison

Once the saving of burned pellets has been defined, it was finally necessary to carry out an economic analysis to understand which plant should be chosen, i.e. which plant produces greater operating savings, compared to the initial investment, at the end of the plant's life.

For the analysis in question was chosen a solar system duration (n) of 20 years [87]. Moreover, was used an interest rate (i) equal to 2.4575% (Chapter 3.2.2) and was assumed that there are no significant variations for energy prices.

Regarding the prices of the main components installed in the solar plant, their values are summarized in the following table:

Table 4.15 Costs of the main components of the solar system installed

Component	Investment cost	Remark	Ref.	Total investment
Vacuum tubes	$I_{VT} = c_{VT} \cdot A_{VT}$	$c_{VT} = 250 \left[\frac{\text{€}}{\text{m}^2} \right]$	[87]	$I_{VT} = 29085 \text{ [€]}$
Flat plates	$I_{FP} = c_{FP} \cdot A_{FP}$	$c_{FP} = 200 \left[\frac{\text{€}}{\text{m}^2} \right]$	[87]	$I_{FP} = 19076 \text{ [€]}$
External heat exchanger	$I_{EHX} = 764 \text{ [\$]}$	Conversion factor dollar euro = 0.9 [88]	[89]	$I_{EHX} = 690 \text{ [€]}$
First storage	$I_{STO_1} = c_{STO_1} \cdot V_{STO_1}$	$c_{STO_1} = 850 \left[\frac{\text{€}}{\text{m}^3} \right]$	[90]	$I_{STO_1} = 6800 \text{ [€]}$
Second storage	$I_{STO_2} = c_{STO_2} \cdot V_{STO_2}$	$c_{STO_2} = 1050 \left[\frac{\text{€}}{\text{m}^3} \right]$	[90]	$I_{STO_2} = 2100 \text{ [€]}$

As can be seen from Table 4.15, the costs of the solar collector refer to the gross area of the panel, while storage costs per unit of volume vary according to the scale effect.

The initial investment sustained in both cases was obtained, through the generic formula:

$$I = I_{SP} + I_{EHX} + I_{STO_1} + I_{STO_2} \quad [\text{€}] \quad (69)$$

obtaining an initial investment cost of 38675 [€] for vacuum tubes and 28666 [€] for the flat plates.

However, these investment costs are amortized thanks to the reduction in operating costs. Every year there is a net saving equal to the difference between the biomass unburned and the electricity used in the pumps. The price of biomass is the same as used

4. Results

in Chapter 3.2.2 $\left(140 \left[\frac{\text{€}}{\text{ton}}\right] [71]\right)$, while the price of electricity was set equal to 0.2293 $\left[\frac{\text{€}}{\text{kWh}}\right]$, that is the average price of electricity in Portugal [91]. Starting from these data, some considerations have been developed in Table 4.16 in terms of energy and monetary savings.

Table 4.16 Annual operating energy and cost savings with the solar configuration

Case	Biomass saved	Electricity consumed	Reduction in operating costs (R)
Vacuum tube	$21.91 \left[\frac{\text{ton}}{\text{year}}\right]$	$38.6 \left[\frac{\text{kWh}}{\text{year}}\right]$	$3059 \left[\frac{\text{€}}{\text{year}}\right]$
	$3067 \left[\frac{\text{€}}{\text{year}}\right]$	$8.85 \left[\frac{\text{€}}{\text{year}}\right]$	
Flat plate	$19.43 \left[\frac{\text{ton}}{\text{year}}\right]$	$36 \left[\frac{\text{kWh}}{\text{year}}\right]$	$2712 \left[\frac{\text{€}}{\text{year}}\right]$
	$2720 \left[\frac{\text{€}}{\text{year}}\right]$	$8.25 \left[\frac{\text{€}}{\text{year}}\right]$	

At this point are known all the parameters necessary to calculate the Net Present Value (NPV), the economic parameter which is calculated through the difference between the present value of the future cash flows and the initial investment.

$$NPV = -I + \frac{(1+i)^n - 1}{i \cdot (1+i)^n} \cdot R \quad [\text{€}] \quad (70)$$

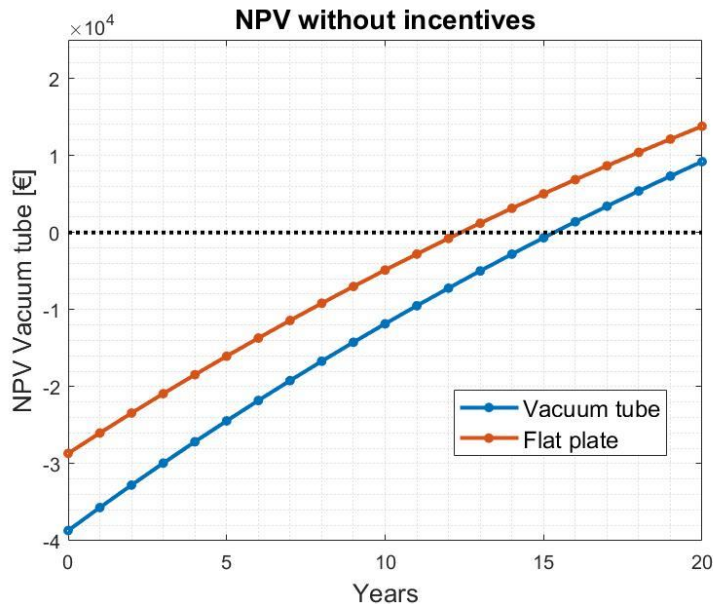


Figure 4.32 Net Present Value of the vacuum tube and flat plate technologies without state incentives

Through Figure 4.32, was chosen the flat plate configuration for the best economic performance. In fact, at the end of the 20 years, was obtained a NPV of 13781 euros for the flat plate configuration, while only 9197.19 euros for the vacuum tube. In addition,

was also estimated a Payback period (PB), i.e. the period necessary to recover the investment, equal to 12 years for the flat plate and 15 years for the vacuum tube.

The vacuum tubes, despite being the most suitable technology for the production of hot water due to the high temperatures that can be reached, do not have the same efficacy in this context. In fact, since the thermal energy must be dissipated at two different sources, there is a general lowering of the temperature of the fluid during the operating conditions and therefore a reduction of the efficiency of the vacuum panel. The installation of the vacuum panels has a greater thermodynamic efficiency, which corresponds to an additional annual saving of about 350 euros compared to the flat plates. However, this is not quickly compensated since there is an initial investment of about 10000 euros more.

The causes of the low annual difference in cost saving are linked to the use of a thermal source converted from a low-cost primary source (pellet) through a highly efficient plant. Therefore, this configuration could be kept attractive for future analyses, if a different energy source were saved, with higher primary source costs and less efficient conversion plants.

However, this result is an approximation, since if a pre-existing DHW plant will be replaced, further financing would be provided in Portugal [92]. The Energy Efficiency Fund, called "AVISO 25 | EFICIÊNCIA ENERGÉTICA EM EDIFÍCIOS" [93], type A2, provides a support of 60% of the investment, up to a maximum of 3000 euros [94]. In this case, therefore, the maximum amount of funding required by law is applied to both cases.

Finally, in Table 4.17 the evolution of the investment is shown, considering the case in which the Italian government funds, granted for thermal renewable resources, are exploited. Currently, for renewable technology, there is the Thermal account 2.0, a Price-based scheme, which provides an incentive for small RES. In accordance with Annex II, 2.2.a of 02.16.2016) [95], if the constraints imposed by law are respected [96], for a solar plant with a gross surface area between 50 and 200 m², which produces DHW and process heat at low temperatures, 0.11 euros per thermal kWh are financed. This entails, for the following analysis, a state financing of 12143 euros for the vacuum tubes and 10767 for flat plates. These values are also within the maximum limit, which provides for a loan of up to a maximum of 65% of the initial investment.

The NPV in 20 years and the PB for all scenarios are summarized in Table 4.17.

4. Results

Table 4.17 Evolution of the investment of the solar system: case without incentives and with Portuguese and Italian incentives.

Case	Parameter	Without funding	With Portuguese funding	With Italian funding
Vacuum tube	Investment [€]	38675	35675	26532
	NPV [€]	9197	12197	21340
	PB [years]	15.5	14	10
Flat plate	Investment [€]	28666	25666	17899
	NPV [€]	13781	16781	24548
	PB [years]	12.5	11	7.5

The state funds in favour of the production of renewable energy, for the case under analysis, allow for a reduction of the PB of about 1.5 years compared to the base scenario in the Portuguese case and of 5-5.5 years in the Italian scenario.

In all cases, even without funding, the scenario with flat plates is economically more convenient, as it has lower investment costs and higher revenues. Therefore, the hybrid solar flat plate configuration is the one suggested for a future implementation.

5. Conclusion

The purpose of this thesis was the optimization, both of the plant structure and of the operating conditions, of an ORC cogeneration plant, powered by biomass and designed for heating the swimming pool water.

Starting from the characteristics of the components installed in the prototype of this plant, designed by the company SCIVEN, a model of it written in MATLAB was created. This model allowed to obtain the thermodynamic characteristics, both in design and off design conditions, as a function of the power and temperature required by the user in the condenser.

From the parametric analysis, obtained by varying the conditions on the condenser, the optimal condition of the plant was identified ($Q_{COND} = 140 \text{ kW}$, $T_7 = 26^\circ\text{C}$ and $T_8 = 32^\circ\text{C}$). This condition allows to reach both the maximum electrical efficiency of the system ($\eta_{el} = 6.62 \%$) and the maximum Primary Energy Savings (PES = 3.30 %). The results have also shown that the optimal point is found for a condenser power of 140 kW, with minimal variations relative to the condenser water temperature. Thus, a strategy for regulating the condenser temperatures was identified to maximize electrical efficiency and primary energy savings, in the case it will be not possible to work in the optimal condition. From the results obtained, it is advisable to minimize the temperature of the water entering the condenser for lower thermal powers and to maximize it for greater thermal powers (Table 4.1 and Figure 4.5). This strategy, linked to the isentropic efficiency of the turbine and the ratio between the mass flow rate of the ORC and the water in the condenser (Figure 4.2), allows to increase the electrical efficiency, with respect to the worst condition in the analysed range, of 0.45% and 0.21% respectively for low and high powers required in the condenser. Finally, the conditions in the condenser that respectively minimize and maximize all the parameters considered in the study were reported (Table 4.6, Table 4.7 and Table 4.8).

Once the energy optimization, regarding the condenser operating conditions, was completed, the system was investigated under the exergetic and exergoeconomic aspect.

The exergetic analysis showed that, in the optimal PES condition ($\dot{Q}_{COND} = 140 \text{ kW}$, $T_7 = 26^\circ\text{C}$ and $T_8 = 32^\circ\text{C}$), the least efficient components are the combustion chamber ($\epsilon_{CC} = 14.23 \%$) and the condenser ($\epsilon_{COND} = 31.56 \%$), while the most irreversible are the combustion chamber ($I_{CC} = 92.25 \%$) and the evaporator ($I_{EVA} = 3.59 \%$).

Starting from the exergetic results, an exergoeconomic analysis was also conducted, exploiting the costs of the components provided by the company SCIVEN (Table 3.3).

The optimization of the costs of the mechanical product, through the parametric analysis of the conditions on the condenser, showed a trend similar to that of electrical efficiency. In general, there is a reduction in the costs of the mechanical product as the heat load of the condenser increases (Figure 4.19). The temperature control strategy that

minimizes the costs of the mechanical product is similar to that adopted in the energy analysis. It allows a maximum unit of exergoeconomic cost savings of $63.4 \left[\frac{\text{€}}{\text{MWh}} \right]$ compared to the worst condition.

The relevant case, instead, is recorded for the minimization of the unit of exergoeconomic cost of the thermal product. Also in this case it is suggested to work at high power of the condenser, however, it is recommended to work with the minimum water temperature difference in the condenser. This regulation allows approximately to halve the costs per unit exergetic with respect to the case with the greater temperature difference, i.e. worst case (Figure 4.23).

The explanation is linked to the fact that decreasing the temperature difference of the water at the ends of the condenser, for the same power required by the condenser, increases the mass flow rate of the pool water. Consequently, the exergy increases (Equation (67) and Figure 4.22) and therefore the unit of exergetic cost of the thermal product is reduced (Figure 4.21).

Since there is a considerable variation in the unit of exergoeconomic cost of the thermal product compared to the mechanical one, and that the thermal power of the plant is up to two orders of magnitude greater than the mechanical one (Table 4.8), it is suggested, from the exergoeconomic point of view, to use the system in the following condenser condition: $\dot{Q}_{COND} = 150 \text{ kW}$, $T_7 = 27^\circ\text{C}$ and $T_8 = 30^\circ\text{C}$.

Finally, to conclude the exergoeconomic analysis, the point where the plant could be improved in the plant structure was investigated through the design improvement analysis.

Starting from the condenser temperature conditions that minimize the unit of exergoeconomic cost ($T_7 = 27^\circ\text{C}$ and $T_8 = 30^\circ\text{C}$), it was noted that the combustion chamber (CC) is the component with the largest cost rate of components and cost rate of irreversibility ($Z + CD$) (Table 4.9) and the major relative cost differences (r_i) (Table 4.10). This is related to the fact that the exergoeconomic factor (f) of the combustion chamber is low (Table 4.11) because the hot water, generated in the combustion chamber, reach temperatures below the boiling point. It is therefore necessary to improve the thermodynamic efficiency of the plant by reducing the contribution of the combustion chamber. In fact, for low powers required by the condenser, and therefore also by the combustion chamber, there is a reduction in the coefficients $Z+CD$ and r_i , while the coefficient f is increased.

To guarantee the delivery of the same power required by the user in the condenser and, at the same time, to reduce the power of the combustion chamber, taking advantage of the hybridization suggestions conducted in previous studies and shown in the introduction, an innovative hybrid biomass-solar thermal model was created (Figure 2.1).

Since the hybridization of the plant was not yet considered by the company, the attention was focused on the design of the solar part of the hybrid plant, i.e. on the

regulation of the three-way valves and on the optimization of the areas of the panels, of the heat exchangers and of the volumes of the storages.

The analysis was carried out both with vacuum tubes and with flat plates. Since the plant will be located inside a sports centre, it was considered useful to expand the thermal products supplied by the installation. The hybrid plant was therefore sized to reduce the consumption of burnt pellets necessary both to feed the cogeneration circuit and to heat the water for 250 daily showers.

The results showed that in the thermodynamically optimized solution it is possible to have a net biomass savings of 21.91 and 19.43 $\left[\frac{\text{ton}}{\text{year}}\right]$, respectively for the vacuum tube and flat plate solution (Table 4.16). Once the characteristics of the plant have been defined, information on the prices of the components has been collected in order to conduct economic optimization (Table 4.15).

From the analysis it emerged that the solution optimized at the economic level is the one with flat plates, since it has both the lowest NPV (equal to € 13781 in 20 years) and PB (12.5 years).

Finally, state funds were considered for the production of renewable energy in the event that the plant was installed in Italy or in Portugal. Has been found for flat plates, i.e. the technology chosen for the installation, a reduction of the PB of about 1.5 years in the case of loans from the Portuguese government and 5 years in the Italian scenario (Table 4.16).

In conclusion, the hybrid solution provides significant annual pellet savings compared to the simple biomass plant and is economically feasible. For these reasons it is suggested, for future works on the plant, to investigate whether this hybrid solution is competitive also from the exergetic and exergoeconomic point of view compared to the cogeneration plant powered only by pellets.

Bibliography

- [1] C. E. Boyd and A. A. McNevin, “World Population,” in *Aquaculture, Resource Use, and the Environment The*, 1st ed., I. John Wiley & Sons, Ed. John Wiley & Sons, Inc., 2015, pp. 21–33.
- [2] A. Korotayev, “A Compact Macromodel of World System Evolution Andrey,” *J. world-systems Res.*, pp. 79–93, 2005.
- [3] IEA, “IEA Headline - International Energy Agency,” 2016. [Online]. Available: https://www.iea.org/media/statistics/IEA_HeadlineEnergyData_2016.xlsx. [Accessed: 14-Mar-2019].
- [4] UNFCCC, “United Nations Framework Convention on Climate Change: What is the Kyoto Protocol.” [Online]. Available: <https://unfccc.int/process-and-meetings/the-kyoto-protocol/what-is-the-kyoto-protocol/what-is-the-kyoto-protocol>. [Accessed: 10-Mar-2019].
- [5] UNFCCC, “United Nations Framework Convention on Climate Change: The Paris Agreement.” [Online]. Available: <https://unfccc.int/process-and-meetings/the-paris-agreement/the-paris-agreement>. [Accessed: 10-Mar-2019].
- [6] IEA, “World Energy Outlook 2018,” 2018. [Online]. Available: <https://www.iea.org/weo2018/>. [Accessed: 14-Mar-2019].
- [7] B. J. Cardoso, A. R. Gaspar, J. C. Góis, and E. Rodrigues, “Energy and water consumption characterization of Portuguese indoor swimming pools,” *CYTEF 2018 VII Congr. Ibérico, Ciencias y técnicas del frío. 19-21 June 2018, Val. Spain*, 2018.
- [8] W. Kampel, B. Aas, and A. Bruland, “Energy-use in Norwegian swimming halls,” *Energy Build.*, vol. 59, no. April, pp. 181–186, 2013.
- [9] W. Kampel, S. Carlucci, B. Aas, and A. Bruland, “A proposal of energy performance indicators for a reliable benchmark of swimming facilities,” *Energy Build.*, vol. 129, no. July, pp. 186–198, 2016.
- [10] J. Oliver-Solà, M. Armero, B. M. de Foix, and J. Rieradevall, “Energy and environmental evaluation of municipal facilities: Case study in the province of Barcelona,” *Energy Policy*, vol. 61, pp. 920–930, 2013.
- [11] BIOS BIOENERGIESYSTEME GmbH Graz, “PROJECTS: OVERALL VIEW.” [Online]. Available: <https://www.bios-bioenergy.at/en/references/all-projects.html#c511>.
- [12] DPSsystem, “COGENERATORE A CIPPATO o PELLETT HKA10,” 2018. [Online]. Available: <https://dpsystem.it/biomassa/legno-cippato-e-cogenerazione/cogeneratore-a-cippato-o-pellett-hka10/>.
- [13] OkoFen, “Pellematic e-max.” [Online]. Available: <https://www.stroomop.be/data/documents/okofen-e-folderemaxen-1.pdf>.

-
- [14] SCIVEN, “SCIVEN Cogeração.” [Online]. Available: <http://www.sciven.com/views/cogeracao.html#Tecno>.
- [15] L. Dong, H. Liu, and S. Riffat, “Development of small-scale and micro-scale biomass-fuelled CHP systems - A literature review,” *Appl. Therm. Eng.*, vol. 29, no. 11–12, pp. 2119–2126, 2009.
- [16] P. Antonio, C. Patrizia, C. Sergio, and S. Nilay, “Thermo-economic assessment of small scale biomass CHP: steam turbines vs ORC in different energy demand segments,” *Energy procedia, 7th Int. Conf. Appl. Energy – ICAE2015*, vol. 75, pp. 1609–1617, 2015.
- [17] R. Matthews *et al.*, “Review of literature on biogenic carbon and life cycle assessment of forest bioenergy,” *Fuel*, vol. 4, no. April, pp. 246–253, 2014.
- [18] J. Portier, S. Gauthier, G. Cyr, and Y. Bergeron, “Does time since fire drive live aboveground biomass and stand structure in low fire activity boreal forests? Impacts on their management,” *J. Environ. Manage.*, vol. 225, no. July, pp. 346–355, 2018.
- [19] C. M. B. Ferreira, “The biomass as an energy vector in Portugal: assessment of availability and of the market features.” Annual report, Renature project, 2018.
- [20] D. Al Katsaprakakis, “Comparison of swimming pools alternative passive and active heating systems based on renewable energy sources in Southern Europe,” *Energy*, vol. 81, pp. 738–753, 2015.
- [21] F. Zuccari, A. Santiangeli, and F. Orecchini, “Energy analysis of swimming pools for sports activities: cost effective solutions for efficiency improvement,” *Energy procedia*, vol. 126, pp. 123–130, 2017.
- [22] I. S. Marinopoulos and K. L. Katsifarakis, “Optimization of Energy and Water Management of Swimming Pools. A Case Study in Thessaloniki, Greece,” *Procedia Environ. Sci.*, vol. 38, pp. 773–780, Jan. 2017.
- [23] FINA, “FACILITIES RULES 2017 – 2021,” 22 September 2017, 2017. [Online]. Available: http://www.fina.org/sites/default/files/2017_2021_facilities_16032018_full_medium.pdf.
- [24] A. Mousia and A. Dimoudi, “Energy performance of open air swimming pools in Greece,” *Energy Build.*, vol. 90, pp. 166–172, 2015.
- [25] Dessau-Roßlau, “Environmental costs in the energy and transport sectors,” *Umweltbundesamt (Federal Environment Agency)*, 2012. [Online]. Available: https://www.umweltbundesamt.de/sites/default/files/medien/378/publikationen/hgp_umweltkosten_en.pdf. [Accessed: 19-Mar-2019].
- [26] F. Calise, R. D. Figaj, and L. Vanoli, “Energy and economic analysis of energy savings measures in a swimming pool centre by means of dynamic simulations,” *Energies*, vol. 11, no. 9, 2018.
- [27] P. Morrone, A. Algieri, and T. Castiglione, “Hybridisation of biomass and concentrated solar power systems in transcritical organic Rankine cycles: A micro combined heat and power application,” *Energy Convers. Manag.*, pp. 757–768, 2019.

- [28] M. Jradi and S. Riffat, “Modelling and testing of a hybrid solar-biomass ORC-based micro-CHP system,” *Int. J. energy Res.*, 2013.
- [29] J. Soares and A. C. Oliveira, “Numerical simulation of a hybrid concentrated solar power/biomass mini power plant,” *Appl. Therm. Eng.*, vol. 111, pp. 1378–1386, 2017.
- [30] E. Açikkalp, T. Zeng, A. Ortwein, H. Burkhardt, and W. Klenk, “Exergy, Exergoeconomic and Enviroeconomic Evaluation of a Biomass Boiler-Steam Engine Micro-CHP System,” *Chem. Eng. Technol.*, vol. 41, no. 11, pp. 2141–2149, 2018.
- [31] M. Creyx, E. Delacourt, C. Morin, S. Lalot, and B. Desmet, “Energetic and exergetic analysis of a heat exchanger integrated in a solid biomass-fuelled micro-CHP system with an Ericsson engine,” *Entropy*, vol. 18, no. 4, 2016.
- [32] T. B. Nur and Sunoto, “Exergy analysis of biomass organic Rankine cycle for power generation,” *IOP Conf. Ser. Mater. Sci. Eng.*, vol. 309, no. 1, 2018.
- [33] J. Pereira, J. Ribeiro, R. Mendes, G. Vaz, and J. André, “ORC based micro-cogeneration systems for residential application – A state of the art review and current challenges,” *Renew. Sustain. Energy Rev.*, vol. 92, pp. 728–743, 2018.
- [34] “KAYMACOR product.” [Online]. Available: <https://www.kaymacor.com/en/products/>. [Accessed: 26-Mar-2019].
- [35] A. Angelo and M. Pietropaolo, “Techno-economic analysis of biomass-fired ORC systems for single-family combined heat and power (CHP) applications,” *Energy Procedia*, 68th Conf. Ital. Therm. Mach. Eng. Assoc., vol. 45, pp. 1285 – 1294, 2014.
- [36] L. Tocci, T. Pal, I. Pesmazoglou, and B. Franchetti, “Small scale Organic Rankine Cycle (ORC): A techno-economic review,” *Energies*, vol. 10, no. 4, pp. 1–26, 2017.
- [37] “Smart Heating Tecnology Brochure.” [Online]. Available: <http://www.smartheating.cz/wp-content/uploads/2014/06/Smart-Biomass-Boilers-150-500-kW-Brochure-1.pdf>.
- [38] L. C.-L. E. em B. S. Centro da Biomassa para a Energia, “Test report N° 377 /18,” 2018.
- [39] European Pellet Council (EPC) and European Biomass Association (AEBIOM), “ENplus® Pellet Bag Design - Requirements,” pp. 1–15, 2018.
- [40] Conselho Nacional de Qualidade, “Diretiva CNQ N.º 23/93 (1993): A Qualidade nas Piscinas de Uso Público,” 1993. [Online]. Available: http://www.buzios.org.pt/CNQ_23_93.pdf. [Accessed: 22-May-2019].
- [41] M. Kaltschmitt, W. Streicher, and A. Wiese, “Renewable Energy: Technology, Economics and Environment, Chapter 4: Solar Thermal Heat Utilisation,” Springer, 2007, pp. 123–168.
- [42] “Planning and Installing Solar Thermal Systems: A guide for installallers, architects and engineers, Chapter 3.5 Planning and dimensioning,” 2010. [Online]. Available:

- https://energiarenovablenec.files.wordpress.com/2015/08/german_solar_energy_society_dgs_planning_and_ibookzz-org.pdf.
- [43] EPA (United States Environmental Protection Agency), “Legionella: Drinking Water Health Advisory,” *Environ. Prot.*, 2015.
- [44] M. O. Lemmon, E. W. Huber, and M. L. McLinden, “NIST Reference Fluid Thermodynamic and Transport Properties (REFPROP) - Version 9.1, National Institute of Standard Technology.” 2013.
- [45] F. P. Incropera, D. P. DeWitt, T. L. Bergman, and A. S. Lavine, *Fundamentals of Heat and Mass Transfer*. John Wiley & Sons, 2007.
- [46] L. I. U. Liuchen, Z. H. U. Tong, G. A. O. Naiping, and G. A. N. Zhongxue, “A review of modeling approaches and tools for the off-design simulation of organic Rankine cycle,” *J. Therm. Sci.*, vol. 27, no. 4, pp. 305–320, 2018.
- [47] D. Ziviani, A. Beyene, and M. Venturini, “Advances and challenges in ORC systems modeling for low grade thermal energy recovery,” *Appl. Energy*, vol. 121, pp. 79–95, 2014.
- [48] R. Dickes, O. Dumont, L. Guillaume, S. Quoilin, and V. Lemort, “Charge-sensitive modelling of organic Rankine cycle power systems for off-design performance simulation,” *Appl. Energy*, vol. 212, no. December 2017, pp. 1262–1281, 2018.
- [49] M. Santos, J. André, S. Francisco, R. Mendes, and J. Ribeiro, “Off-design modelling of an organic Rankine cycle micro-CHP: Modular framework, calibration and validation,” *Appl. Therm. Eng.*, vol. 137, no. December 2017, pp. 848–867, 2018.
- [50] A. Muley and R. M. Manglik, “Experimental study of turbulent flow heat transfer and pressure drop in a plate heat exchanger with chevron plates,” *J. Heat Transf. ASME 121*, pp. 110–117, 1999.
- [51] B. Thonon, “A review of hydrocarbon two-phase heat transfer in compact heat exchangers and enhanced geometries,” *Int. J. Refrig. 31*, pp. 633–642, 2008.
- [52] A. Maslov and L. Kovalenko, “Hydraulic resistance and heat transfer in plate heat exchangers,” *Molochnaya Promyshlennost. 10*, pp. 20–22, 1972.
- [53] H. Kumar, “The plate heat exchanger: construction and design,” *roc. First UK Natl. Conf. Heat Transf. Univ. Leeds, Inst. Chem. Symp.*, pp. 1275–1288, 1984.
- [54] A. S. Wanniarachchi and U. Ratman, “Approximate correlations for chevron-type plate heat exchangers,” *Proc. 30th Natl. Heat Transf. Conf. ASME-vol*, pp. 145–151, 1995.
- [55] Y. Y. Yan, H. C. Lio, and T. F. Lin, “Condensation heat transfer and pressure drop of refrigerant R134a in a plate heat exchanger,” *Int. J. Heat Mass Transf. 42*, pp. 993–1006, 1999.
- [56] D. H. Han, K. J. Lee, and Y. H. Kim, “The characteristics of condensation in brazed plate heat exchangers with different chevron angles,” *J. Korean Phys. Soc. 43*, pp. 66–73, 2003.
- [57] CLIMATE-DATA.ORG, “Climate: Coimbra.” [Online]. Available:

- <https://it.climate-data.org/europa/portogallo/coimbra/coimbra-160/>. [Accessed: 08-May-2019].
- [58] Y. A. Cenghel and M. A. Boles, "Thermodynamics: An Engineering Approach, Chapter 15," 5th ed., 2004.
- [59] M. J. Moran, H. N. Shapiro, D. D. Boettner, and M. B. Bailey, "Table A-25E," in *FUNDAMENTALS OF ENGINEERING THERMODYNAMICS*, Eighth Edi., 2014.
- [60] J. Zueco, "An educational laboratory virtual EES for encouraging the use of computer programming in thermal engineering problems," *Comput. Appl. Eng. Educ.*, vol. 21, no. 4, pp. 691–697, 2013.
- [61] L. Borel and D. Favrat, "Energy and exergies analyses," in *Thermodynamics and energy systems analysis: form energy to exergy*, 2010, pp. 399–490.
- [62] M. De Rosa, R. Douglas, and S. Glover, "Numerical Analysis on a Dual-Loop Waste Heat Recovery System Coupled with an ORC for Vehicle Applications," *SAE Tech. Pap. Ser.*, vol. 1, 2016.
- [63] J. M. Moran, S. N. Howard, D. D. Boettner, and B. B. Margaret, *Fundamentals of engineering thermodynamics (8th edition)*, TABLE A-26, 8th editio. Wiley, 2014.
- [64] F. Gharagheizi, P. Ilani-Kashkouli, A. H. Mohammadi, and D. Ramjugernath, "A group contribution method for determination of the standard molar chemical exergy of organic compounds," *Energy*, vol. 70, pp. 288–297, 2014.
- [65] F. Heberle and D. Brüggemann, "Exergy based fluid selection for a geothermal Organic Rankine Cycle for combined heat and power generation," *Appl. Therm. Eng.*, vol. 30, no. 11–12, pp. 1326–1332, 2010.
- [66] M. A. Al-Weshahi, A. Anderson, and G. Tian, "Organic Rankine Cycle recovering stage heat from MSF desalination distillate water," *Appl. Energy*, vol. 130, pp. 738–747, 2014.
- [67] J. Chen, H. Havtun, and B. Palm, "Conventional and advanced exergy analysis of an ejector refrigeration system," *Appl. Energy*, vol. 144, pp. 139–151, 2015.
- [68] F. I. Abam, E. B. Ekwe, S. O. Effiom, M. C. Ndukwu, T. A. Briggs, and C. H. Kadurumba, "Optimum exergetic performance parameters and thermo-sustainability indicators of low-temperature modified organic Rankine cycles (ORCs)," *Sustain. Energy Technol. Assessments*, vol. 30, no. October 2017, pp. 91–104, 2018.
- [69] G. Song, L. Shen, and J. Xiao, "Estimating specific chemical exergy of biomass from basic analysis data," *Ind. Eng. Chem. Res.*, vol. 50, no. 16, pp. 9758–9766, 2011.
- [70] M. A. Lozano and A. Valero, "Theory of the exergetic cost," *Energy*, vol. 18, no. 9, pp. 939–960, 1993.
- [71] A. Rodzkin, S. Kundas, Y. Charnenak, B. Khroustalev, and W. Wichtmann, "The assessment of cost of biomass from post-mining peaty lands for pellet fabrication," *Environ. Clim. Technol.*, vol. 22, no. 1, pp. 118–131, 2018.
- [72] US Department of Energy, "Quality Guideline for Energy System Studies (QGESS) - Cost Estimation Methodology for NETL Assessments of Power Plant

- Performance,” 2011.
- [73] Trading Economics, “Portugal Government Bond 10Y,” 2019. [Online]. Available: <https://tradingeconomics.com/portugal/government-bond-yield%0D>. [Accessed: 17-Jul-2019].
- [74] Jornal de negocios, “Obrigações Portugal paga 0,51% para emitir dívida a 10 anos.axa cai para metade em dois meses,” 2019. [Online]. Available: <https://www.jornaldenegocios.pt/mercados/obrigacoes/detalhe/portugal-paga-051-para-emitir-divida-a-10-anos%0D>. [Accessed: 17-Jul-2019].
- [75] kpmg, “Equity Market Risk Premium – Research Summary,” 2019. [Online]. Available: <https://assets.kpmg/content/dam/kpmg/nl/pdf/2019/advisory/equity-market-risk-premium-research-summary-31032019.pdf>. [Accessed: 17-Jul-2019].
- [76] Il sole 24 ore, “EURIRS,” 2019. [Online]. Available: <https://mutuionline.24oreborsaonline.ilsole24ore.com/guide-mutui/irs.asp#storico>. [Accessed: 17-Jul-2019].
- [77] N. Shokatia, R. Faramarz, and Y. Mortaza, “A comprehensive exergoeconomic analysis of absorption power and cooling cogeneration cycles based on Kalina, part 1: Simulation,” *Energy Convers. Manag.*, vol. 158, pp. 437–459, 2018.
- [78] SWEP, “SSP Online Calculation Software,” 2019. [Online]. Available: <http://www.ssonline.swep.net/>.
- [79] ASHRAE, *ASHRAE Handbook—Fundamentals (SI)*. 2009.
- [80] Honeywell, “Honeywell: Physical Properties of Genetron® 245fa (R-245fa).” [Online]. Available: <https://www.honeywell-refrigerants.com/europe/product/genetron-245fa/>. [Accessed: 01-Jun-2019].
- [81] SWEP, “SWEP products, B25T technical features,” 2019. [Online]. Available: <https://www.swep.net/products/B25T>.
- [82] A. Davis, “The Efficiency of Solar Thermal Heating,” 2017. [Online]. Available: <https://www.oxfordrenewables.co.uk/the-efficiency-of-solar-thermal-heating>.
- [83] DEA - Dipartimento di Energia e Ambiente - CISM, “La cogenerazione ad alto rendimento.”
- [84] European Parliament and European Council, “Directive 2012/27/EU,” *Off. J. Eur. Union. L315/1*, pp. 1–56, 2012.
- [85] J. S. Pereira, J. B. Ribeiro, M. Ricardo, and J. C. André, “Analysis of a hybrid (topping/bottoming) ORC based CHP configuration integrating a new evaporator design concept for residential applications,” *Appl. Therm. Eng.*, 2019.
- [86] European Commission, “COMMISSION DELEGATED REGULATION (EU) 2015/2402 of 12 October 2015 reviewing harmonised efficiency reference values for separate production of electricity and heat in application of Directive 2012/27/EU of the European Parliament and of the Council and rep,” *Off. J. Eur. Union L 333/54*, pp. 54–61, 2015.
- [87] T. Bouhal *et al.*, “Technical assessment, economic viability and investment risk analysis of solar heating/cooling systems in residential buildings in Morocco,” *Sol.*

- Energy*, vol. 170, pp. 1043–1062, 2018.
- [88] Il sole 24 ore, “Tassi e Valute,” 27-08-2019, 2019. [Online]. Available: <https://mercati.ilsole24ore.com/tassi-e-valute>.
- [89] HVACBRAIN, “SWEP B25T cost.” [Online]. Available: <https://www.hvacbrain.com/SWEP-15010-030-1/>. [Accessed: 27-Aug-2019].
- [90] V. A., J. J., and K. R., “A cost-optimal solar thermal system for apartment buildings with district heating in a cold climate,” *Int. J. Sustain. Energy*, vol. 38, no. 2, pp. 141–162, 2018.
- [91] Eurostat, “Electricity price statistics,” 2019. [Online]. Available: https://ec.europa.eu/eurostat/statistics-explained/index.php/Electricity_price_statistics.
- [92] Res-legal.eu (EU), “Promotion in Portugal, Subsidy (Energy Efficiency Fund),” 2019. [Online]. Available: <http://www.res-legal.eu/search-by-country/portugal/tools-list/c/portugal/s/res-hc/t/promotion/sum/180/lpid/179/>.
- [93] Plano nacional de ação para a eficiência energética, “AVISO 25 | EFICIÊNCIA ENERGÉTICA EM EDIFÍCIOS,” 2018.
- [94] Plano nacional de ação para a eficiência energética, “Aviso 25 | Processo da Candidatura ao Apoio do FEE, TIPOLOGIA DE MEDIDA: A2,” 2018. [Online]. Available: http://www.pnaee.pt/images/files/aviso25/Tipologia_A2.pdf.
- [95] MISE (Ministero dello Sviluppo Economico), “Decreto interministeriale 16 febbraio 2016, Annex,” 2016. [Online]. Available: https://www.mise.gov.it/images/stories/normativa/https://www.mise.gov.it/images/stories/normativa/allegato_decreto_interministeriale_16_febbraio_2016_aggiornamento_conto_termico.pdf.
- [96] MISE (Ministero dello Sviluppo Economico), “Decreto interministeriale 16 febbraio 2016,” 2016. [Online]. Available: https://www.mise.gov.it/images/stories/normativa/decreto_interministeriale_16_febbraio_2016_aggiornamento_conto_termico.pdf.

Appendix

Appendix A

Stream	ORC				Hot water		Pool water		Air	Pellet	Combustion gas	Mechanical energy		
	ORC ₁	ORC ₂	ORC ₃	ORC ₄	HW _{in}	HW _{out}	PW _{in}	PW _{out}	Air	P	GAS _{out}	Em ₁	Em ₂	
Subsystem	E1	E2	E3	E4	E5	E6	E7	E8	E9	E10	E11	E12	E13	
CC	0	0	0	0	-1	1	0	0	1	1	-1	0	0	A
EVA	1	-1	0	0	1	-1	0	0	0	0	0	0	0	
TURB	0	1	-1	0	0	0	0	0	0	0	0	-1	-1	
COND	0	0	1	-1	0	0	1	-1	0	0	0	0	0	
PUMP	-1	0	0	1	0	0	0	0	0	0	0	0	1	
Inlet air	0	0	0	0	0	0	0	0	1	0	0	0	0	α_e
Inlet fuel	0	0	0	0	0	0	0	0	0	1	0	0	0	
Inlet water	0	0	0	0	0	0	1	0	0	0	0	0	0	
Exhausted gas	0	0	0	0	0	0	0	0	0	0	1	0	0	
EVA	0	0	0	0	$-\frac{E_6}{E_5}$	1	0	0	0	0	0	0	0	α_x
TURB	0	$-\frac{E_3}{E_2}$	1	0	0	0	0	0	0	0	0	0	0	
COND	0	0	$-\frac{E_4}{E_3}$	1	0	0	0	0	0	0	0	$-\frac{E_{13}}{E_{12}}$	1	

Figure A.1 Cost matrix

0
0
0
0
0
E_9
E_{10}
E_7
0
0
0
0
0

Figure A.2 Vector of external assessment

Appendix B

\dot{Q}_{COND}	c_r				
	CC	EVA	TURB	COND	PUMP
80	27.93	322.67	467.94	467.94	882.95
90	27.94	299.15	417.05	417.05	687.58
100	27.94	279.88	379.42	379.42	570.77
110	27.94	263.88	350.78	350.78	498.61
120	27.94	250.36	328.53	328.53	454.99
130	27.95	238.57	311.01	311.01	431.80
140	27.95	227.17	297.06	297.06	424.95
150	27.95	205.46	285.90	285.90	432.94

Figure B.1 Unit cost of resources

\dot{Q}_{COND}	c_p				
	CC	EVA	TURB	COND	PUMP
80	422.74	462.73	882.95	1591.82	1133.81
90	441.62	413.00	687.58	1396.07	863.04
100	481.36	376.12	570.77	1254.00	699.94
110	552.35	347.93	498.61	1149.78	597.69
120	679.10	325.91	454.99	1073.55	533.74
130	929.58	308.42	431.80	1018.91	496.42
140	1576.24	294.29	424.95	981.11	479.55
150	2112.16	282.72	432.94	956.91	480.36

Figure B.1 Unit cost of product

Appendix C

Exergy and exergoeconomic models

```
clc
clear all
close all

QQ_cond=[80:10:150];
TT_in=[25:1:27];
TT_out=[30:1:32];

%% Reference definition

P0=101.325;
Tref = 25+273.15;

T0_1=Tref;
T0_2=Tref;
T0_3=Tref;
T0_4=Tref;
T0_5=Tref;
T0_6=Tref;
T0_7=Tref;
T0_8=Tref;
T0_9=Tref;
T0_10=Tref;
T0_11=Tref;

T0 =[T0_1,T0_2,T0_3,T0_4,T0_5,T0_6,T0_7,T0_8,T0_9,T0_10,T0_11]; % [K]

%% Chemical exergy data

MM_N2= 28.01;
MM_O2= 32.00;
MM_CO2=44.01;
MM_H2O=18.02;

RR=8314; % Universal Gas Constant [J/kmolK]
RR_N2= RR/MM_N2;
RR_O2= RR/MM_O2;
RR_CO2=RR/MM_CO2;
RR_H2O=RR/MM_H2O;
```

Appendix

```
b_0_N2 = 720000/MM_N2;      %[J/kg]=[J/kmol]*MM
b_0_O2 = 3970000/MM_O2;    %[J/kg]=[J/kmol]*MM
b_0_CO2 = 19870000/MM_CO2; %[J/kg]=[J/kmol]*MM
b_0_H2O_v=9500000/MM_H2O;  %[J/kg]=[J/kmol]*MM
```

%% Matrix

```
AA=[0 0 0 0 -1 1 0 0 1 1 -1 0 0
    1 -1 0 0 1 -1 0 0 0 0 0 0 0
    0 1 -1 0 0 0 0 0 0 0 0 -1 -1
    0 0 1 -1 0 0 1 -1 0 0 0 0 0
    -1 0 0 1 0 0 0 0 0 0 0 0 1];
```

```
ae=[0 0 0 0 0 0 0 0 1 0 0 0 0
    0 0 0 0 0 0 0 0 0 1 0 0 0
    0 0 0 0 0 0 1 0 0 0 0 0 0
    0 0 0 0 0 0 0 0 0 0 1 0 0];
```

%% Economic Parameters

```
Eq=0.25;    % Equity
Deb=0.75;   % Debt
```

```
Rf=0.51/100;      % Risk free interest
Rs=0/100;         % Small stock premium
bb_fluid=1;       % Coefficient that account the specific sector in the market
EMRP=5.75/100;   % Equity Market Risk Premium
premium=Rs+bb_fluid*EMRP;
```

```
ke=Rf+premium;    % Cost of equity
```

```
IRS=0.19/100;    % Interest Rate Swap
spread=1/100;    % Increase of the interest rate depending on the capability
of the investor to return the capital
```

```
kd=IRS+spread;   % Cost of debt
```

```
WACC=ke*(Eq/(Eq+Deb))+kd*(Deb/(Eq+Deb)); % Weighted average cost of capital
```

```
nn=20;           % Plant lifetime
AF=0.57;         % Availability factor
DRF=((((WACC+1)^nn)*WACC)/(((WACC+1)^nn)-1)); % Discount Rate Factor
```

%% Component and fuel cost

```

c_Cc=44000;           % [€] Cost of Combustion chamber [SMART 180 kW]
c_Eva=500;           % [€] Cost of Evaporator [SWEP B200THx110/1P-NC-M
(2 1/2"+2 1/2"+2x2 1/2")]
c_Turb=30000;        % [€] Cost of Turbine [DEPRAG Turbine Generator GET11
kW]
c_Cond=350;          % [€] Cost of Condenser [KELVION BPHE GmbH
GBS757M-60]
c_Pump=800;          % [€] Cost of Pump [MPO 3R series]

c_bio=0.14;          % [€/kg] Cost of Biomass per unit of mass [pellet]
bio_energy=18000000; % [J/kg] Biomass energy per unit of mass
c_energy_bio=c_bio/bio_energy; % [€/J] Cost of Biomass per unit of energy [pellet]

BEC=[c_Cc;c_Eva;c_Turb;c_Cond;c_Pump]; % [€] Bare erected Cost

aa_EPCC=1.1;         % [-] Engineering,Procurement and Construction Cost
coefficient
aa_TPC=1.2;          % [-] Total Plant Cost coefficient
aa_TOC=1.15;         % [-] Total Overnight cost coefficient
aa_TASC=1;           % [-] Total As-Spent Cost coeffiecnt

EPCC=aa_EPCC*BEC;   % [€] Engineering,Procurement and Construction Cost
TPC =aa_TPC*EPCC;   % [€] Total Plant Cost
TOC =aa_TOC*TPC;    % [€] Total Overnight cost
TASC=aa_TASC*TOC;   % [€] Total As-Spent Cost

Case=1;
Subcase=1;

for(QQ_i=1:length(QQ_cond))
    for(TT_in_i=1:length(TT_in))
        for(TT_out_i=1:length(TT_out))

            Subcase

            ORCcycle
            Combustion_chamber

            eta_el=(Pe_net/(LCV*m_BIO))*100;
            eta_th=(Q_out_cond/(LCV*m_BIO))*100;

            %% Collected data

            TT_case=[T1,T2,T3,T4,T5,T6,T7,T8,T_amb,T_amb,T_exit];

```

```

PP_case=[P1,P2,P3,P4,PP_c,PP_c,PP_eva,PP_eva,P0,P0,P0];

%% Dead state enthalpies and entropies

h0_1 = refpropm('H','T',T0_1,'P',P0,'R245fa');
h0_2 = h0_1;
h0_3 = h0_1;
h0_4 = h0_1;
h0_5 = refpropm('H','T',T0_5,'P',P0,'water');
h0_6 = h0_5;
h0_7 = h0_5;
h0_8 = h0_5;
h0_9
                                                    =
fkg_air_N2*refpropm('H','T',T0_9,'P',P0,'nitrogen')+fkg_air_O2*refpropm('H','T',T0_9,'
P',P0,'oxygen')+fkg_air_H2O*refpropm('H','T',T0_9,'P',P0,'water');
h0_10 = 0;
                                                    % not physical exergy
h0_11
                                                    =
fkg_CO2*refpropm('H','T',T0_11,'P',P0,'CO2')+fkg_O2*refpropm('H','T',T0_11,'P',P0,'o
xygen')+fkg_N2*refpropm('H','T',T0_11,'P',P0,'nitrogen')+fkg_H2O*refpropm('H','T',
T0_11,'P',P0,'water');

s0_1 = refpropm('S','T',T0_1,'P',P0,'R245fa');
s0_2 = s0_1;
s0_3 = s0_1;
s0_4 = s0_1;
s0_5 = refpropm('S','T',T0_5,'P',P0,'water');
s0_6 = s0_5;
s0_7 = s0_5;
s0_8 = s0_5;
s0_9
                                                    =
fkg_air_N2*refpropm('S','T',T0_9,'P',P0,'nitrogen')+fkg_air_O2*refpropm('S','T',T0_9,'
P',P0,'oxygen')+fkg_air_H2O*refpropm('S','T',T0_9,'P',P0,'water');
s0_10 = 0;
                                                    % not physical exergy
s0_11
                                                    =
fkg_CO2*refpropm('S','T',T0_11,'P',P0,'CO2')+fkg_O2*refpropm('S','T',T0_11,'P',P0,'o
xygen')+fkg_N2*refpropm('S','T',T0_11,'P',P0,'nitrogen')+fkg_H2O*refpropm('S','T',T0
_11,'P',P0,'water');

hh_0=      [h0_1,h0_2,h0_3,h0_4,h0_5,h0_6,h0_7,h0_8,h0_9,h0_10,h0_11];
%[J/kg]
ss_0 = [s0_1,s0_2,s0_3,s0_4,s0_5,s0_6,s0_7,s0_8,s0_9,s0_10,s0_11];  %[J/(kg
K)]

%% Mass flow rates

```

```

m1=m_ORC;
m2=m_ORC;
m3=m_ORC;
m4=m_ORC;
m5=m_B_water;
m6=m_B_water;
m7=m_SP_water;
m8=m_SP_water;
m9=m_AIR;
m10=m_BIO;
m11=m_GAS;

%% Vectors for exergy calculations
mm = [m1,m2,m3,m4,m5,m6,m7,m8,m9,m10,m11];
hh_real=[h1,h2,h3,h4,h5,h6,h7,h8,h9,h10,h11];           %[J/kg]
ss_real=[s1,s2,s3,s4,s5,s6,s7,s8,s9,s10,s11];           %[J/(kg K)]

%% Physical exergy

for(ii=1:length(hh_real))
    e_ph(ii)=hh_real(ii)-hh_0(ii)-T0(ii)*(ss_real(ii)-ss_0(ii));
end

%% Chemical exergy

e_ch=zeros(1,length(hh_real));
e_ch(9)=
f_mol_N2*b_0_N2+f_mol_O2*b_0_O2+f_mol_H2O*b_0_H2O_v+T0_9*(RR_
_N2*f_mol_N2*log(f_mol_N2)+RR_O2*f_mol_O2*log(f_mol_O2)+RR_H
2O*f_mol_H2O*log(f_mol_H2O));

e_ch(10)=1000*(1812.5+295.606*C_kg*100+587.354*H_kg*100+17.506*O_kg*100+
17.735*N_kg*100-31.8*ASH*100);

e_ch(11)=f_mol_N2*b_0_N2+f_mol_O2*b_0_O2+f_mol_CO2*b_0_CO2+f_mol_H2O*b_
0_H2O_v+T0_11*(RR_N2*f_mol_N2*log(f_mol_N2)+RR_O2*f_mol_O2*log(f_mol_O2)
+RR_CO2*f_mol_CO2*log(f_mol_CO2)+RR_H2O*f_mol_H2O*log(f_mol_H2O));

%% Total exergy [W]

for(qq=1:length(hh_real))
    ee(qq)=e_ph(qq)+e_ch(qq);
    EE(qq)=ee(qq)*mm(qq);

```

```

end

EE(12)=W_net_W;
EE(13)=W_in_W;

%% Irreversibilities

II=AA*EE';      % Irreversibilities for each component

II_tot=sum(II); % Total irreversibilities

Irr=II./II_tot.*100; % Fraction of irreversibilities for each component

% %% Fraction of irreversibilities for each component figure
%
% figure (1)
% xx={'CC','EVA','TURB','COND','PUMP'};
% bar(Irr);
% box on
% title('Irreversibilities')
% set(gca,'xticklabel',xx)
% for i1=1:numel(Irr)
%
text(i1,Irr(i1),num2str(Irr(i1),'%0.2f'),'HorizontalAlignment','center','VerticalAlignment',
'bottom')
% end

%% Exergy cost of a stream calculation

ax=[0 0 0 0 -(EE(6)/EE(5)) 1 0 0 0 0 0 0 0
0 -(EE(3)/EE(2)) 1 0 0 0 0 0 0 0 0 0 0
0 0 0 0 0 0 0 0 0 0 -(EE(13)/EE(12)) 1
0 0 -(EE(4)/EE(3)) 1 0 0 0 0 0 0 0 0 0];

Ac=[AA;ae;ax]; % Cost matrix

Ye=[0;0;0;0;0;EE(9);EE(10);EE(7);0;0;0;0;0]; %Vector of external assessment

EE_c=inv(Ac)*Ye; % Exergy cost of a stream

% %% Exergy cost of a stream figure
%
% figure (2)

```

```

%
xx={'E_c1','E_c2','E_c3','E_c4','E_c5','E_c6','E_c7','E_c8','E_c9','E_c10','E_c11','E_c12',
'E_c13'};
%   bar(EE_c);
%   box on
%   title('Exergy cost of a stream')
%   set(gca,'xticklabel',xx)

%% Unit of exergy cost of a stream calculation

kk=EE_c./EE';      % Unit of exergy cost of a stream

%% Unit of exergy cost of a stream figure

%   figure (3)
%
xx={'E_c1','E_c2','E_c3','E_c4','E_c5','E_c6','E_c7','E_c8','E_c9','E_c10','E_c11','E_c12',
'E_c13'};
%   bar(kk);
%   box on
%   title('Unit of exergy cost')
%   set(gca,'xticklabel',xx)

%% EXERGO-ECONOMIC analysis

Annuity=DRF*TASC;      % [€/year]
ZZ=Annuity/(60*60*24*365)/AF; % [€/s] Component cost contribution

C_e=[0;c_energy_bio*EE(10);0;0]; % [€/s] Cost of the stream delivered to the
plat and cost of the discharged streams

Ze=[-ZZ;C_e;0;0;0;0]; % [€/s] Vector of external assessment

CC_i=inv(Ac)*Ze;      % [€/s] Vector of exergo economic cost
cc_i=(CC_i./EE')*10^6*3600; % [€/MWh] Vector of unit exergo economic
cost

%% Design improvement

% Exergo economic unit cost of the fuel

cf=[(cc_i(9)*EE(9)+cc_i(10)*EE(10))/(EE(9)+EE(10));cc_i(5);cc_i(2);cc_i(3);cc_i(13)]
;

```

```

% Exergo economic unit cost of the product
cp=[(cc_i(5)*EE(5)-cc_i(6)-EE(6))/(EE(5)-EE(6));(cc_i(2)*EE(2)-
cc_i(1)*EE(1))/(EE(2)-EE(1));cc_i(12);(cc_i(8)*EE(8)-cc_i(7)*EE(7))/(EE(8)-
EE(7));(cc_i(1)*EE(1)-cc_i(4)*EE(4))/(EE(1)-EE(4))];

% Relative cost difference
ri=[(cp(1)-cf(1))/cf(1);(cp(2)-cf(2))/cf(2);(cp(3)-cf(3))/cf(3);(cp(4)-
cf(4))/cf(4);(cp(5)-cf(5))/cf(5)];

% Cost of exergy destroyed
C_D=[cf(1)*II(1);cf(2)*II(2);cf(3)*II(3);cf(4)*II(4);cf(5)*II(5)]/(10^6*3600);

ZZ_plus_C_D=ZZ+C_D;

%% Exergo economic factor
ff=ZZ./ZZ_plus_C_D;

%% Parametrical results
EE_parametric(TT_out_i,:)=EE;           % Exergies
Irr_parametric(TT_out_i,:)=Irr;         % Fraction of irreversibilities for
each component
EE_c_parametric(TT_out_i,:)=EE_c;       % Exergy cost of a stream
kk_parametric(TT_out_i,:)=kk;           % Unit of exergy cost of a stream
CC_i_parametric(TT_out_i,:)=CC_i;       % [€/s] Vector of exergo economic
cost
cc_i_parametric(TT_out_i,:)=cc_i;       % [€/MWh] Vector of unit exergo
economic cost
cf_parametric(TT_out_i,:)=cf;           % Exergo economic unit cost of the
fuel
cp_parametric(TT_out_i,:)=cp;           % Exergo economic unit cost of the
product
ri_parametric(TT_out_i,:)=ri;           % Relative cost difference
ZZ_plus_C_D_parametric(TT_out_i,:)=ZZ_plus_C_D;
ff_parametric(TT_out_i,:)=ff;           % Exergo economic factor
eta_el_parametric(TT_out_i,:)=eta_el;   % Electric efficiency
eta_th_parametric(TT_out_i,:)=eta_th;   % Thermal efficiency
mm_parametric(TT_out_i,:)=mm;
Pe_in_W_parametric(TT_out_i,:)=Pe_in_W;
Pe_out_W_parametric(TT_out_i,:)=Pe_out_W;
Pe_net_W_parametric(TT_out_i,:)=Pe_net_W;
W_in_W_parametric(TT_out_i,:)=W_in_W;
W_out_W_parametric(TT_out_i,:)=W_out_W;
W_net_W_parametric(TT_out_i,:)=W_net_W;
TT_case_parametric(TT_out_i,:)=TT_case;

```

```

PP_case_parametric(TT_out_i,:)= PP_case;
hh_real_parametric(TT_out_i,:)= hh_real;
ss_real_parametric(TT_out_i,:)= ss_real;
Q_EHE_parametric(TT_out_i,:)= Q_EHE;

TT_input=TT_in(TT_in_i)*ones(TT_out_i,1);
QQ_condenser=QQ_cond(QQ_i)*ones(TT_out_i,1);

Subcase=Subcase+1;
end

table_fluid=[QQ_condenser,TT_input,TT_out',eta_el_parametric,eta_th_parametric,EE
_parametric,EE_c_parametric,kk_parametric,CC_i_parametric,cc_i_parametric];

table_component=[QQ_condenser,TT_input,TT_out',Irr_parametric,cf_parametric,cp_p
arametric,ri_parametric,ZZ_plus_C_D_parametric,ff_parametric];

table_data=[QQ_condenser,TT_input,TT_out',Q_EHE_parametric,mm_parametric,Pe_i
n_W_parametric,Pe_out_W_parametric,Pe_net_W_parametric,W_in_W_parametric,W
_out_W_parametric,W_net_W_parametric,TT_case_parametric,PP_case_parametric,hh
_real_parametric,ss_real_parametric];

% File in order to check only some values

table_extra=[QQ_condenser,TT_input,TT_out',Q_EHE_parametric,Pe_out_W_paramet
ric,QQ_condenser,Pe_in_W_parametric,Pe_net_W_parametric,eta_el_parametric,eta_th
_parametric,mm_parametric,TT_case_parametric,PP_case_parametric,hh_real_paramet
ric,ss_real_parametric];
if Case==1
    [row_fluid,column_fluid]=size(table_fluid);
    bb_fluid=zeros(row_fluid,column_fluid);
    [row_component,column_component]=size(table_component);
    bb_component=zeros(row_component,column_component);
    [row_data,column_data]=size(table_data);
    bb_data=zeros(row_data,column_data);
    [row_extra,column_extra]=size(table_extra);
    bb_extra=zeros(row_extra,column_extra);
end

table2_fluid((1+(Case-1)*row_fluid:(Case-
1)*row_fluid+row_fluid,:)=table_fluid(:,:);
table2_component((1+(Case-1)*row_component:(Case-
1)*row_component+row_component,:)=table_component(:,:);

```

```
    table2_data((1+(Case-1)*row_data:(Case-
1)*row_data+row_data),:)=table_data(:,:);
    table2_extra((1+(Case-1)*row_extra:(Case-
1)*row_extra+row_extra),:)=table_extra(:,:);
    Case=Case+1;

%% Excel files creation

Plant_fluid_results='parametric_fluid.xls';
xlswrite('Plant_fluid_results', table2_fluid)

Plant_component_results='parametric_component.xls';
xlswrite('Plant_component_results', table2_component)

Plant_data_results='parametric_data.xls';
xlswrite('Plant_data_results', table2_data)

Plant_extra_results='parametric_extra.xls';
xlswrite('Plan_extra_results', table2_extra)
end
end
```

Appendix D

ORC model

```

%% Inputs
% Q_out_cond=110;           % Only one case; the parametrical is in the file
exergetic analysis

Q_out_cond=QQ_cond(QQ_i);   % Parametrical study
Q_out_cond_n=147.41;
T8=TT_out(TT_out_i);       % Parametrical study
T7=TT_in(TT_in_i);        % Parametrical study
T5=95;                     % Fix value
T2=90;                     % Fix value
subcooling=5;

P2_n=892.7842;
mf_n=0.667;
T2_n=90;
rp_n=3.71;
eta_th_n=0.8;
eta_me_n=0.88;

P3=250;                    % Initial guess
mf=(Q_out_cond/Q_out_cond_n)*mf_n; % Initial guess
error1=1;
error2=1;
toll=5e-5;

while ((error1>toll) && (error2>toll))
    % Point 2
    P2=mf/mf_n*sqrt((T2+273.15)/(T2_n+273.15))*P2_n;

    % Point 3
    rp=(P2/P3);
    eta_th=(-2.1122*((rp/rp_n)^2)+3.9773*(rp/rp_n)-0.8683)*eta_th_n;

    h2=refpropm('H','T',T2+273.15,'P',P2,'R245fa');
    s2=refpropm('S','T',T2+273.15,'P',P2,'R245fa');
    h3_i=refpropm('H','P',P3,'S',s2,'R245fa');
    h3=h2-eta_th*(h2-h3_i);
    T3=refpropm('T','H',h3,'P',P3,'R245fa')-273.15;
    s3=refpropm('S','T',T3+273.15,'P',P3,'R245fa');

```

```

% Point 4
P4=P3;
mf_old=mf;
condenser % The condenser function is used
mf=mf_new;
P3old=P3;
P3new=refpropm('P','T',T4+subcooling+273.15,'Q',0,'R245fa');

error1=abs((mf-mf_old)/mf);
error2=abs((P3new-P3old)/P3new);

if ((error1>toll) && (error2>toll))
    P3=0.65*P3old+0.35*refpropm('P','T',T4+subcooling+273.15,'Q',0,'R245fa');
end

end

%% New calculation with P3 and mf known
m_ORC=mf;
m_SP_water=mc;

h7=refpropm('H','T',T7+273.15,'P',Pc,'water');
h8=refpropm('H','T',T8+273.15,'P',Pc,'water');
s7=refpropm('S','T',T7+273.15,'P',Pc,'water');
s8=refpropm('S','T',T8+273.15,'P',Pc,'water');

% Tsat_cond=refpropm('T','P',P3,'Q',1,'R245fa')-273.15

% Point 1
eta_th_pump = 0.98;
P1=P2;
h4 = refpropm('H','T',T4+273.15,'P',P4,'R245fa');
s4 = refpropm('S','T',T4+273.15,'P',P4,'R245fa');
h1_i = refpropm('H','P',P1,'S',s4,'R245fa');
h1 = h4+(h1_i-h4)/eta_th_pump;
T1 = refpropm('T','H',h1,'P',P1,'R245fa')-273.15;
s1 = refpropm('S','T',T1+273.15,'P',P1,'R245fa');

evaporator % The evaporator function is used
m_B_water=mh;

h5=refpropm('H','T',T5+273.15,'P',Ph,'water');
h6=refpropm('H','T',T6+273.15,'P',Ph,'water');

```

```

s5=refpropm('S','T',T5+273.15,'P',Ph,'water');
s6=refpropm('S','T',T6+273.15,'P',Ph,'water');
Tsat_eva=refpropm('T','P',P1,'Q',1,'R245fa')-273.15

% Final calculation
eta_me_pump = 0.6;
W_out = (mf*(h2-h3))/1000;           % kW
Pe_out = (eta_me_n*W_out);         % kW
W_in = (mf*(h1-h4))/1000;         % kW
Pe_in = (eta_me_pump*W_in);       % kW

Pe_net=Pe_out-Pe_in;              % kW
W_net=W_out-W_in;                % kW

Pe_in_W=Pe_in*1000;              % W
Pe_out_W=Pe_out*1000;            % W
Pe_net_W=Pe_net*1000;            % W

W_in_W=W_in*1000;                % W
W_out_W=W_out*1000;              % W
W_net_W=W_net*1000;              % W
WW=[W_net_W,W_in_W,0,0,0,0,0,0,0,0]; % W
% P3
%
% For polysun
%                               Qso_max=mf*(refpropm('H','T',73+273.15,'P',P1,'R245fa')-
refpropm('H','T',T1+273.15,'P',P1,'R245fa'))

```

Appendix E

Evaporator model

%% Manufacturer's Inputs

```

o = 1.17;           % Enlargement factor
Beta = 27.5;       % Channel angle on the plate
pco = 0.0046;      % Longitudinal step from correlation

tt=0.00244;        % Thickness of channels
Dentradas=0.060;  % Entrance diameter
L=0.450;           % Plate length
w=0.243;           % Plate width
Ap=0.1300;         % Plate area
Np=107;            % Number of plates

Rfc = 0;           % Fouling factor in cold fluid channels
Rfh = 0;           % Fouling factor in hot fluid channels

```

%% Model inputs

```

Th_in=T5;
Ph=300;            % Hot pressure
PP_eva=Ph;        % Evaporator pressure

```

```

Tc_out=T2;
Tc_in=T1;
mc=mf;
Pc=P1;

```

```

Area = Np*Ap;

```

%% Balance

```

hc_in=refpropm('H','T',Tc_in+273.15,'P',Pc,'R245fa'); %h1
hc_out=refpropm('H','T',Tc_out+273.15,'P',Pc,'R245fa'); %h2
Q=mc*(hc_out-hc_in);

```

```

hh_in=refpropm('H','T',Th_in+273.15,'P',Ph,'water'); %h5

```

```

error=1;
Th_out=Th_in-3;    % guess
A2=3;              % guess

```

```

while (error>0.0001)

```

```

    T6=Th_out;

```

```

    hh_out=refpropm('H','T',Th_out+273.15,'P',Pc,'water'); %h6
    mh=Q/(hh_in-hh_out);

```

% 3 zone

```

    Tsat=refpropm('T','P',Pc,'Q',0,'R245fa')-273.15; %Tboil_h

```

```

hc_1=hc_out;
hc_2=refpropm('H','P',Pc,'Q',1,'R245fa');
hc_3=refpropm('H','P',Pc,'Q',0,'R245fa');
hc_4=hc_in;

Tc_1=T2;
Tc_2=Tsats;
Tc_3=Tsats;
Tc_4=T1;

Q1=mc*(hc_1-hc_2);
Q2=mc*(hc_2-hc_3);
Q3=mc*(hc_3-hc_4);

hh_1=hh_in;
hh_2=hh_1-Q1/mh;
hh_3=hh_2-Q2/mh;
hh_4=hh_out;

Th_1=T5;
Th_2=refpropm('T','H',hh_2,'P',Ph,'water')-273.15;
Th_3=refpropm('T','H',hh_3,'P',Ph,'water')-273.15;
Th_4=T6;

% Calculation h(...)
Ncp = (Np-1)/2;

%hh1
D = 2*tt;
Gf = mh/(Ncp*tt*w);
mu = refpropm('V','H',(hh_1+hh_2)/2,'P',Ph,'water');
Re_h1 = (Gf*D)/mu;
Pr_h1 = refpropm('^','H',(hh_1+hh_2)/2,'P',Ph,'water');
Nu_h1 = 0.78*(Re_h1^0.5)*(Pr_h1^(1./3.));
k = refpropm('L','H',(hh_1+hh_2)/2,'P',Ph,'water');
hh1 = (Nu_h1*k)/D;

%hc1
D=2*tt;
Gf = mc/(Ncp*tt*w);
mu = refpropm('V','H',(hc_1+hc_2)/2,'P',Pc,'R245fa');
Re_c1 = (Gf*D)/mu;
Pr_c1 = refpropm('^','H',(hc_1+hc_2)/2,'P',Pc,'R245fa');
Nu_c1 = 0.78*(Re_c1^0.5)*(Pr_c1^(1./3.));
k = refpropm('L','H',(hc_1+hc_2)/2,'P',Pc,'R245fa');
hc1 = (Nu_c1*k)/D;

U1=1/((1/hc1)+Rfc+Rfh+(1/hh1));

```

%hh2

```

D = 2*tt;
Gf = mh/(Ncp*tt*w);
mu = refpropm('V','H',(hh_2+hh_3)/2,'P',Ph,'water');
Re_h2 = (Gf*D)/mu;
Pr_h2 = refpropm('^','H',(hh_2+hh_3)/2,'P',Ph,'water');
Nu_h2 = 0.78*(Re_h2^0.5)*(Pr_h2^(1./3.));
k = refpropm('L','H',(hh_2+hh_3)/2,'P',Ph,'water');
hh2 = (Nu_h2*k)/D;

```

%hc2

```

D = (2*tt)/o;
Gf = mc/(Ncp*tt*w);
mu = refpropm('V','P',Pc,'Q',0,'R245fa');
xm=0.5;
rho_l=refpropm('D','P',Pc,'Q',0,'R245fa');
rho_v=refpropm('D','P',Pc,'Q',1,'R245fa');
Gfeq = Gf*(1+xm*(((rho_l/rho_v)^(1./2.))-1));
Re_c2 = (Gfeq*D)/mu;

k = refpropm('L','P',Pc,'Q',0,'R245fa');
cp_l=refpropm('C','P',Pc,'Q',0,'R245fa');
cp_v=refpropm('C','P',Pc,'Q',1,'R245fa');
cp_m=(cp_l+cp_v)/2;
Pr_c2 = (cp_m*mu)/k;

Ge1 = 2.81*((pco/D)^(-0.041))*(((pi/2)*((Beta*pi)/180))^(-2.83));
Ge2 = 0.746*((pco/D)^(-0.082))*(((pi/2)*((Beta*pi)/180))^(0.61));
Bo = mc/(Gfeq*A2);
Nu_c2 = Ge1*(Re_c2^Ge2)*(Bo^0.3)*(Pr_c2^0.4);

hc2 = (Nu_c2*k)/D;

```

```

U2=1/((1/hc2)+Rfc+Rfh+(1/hh2));

```

%hh3

```

D = 2*tt;
Gf = mh/(Ncp*tt*w);
mu = refpropm('V','H',(hh_3+hh_4)/2,'P',Ph,'water');
Re_h3 = (Gf*D)/mu;
Pr_h3 = refpropm('^','H',(hh_3+hh_4)/2,'P',Ph,'water');
Nu_h3 = 0.78*(Re_h3^0.5)*(Pr_h3^(1./3.));
k = refpropm('L','H',(hh_3+hh_4)/2,'P',Ph,'water');
hh3 = (Nu_h3*k)/D;

```

%hc3

```

D = 2*tt;
Gf = mc/(Ncp*tt*w);

```

```

mu = refpropm('V','H',(hc_3+hc_4)/2,'P',Pc,'R245fa');
Re_c3 = (Gf*D)/mu;
Pr_c3 = refpropm('^','H',(hc_3+hc_4)/2,'P',Pc,'R245fa');
C1 = 0.2946;
m = 0.7;
Nu_c3 = C1*(Re_c3^m)*(Pr_c3^(1./3.));
k = refpropm('L','H',(hc_3+hc_4)/2,'P',Pc,'R245fa');
hc3 = (Nu_c3*k)/D;

U3=1/((1/hc3)+Rfc+Rfh+(1/hh3));

dt1 = Th_1-Tc_1;
dt2 = Th_2-Tc_2;
dTml_1 = (dt1-dt2)/(log(dt1/dt2));

dt1 = Th_2-Tc_2;
dt2 = Th_3-Tc_3;
dTml_2 = (dt1-dt2)/(log(dt1/dt2));

dt1 = Th_3-Tc_3;
dt2 = Th_4-Tc_4;
dTml_3 = (dt1-dt2)/(log(dt1/dt2));

A1=Q1/(U1*dTml_1);
A2=Q2/(U2*dTml_2);
A3=Q3/(U3*dTml_3);

AT=A1+A2+A3;
error= abs((Area-AT)/Area);

Th_out = Th_out-((Area-AT)/Area);
end

T6=Th_out;
pp_evap=Th_3-Tc_3;
Q_EHE=Q/1000;

```

Appendix F

Condenser model

%% Manufacturer's Inputs

```

o = 1.17;           % Enlargement factorEnlargement factor
Beta = 27.5;       % Channel angle of the plate
pco = 0.0046;      % Longitudinal step from correlation
tc=0.00225;        % Thickness of channels
Dentradas=0.060;   % Entrance diameter
L=0.460;           % Plate length
w=0.281;           % Plate width
Ap=0.1600;         % Plate area
Np=58;             % Number of plates

Rfc = 0;           % Fouling factor in cold fluid channels
Rfh = 0;           % Fouling factor in hot fluid channels

```

%% Model inputs

```

Q=Q_out_cond;
Th_in=T3;
Ph=P3;

Tc_out=T8;
Tc_in=T7;
Pc=300;           % Cold side pressure
PP_c=Pc;          % Condenser pressure

```

```

Area = Np*Ap;

```

%% Balance

```

hc_in=refpropm('H','T',Tc_in+273.15,'P',Pc,'water'); %h7
hc_out=refpropm('H','T',Tc_out+273.15,'P',Pc,'water'); %h8
mc=Q*1000/(hc_out-hc_in);

```

```

hh_in=refpropm('H','T',Th_in+273.15,'P',Ph,'R245fa'); %h3

```

```

error=1;

```

```

toll_cond=1e-5;

```

```

Th_out=T8; % guess

```

```

while (error>toll_cond)

```

```

    T4=Th_out;

```

```

    hh_out=refpropm('H','T',Th_out+273.15,'P',Ph,'R245fa'); %h3

```

```

    mh=Q*1000/(hh_in-hh_out);

```

```

    % 3 zone

```

```

    Tsat=refpropm('T','P',Ph,'Q',0,'R245fa')-273.15; %Tboil_h

```

```

    hh_1=hh_in;

```

```

    hh_2=refpropm('H','P',Ph,'Q',1,'R245fa');

```

```

hh_3=refpropm('H','P',Ph,'Q',0,'R245fa');
hh_4=hh_out;

Th_1=T3;
Th_2=Tsats;
Th_3=Tsats;
Th_4=T4;

Q1=mh*(hh_1-hh_2);
Q2=mh*(hh_2-hh_3);
Q3=mh*(hh_3-hh_4);

hc_1=hc_out;
hc_2=hc_1-Q1/mc;
hc_3=hc_2-Q2/mc;
hc_4=hc_in;

Tc_1=T8;
Tc_2=refpropm('T','H',hc_2,'P',Pc,'water')-273.15;
Tc_3=refpropm('T','H',hc_3,'P',Pc,'water')-273.15;
Tc_4=T7;

% Calculation h(...)
%hh1
D = 2*tc;
Ncp = Np/2;
Gf = mh/(Ncp*tc*w);
mu = refpropm('V','H',(hh_1+hh_2)/2,'P',Ph,'R245fa');
Re_h1 = (Gf*D)/mu;
Pr_h1 = refpropm('^','H',(hh_1+hh_2)/2,'P',Ph,'R245fa');
Nu_h1 = 0.78*(Re_h1^0.5)*(Pr_h1^(1./3.));
k = refpropm('L','H',(hh_1+hh_2)/2,'P',Ph,'R245fa');
hh1 = (Nu_h1*k)/D;

%hc1
D = 2*tc;
Gf = mc/(Ncp*tc*w);
mu = refpropm('V','H',(hc_1+hc_2)/2,'P',Pc,'water');
Re_c1 = (Gf*D)/mu;
Pr_c1 = refpropm('^','H',(hc_1+hc_2)/2,'P',Pc,'water');
Nu_c1 = 0.78*(Re_c1^0.5)*(Pr_c1^(1./3.));
k = refpropm('L','H',(hc_1+hc_2)/2,'P',Pc,'water');
hc1 = (Nu_c1*k)/D;

U1=1/((1/hc1)+Rfc+Rfh+(1/hh1));

%hh2
D = (2*tc)/o;
Gf = mh/(Ncp*tc*w);

```

```

mu = refpropm('V','P',Ph,'Q',0,'R245fa');
xm=0.5;
rhol=refpropm('D','P',Ph,'Q',0,'R245fa');
rhov=refpropm('D','P',Ph,'Q',1,'R245fa');
Gfeq = Gf*(1+xm*(((rhol/rhov)^(1./2.))-1));
Re_h2 = (Gfeq*D)/mu;

k = refpropm('L','P',Ph,'Q',0,'R245fa');
cp_l=refpropm('C','P',Ph,'Q',0,'R245fa');
cp_v=refpropm('C','P',Ph,'Q',1,'R245fa');
cp_m=(cp_l+cp_v)/2;
Pr_h2 = (cp_m*mu)/k;

Ge1=11.22*((pco/D)^(-2.83))*(((pi/2)*((Beta*pi)/180))^(-4.5));
Ge2=0.35*((pco/D)^(0.23))*(((pi/2)*((Beta*pi)/180))^(1.48));
Nu_h2=Ge1*(Re_h2^Ge2)*Pr_h2^(1./3.);

hh2=(Nu_h2*k)/D;

%hc2
D = 2*tc;
Gf = mc/(Ncp*tc*w);
mu = refpropm('V','H',(hc_2+hc_3)/2,'P',Pc,'water');
Re_c2 = (Gf*D)/mu;
Pr_c2 = refpropm('^','H',(hc_2+hc_3)/2,'P',Pc,'water');
Nu_c2 = 0.78*(Re_c2^0.5)*(Pr_c2^(1./3.));
k = refpropm('L','H',(hc_2+hc_3)/2,'P',Pc,'water');
hc2 = (Nu_c2*k)/D;

U2=1/((1/hc2)+Rfc+Rfh+(1/hh2));

%hh3
D = 2*tc;
Gf = mh/(Ncp*tc*w);
mu = refpropm('V','H',(hh_3+hh_4)/2,'P',Ph,'R245fa');
Re_h3 = (Gf*D)/mu;
Pr_h3 = refpropm('^','H',(hh_3+hh_4)/2,'P',Ph,'R245fa');
Nu_h3 = 0.78*(Re_h3^0.5)*(Pr_h3^(1./3.));
k = refpropm('L','H',(hh_3+hh_4)/2,'P',Ph,'R245fa');
hh3 = (Nu_h3*k)/D;

%hc3
D = 2*tc;
Gf = mc/(Ncp*tc*w);
mu = refpropm('V','H',(hc_3+hc_4)/2,'P',Pc,'water');
Re_c3 = (Gf*D)/mu;
Pr_c3 = refpropm('^','H',(hc_3+hc_4)/2,'P',Pc,'water');
Nu_c3 = 0.78*(Re_c3^0.5)*(Pr_c3^(1./3.));
k = refpropm('L','H',(hc_3+hc_4)/2,'P',Pc,'water');
hc3 = (Nu_c3*k)/D;

```

```
U3=1/((1/hc3)+Rfc+Rfh+(1/hh3));

dt1 = Th_1-Tc_1;
dt2 = Th_2-Tc_2;
dTml_1 = (dt1-dt2)/(log(dt1/dt2));

dt1 = Th_2-Tc_2;
dt2 = Th_3-Tc_3;
dTml_2 = (dt1-dt2)/(log(dt1/dt2));

dt1 = Th_3-Tc_3;
dt2 = Th_4-Tc_4;
dTml_3 = (dt1-dt2)/(log(dt1/dt2));

A1=Q1/(U1*dTml_1);
A2=Q2/(U2*dTml_2);
A3=Q3/(U3*dTml_3);

AT=A1+A2+A3;

error=abs((Area-AT)/Area);
Th_out=Th_out-((Area-AT)/Area);
end

%pp_cond=Th_2-Tc_2;
mf_new=mh;
% Ph
% Th_in
% Th_out
```

Appendix G

Combustion chamber model

%% Combustion calculations

$\text{bio_hum_kg} = 0.048;$ % Moisture content in dry biomass
 $[\text{kg_H}_2\text{O_l}/\text{kg_bio_s}]$
 $\text{Qw} = \text{Q_EHE};$ % Power absorbed by water [kW]
 $\text{T_amb} = 16.1;$ % Room temperature [°C]
 $\text{T_exit} = 0.3761 * \text{Qw} + 56.229;$ % Gas outlet temperature at nominal boiler point
 $[\text{°C}]$
 $\text{CO}_2_\text{xbio} = (0.0352 * \text{Qw} + 5.7665) / 100;$ % Percentage of CO₂ in the combustion gases
 in the nominal condition of the boiler and considering a dry basis

%Biomass mass fractions (pellets) for a dry basis in a mass percentage [kg_i/kg_bio_seca]

$\text{C_kg} = 0.494;$
 $\text{H_kg} = 0.061;$
 $\text{N_kg} = 0.001;$
 $\text{O_kg} = 0.437;$
 $\text{ASH} = 0.006;$
 $\text{H}_2\text{Oa_rel_hum} = 0.6;$ %Relative humidity

%Molar mass of different components [kg/kmol]

$\text{MM_CO}_2 = 44.01;$
 $\text{MM_H}_2\text{O} = 18.02;$
 $\text{MM_O}_2 = 32;$
 $\text{MM_N}_2 = 28.01;$
 $\text{MM_air} = 28.96;$
 $\text{MM_C} = 12.01;$
 $\text{MM_H} = 1.008;$
 $\text{MM_N} = 14.01;$
 $\text{MM_O} = 16;$
 $\text{MM_bio} = 1;$

%Biomass mole fractions for $\text{MM_bio_s} = 1$

$\text{C} = \text{C_kg} / \text{MM_C};$
 $\text{H} = \text{H_kg} / \text{MM_H};$
 $\text{N} = \text{N_kg} / \text{MM_N};$
 $\text{O} = \text{O_kg} / \text{MM_O};$

%% Influence of moisture present on ambient air

$\text{psat_air_H}_2\text{O} = \text{refpropm}(\text{'P','T'}, \text{T_amb} + 273.15, \text{'Q'}, 0, \text{'water'});$ % Water saturation
 pressure at room temperature [kPa]
 $\text{pp_air_H}_2\text{O} = \text{H}_2\text{Oa_rel_hum} * \text{psat_air_H}_2\text{O};$ % Partial humidity present in ambient
 air [kPa]
 $\text{H}_2\text{Oa} = (\text{pp_air_H}_2\text{O} / 101.325);$ % H₂O moles present in the reagents

$$H2O1bio = bio_hum_kg/MM_H2O;$$

%% Stoichiometric calculations, theoretical reaction

% Considering the humidity of biomass and air, according to the equation:

$$\% 1 * (C,H,N,O,H2O1bio) + air * (O2 + 3,76N2 + H2Oa) ===== a * (CO2) + c * (N2) + d * (H2O)$$

$$CO2_st_hh = C; \quad \% \text{ Chemical balance of species - C}$$

$$air_st_hh = (4 * CO2_st_hh + H - 2 * O) / 4; \quad \% \text{ Chemical balance of species - O}$$

$$H2O_st_hh = (H + 2 * H2O1bio + 2 * air_st_hh * H2Oa) / 2; \quad \% \text{ Chemical balance of species - H}$$

$$N2_st_hh = (N + 2 * 3.76 * air_st_hh) / 2; \quad \% \text{ Chemical balance of species - N}$$

%% Molar coefficients for x moles of dry biomass, with humidity in the air - according to equation:

$$\% x * (C,H,N,O) + air * (O2 + 3,76N2 + H2Oa) ===== a * (CO2) + b * (O2) + c * (N2) + d * (H2O)$$

$$xbio_sh = CO2_xbio / C;$$

$$O2_xbio_sh = (3.76*xbio_sh*O+2-2*CO2_xbio-xbio_sh*N-2*3.76*CO2_xbio - ((3.76*xbio_sh*H)/2)) / (2*3.76 + 2);$$

$$air_xbio_sh = (2-2*CO2_xbio-xbio_sh*N-2*O2_xbio_sh)/(2*3.76);$$

$$H2O_xbio_sh = (xbio_sh*H+2*air_xbio_sh*H2Oa)/2;$$

$$N2_xbio_sh = 1 - O2_xbio_sh - CO2_xbio;$$

%Mole coefficients for 1 kmol of dry biomass

% Reagents:

$$bio1_sh = xbio_sh / xbio_sh; \quad \% \text{ Dry biomass}$$

$$air_1bio_sh = air_xbio_sh / xbio_sh; \quad \% \text{ Air for the combustion of dry biomass}$$

% Products:

$$CO2_1bio_sh = CO2_xbio / xbio_sh;$$

$$O2_1bio_sh = O2_xbio_sh / xbio_sh;$$

$$N2_1bio_sh = N2_xbio_sh / xbio_sh;$$

$$H2O_1bio_sh = H2O_xbio_sh / xbio_sh;$$

%% Molar coefficients for x moles of biomass, considering the humidity of biomass and air - according to equation:

$$\% x * (C,H,N,O,H2O1bio) + air * (O2 + 3,76N2 + H2Oa) ===== CO2_xbio * (CO2) + O2_xbio_h * (O2) + N2_xbio_h * (N2) + H2O_xbio_h * (H2O)$$

$$xbio_hh = CO2_xbio / C;$$

$$O2_xbio_hh = (3.76*xbio_hh*O+2-2*CO2_xbio-xbio_hh*N-2*3.76*CO2_xbio - ((3.76*xbio_hh*H)/2)) / (2*3.76 + 2);$$

$$\text{air_xbio_hh} = (2 - 2 \cdot \text{CO2_xbio} - \text{xbio_hh} \cdot \text{N} - 2 \cdot \text{O2_xbio_hh}) / (2 \cdot 3.76);$$

$$\text{H2O_xbio_hh} = (\text{xbio_hh} \cdot \text{H} + 2 \cdot \text{xbio_hh} \cdot \text{H2O} + 2 \cdot \text{air_xbio_hh} \cdot \text{H2Oa}) / 2;$$

$$\text{N2_xbio_hh} = 1 - \text{O2_xbio_hh} - \text{CO2_xbio};$$

%Mole coefficients for 1 kmol of biomass

% Reagents:

$$\text{bio1_hh} = \text{xbio_hh} / \text{xbio_hh};$$

$$\text{air_1bio_hh} = \text{air_xbio_hh} / \text{xbio_hh}; \quad \text{\%Air for the combustion of biomass, considering its biomass and aria humidity}$$

%Products:

$$\text{CO2_1bio_hh} = \text{CO2_xbio} / \text{xbio_hh}; \quad \text{\%Value of CO2, considering the biomass and aria humidity, per kmol of biomass}$$

$$\text{O2_1bio_hh} = \text{O2_xbio_hh} / \text{xbio_hh}; \quad \text{\%Value of O2, considering the biomass and aria humidity, per kmol of biomass}$$

$$\text{N2_1bio_hh} = \text{N2_xbio_hh} / \text{xbio_hh}; \quad \text{\%Value of N2, considering the biomass and aria humidity, per kmol of biomass}$$

$$\text{H2O_1bio_hh} = \text{H2O_xbio_hh} / \text{xbio_hh}; \quad \text{\%Value of H2O, considering the biomass and aria humidity, per kmol of biomass}$$

%% Calculation of the AF ratio and excess air

$$\text{l_ca} = ((\text{air_1bio_hh} / \text{air_st_hh}) * 100); \quad \text{\% Air of combustion}$$

$$\text{l_ea} = ((\text{air_1bio_hh} / \text{air_st_hh}) * 100) - 100; \quad \text{\% Excess of air}$$

$$\text{AF_hh} = (\text{air_1bio_hh} * \text{MM_air} * (4.76 + \text{H2Oa})) ; \quad \text{\%Air-to-fuel mass ratio [kg_ar/kg_fuel]}$$

%% Molar fractions of air considering the humidity

$$\text{sum_mol_air} = 4.76 + \text{H2Oa};$$

$$\text{fmol_air_N2} = 3.76 / \text{sum_mol_air};$$

$$\text{fmol_air_O2} = 1 / \text{sum_mol_air};$$

$$\text{fmol_air_H2O} = \text{H2Oa} / \text{sum_mol_air};$$

$$\text{fmol_air} = [\text{fmol_air_N2}; \text{fmol_air_O2}; 0; \text{fmol_air_H2O}];$$

%% Moisture fractions of the combustion air considering the humidity

$$\text{sum_kg_air} = \text{H2Oa} * \text{MM_H2O} + 3.76 * \text{MM_N2} + 1 * \text{MM_O2};$$

$$\text{fkg_air_N2} = (3.76 * \text{MM_N2}) / \text{sum_kg_air};$$

$$\text{fkg_air_O2} = (1 * \text{MM_O2}) / \text{sum_kg_air};$$

$$\text{fkg_air_H2O} = (\text{H2Oa} * \text{MM_H2O}) / \text{sum_kg_air};$$

$$\text{fkg_air} = [\text{fkg_air_N2}; \text{fkg_air_O2}; 0; \text{fkg_air_H2O}];$$

%% Molar fractions of the combustion products considering the humidity and 1 kmol/kg of biomass

```
sum_mol_prod = H2O_1bio_hh + N2_1bio_hh + O2_1bio_hh + CO2_1bio_hh;
fmol_CO2 = CO2_1bio_hh / sum_mol_prod;
fmol_O2 = O2_1bio_hh / sum_mol_prod;
fmol_N2 = N2_1bio_hh / sum_mol_prod;
fmol_H2O = H2O_1bio_hh / sum_mol_prod;
```

```
fmol_gas=[fmol_N2; fmol_O2; fmol_CO2; fmol_H2O];
%% Moisture fractions of the combustion products considering moisture and 1 kmol/kg of biomass
```

```
sum_kg_prod = H2O_1bio_hh*MM_H2O + N2_1bio_hh*MM_N2 +
O2_1bio_hh*MM_O2 + CO2_1bio_hh*MM_CO2;
fkg_CO2 = (CO2_1bio_hh*MM_CO2) / sum_kg_prod;
fkg_O2 = (O2_1bio_hh*MM_O2) / sum_kg_prod;
fkg_N2 = (N2_1bio_hh*MM_N2) / sum_kg_prod;
fkg_H2O = (H2O_1bio_hh*MM_H2O) / sum_kg_prod;
```

```
fkg_gas=[fkg_N2; fkg_O2; fkg_CO2; fkg_H2O];
```

%% Partial pressures (molar fractions are always used to calculate partial pressures):

```
pb= 101.325; % Pressure boiler [kPa] - The atmospheric pressure was assumed
pb_atm= 1; % Pressure boiler [atm] - The atmospheric pressure was assumed
pp_CO2= fmol_CO2*pb; % Partial pressure of CO2 [kPa]
pp_H2O= fmol_H2O*pb; % Partial pressure of H2O [kpa]
pp_N2= fmol_N2*pb; % Partial pressure of N2 [kPa]
pp_O2= fmol_O2*pb; % Partial pressure of O2 [kPa]
pp_CO2_atm= fmol_CO2*pb_atm; % Partial pressure of CO2 [atm]
pp_H2O_atm= fmol_H2O*pb_atm; % Partial pressure of H2O [atm]
pp_N2_atm= fmol_N2*pb_atm; % Partial pressure of N2 [atm]
pp_O2_atm= fmol_O2*pb_atm; % Partial pressure of O2 [atm]
```

%% CONTROL

```
Tsat_H2O_gas=refpropm('T','P',pp_H2O,'Q',0,'water')-273.15;
```

```
if Tsat_H2O_gas>T_exit
```

```
error('The stoichiometric balance is not correct because part of the water contained in the gases at the chimney is condensed')
```

```
end
```

%% Enthalpy of formation and PC [kJ/kmol]

```
hf_H2O_l = -285830;
hf_H2O_g = -241820;
hf_CO2 = -393520;
```

```
LCV = 18 * 1000; %kJ/kg in dry biomass supplied
```

%% Enthalpy in the reference state [kJ/kmol] - EES (Input in [°C])

T_ref= 25;

h_CO2_ref = 0.0061*(T_ref^2) + 43.985*T_ref - 395277;
 h_N2_ref = 0.0025*(T_ref^2) + 28.796*T_ref - 757.38;
 h_water_l_ref = -0.0025*(T_ref^2) + 75.518*T_ref + 2.6114;
 h_water_g_ref = 0.006*(T_ref^2) + 32.597*T_ref - 242620;
 h_O2_ref = 0.0025*(T_ref^2) + 30.758*T_ref - 952.61;
 h_C_ref = -3E-05*(T_ref^2) + 20.84*T_ref + 716115;
 h_H_ref = 0.0001*(T_ref^2) + 20.78*T_ref + 217466;
 h_N_ref = 8E-05*(T_ref^2) + 20.782*T_ref + 472131;
 h_O_ref = -0.0029*(T_ref^2) + 22.065*T_ref + 248610;
 h_bio_ref = C*h_C_ref + H*h_H_ref + N*h_N_ref + O*h_O_ref;

%in

T_in=T_amb;

h_C_in = -3E-05*(T_in^2) + 20.84*T_in + 716115;
 h_H_in = 0.0001*(T_in^2) + 20.78*T_in + 217466;
 h_N_in = 8E-05*(T_in^2) + 20.782*T_in + 472131;
 h_N2_in = 0.0025*(T_in^2) + 28.796*T_in - 757.38;
 h_O_in = -0.0029*(T_in^2) + 22.065*T_in + 248610;
 h_bio_in = C*h_C_in + H*h_H_in + N*h_N_in + O*h_O_in;
 h_water_l_in = -0.0025*(T_in^2) + 75.518*T_in + 2.6114;
 h_water_g_in = 0.006*(T_in^2) + 32.597*T_in - 242620;
 h_O2_in = 0.0025*(T_in^2) + 30.758*T_in - 952.61;

%% Enthalpies in the chimney [kJ/kmol] - EES (Input in [°C])

h_CO2_exit = 0.0061*(T_exit^2) + 43.985*T_exit - 395277;
 h_water_g_exit = 0.006*(T_exit^2) + 32.597*T_exit - 242620;
 h_N2_exit = 0.0025*(T_exit^2) + 28.796*T_exit - 757.38;
 h_O2_exit = 0.0025*(T_exit^2) + 30.758*T_exit - 952.61;

%% Enthalpy formation and calculation of available energy - q_available [kJ/kg]

hf_bio_sh = LCV + (CO2_1bio_sh * hf_CO2 + H2O_1bio_sh * hf_H2O_g);

%Enthalpy of biomass formation [kJ/kmol]

q_reagentes = ((bio1_hh*hf_bio_sh + H2O1bio*hf_H2O_l) + (bio1_hh*(h_bio_in-
 h_bio_ref) + H2O1bio*(h_water_l_in-h_water_l_ref) +
 ((air_1bio_hh*H2Oa*hf_H2O_g)+(air_1bio_hh*H2Oa*(h_water_g_in-h_water_g_ref))
 + (air_1bio_hh*3.76*(h_N2_in-h_N2_ref)) + (air_1bio_hh*1*(h_O2_in-h_O2_ref))));
 q_productos = (CO2_1bio_hh*hf_CO2 + H2O_1bio_hh*hf_H2O_g) +
 (CO2_1bio_hh*(h_CO2_exit-h_CO2_ref) + O2_1bio_hh*(h_O2_exit-h_O2_ref) +
 N2_1bio_hh*(h_N2_exit-h_N2_ref) + H2O_1bio_hh*(h_water_g_exit-h_water_g_ref));
 q_gq = q_reagentes - q_productos;

%% Calculation of the flue gas flow rate

%Air-to-fuel ratio AF

```
s9 = fkg_air_N2*refpropm('S','T',T_amb+273.15,'P',P0,'nitrogen')+fkg_air_O2*refpropm('S',  
'T',T_amb+273.15,'P',P0,'oxygen')+fkg_air_H2O*refpropm('S','T',T_amb+273.15,'P',P0  
, 'water');  
s10 = 0; %not physical exergy  
% s11_flame =  
fkg_CO2*refpropm('S','T',T_flame+273.15,'P',P0,'CO2')+fkg_O2*refpropm('S','T',T fla  
me+273.15,'P',P0,'oxygen')+fkg_N2*refpropm('S','T',T_flame+273.15,'P',P0,'nitrogen')  
+fkg_H2O*refpropm('S','T',T_flame+273.15,'P',P0,'water');  
s11 = fkg_CO2*refpropm('S','T',T_exit+273.15,'P',P0,'CO2')+fkg_O2*refpropm('S','T',T_exit  
+273.15,'P',P0,'oxygen')+fkg_N2*refpropm('S','T',T_exit+273.15,'P',P0,'nitrogen')+fkg_  
H2O*refpropm('S','T',T_exit+273.15,'P',P0,'water');
```